The effects of vegetation on the estimation of low flows: a high-resolution study in natural streams featuring novel techniques

by

Lorenzo Brignoli

A thesis

presented to the University of Waterloo

in fulfillment of the

thesis requirement for the degree of

Doctor of Philosophy

in

Civil Engineering

Waterloo, Ontario, Canada, 2018

Examining Committee Membership

The following served on the Examining Committee for this thesis. The decision of the Examining Committee is by majority vote.

External Examiner	Andrea Bradford Professor
Supervisor(s)	William K. Annable Associate Professor
Internal Member	Bruce MacVicar Associate Professor
Internal Member	Nicholas Kouwen Distinguished Professor Emeritus
Internal-external Member	Mike Stone Professor

Author’s Declaration

This thesis consists of material all of which I authored or co-authored: see Statement of Contributions included in the thesis. This is a true copy of the thesis, including any required final revisions, as accepted by my examiners.

I understand that my thesis may be made electronically available to the public.

Statement of Contributions

Chapter 2 was prepared in collaboration with Dr. Ben D. Plumb, of GeoProcess Research Associates, who is also an University of Waterloo alumnus (Civil Engineering). Ben assisted by starting the data collection process using his personal UAV and providing guidance throughout as the process evolved from its initial stages to the final stage. Ben also provided helpful inputs regarding the image stitching techniques and helped in the review phase as the paper got submitted, and eventually accepted, by a Journal; his help was crucial for the paper to succeed.

Experimental work for Chapter 3 was prepared with help from Terry Ridgway, of the University of Waterloo (Civil Engineering). Terry was instrumental in helping setting up the experiment, find the right materials for the test and suggesting improvements to the experimental apparatus.

Abstract

Accurate measurement of stream discharge under low-flow conditions is of utmost importance to many water resources practitioners. In most of the world, discharge is estimated at gauging stations using rating curves. These relate observed water level to field measured discharge, under the assumption that a direct proportionality exists between the two. However, if seasonal aquatic vegetation growth occurs, water levels (or stages) will rise as macrophytes increase flow resistance. Consequently, if this effect is not accounted for, the increase in water levels may be mistaken as an increase in discharge. Current methods to correct these errors in flow calculations can be time-consuming and do not always perform consistently, as they rely on sporadic discharge measurements and qualitative observations. As such, it is not uncommon for flow records to be discontinued during the summer, a period often coinciding with the low flow season in many climatic regions. During these months, incorrectly estimated flow values, or lack of flow records can have problematic consequences. For instance, reliable flow estimations are required to provide adequate water apportionments between parties, while avoiding water scarcity issues in downstream communities. Furthermore, the assessment of ecological low flow requirements for fish and benthic communities often depends on available flow records. As such, methods to aid in the estimation of flow records are warranted, especially at a time when climate change is being proven to exacerbate the severity of low flow extremes.

There has been extensive research regarding the general relationship between aquatic vegetation and flow resistance. However, a lack of standardization has resulted in different methods of data collection and results, thus preventing universal comparison and the achievement of conclusive results. Consequently, reliable methods of quantifying vegetative flow resistance have not been established. This thesis is aimed at obtaining a thorough understanding of the effects of vegetation on flow resistance and using this knowledge to provide reliable methods to estimate low flow rates at gauging stations during the macrophytes growing season. To achieve this, it was paramount that the methods developed were capable of assessing vegetative flow resistance reliably and consistently. This was done by thoroughly quantifying the parameters often found proportional to channel roughness, such as plants stiffness and density, while flow and water level conditions were continuously monitored.

A simple image processing technique was developed to map aquatic plants at the reach scale by analyzing aerial photogrammetry data, obtained using an Unmanned Aerial Vehicle (UAV). The data collection and processing methods presented are simple, reproducible, and allow for the high-resolution mapping of aquatic plants in a time-efficient manner. Results showed that the algorithm presented here consistently out-performed conventional manual post-processing techniques and in-stream surveys. Post-processed data

were also used to estimate how ground data resolution affects the accuracy of flow resistance formulae, which in turn was used to assess the sensitivity of discharge estimates on vegetation mapping.

A simple and cost-effective test, and associated testing apparatus, were developed to measure plants biomechanical properties (stiffness and density). Different than most methods found in literature, the test is not disruptive and can be undertaken on both submerged and emergent vegetation. It was first calibrated with artificial vegetation, of known biomechanical properties, and then tested on natural plants. Results showed that plants biomechanics evolve temporally following the growth and decay cycle of macrophytes. Therefore, these findings have useful implications for understanding seasonal changes in vegetative flow resistance which can impair rating curves during the low flow season.

To gain a thorough insight on how vegetation can affect stage-discharge relationships, a three-year investigation was undertaken at two separate reaches (~100 m in length) located on a Southern Ontario stream. Here, it was determined that using conventional rating curves, average daily discharge can be overestimated up to 100%. Published equations to determine flow resistance were not capable of correcting these estimates. Different to most published studies, flow resistance was not found proportional to the average spatial density of vegetation, rather it was correlated to the distribution of macrophytes in the most densely vegetated parts of the reach. By characterizing the spatial distribution of vegetation, it was then possible to successfully correct flow estimates at the study reaches for the period of record affected by macrophyte growth. The developed correction procedure was also validated on three additional streams, with successful results. Therefore, these findings can be applied to other gauged sites affected by aquatic plant growth to provide accurate low flow records.

Results from this thesis were obtained through a large dataset, both in terms of temporal and spatial resolution, and significantly expand previous findings regarding vegetative flow resistance. The methods presented herein can be readily applied to correct rating curves affected by vegetation growth in a time and cost-efficient manner. This can improve the estimation of environmental flows to aid in important water management decisions, such as water allocations for agricultural or potable water use. Further, more accurate aquatic habitat sustainability assessments can be achieved by using improved flow records. In turn, as these would reflect actual low flow conditions, they can be used to develop appropriate water taking targets that will not impact the environment negatively.

Acknowledgements

I would like to thank my advisor, Dr. Bill Annable, for taking a chance with me, first when I was a visiting student and later as a PhD student. I learned a lot from Bill's mentorship, not only within this project, and became a better scientist thanks to him. It was always stimulating to discuss scientific topics with Bill, thanks to his extensive knowledge and world-wide experience. His vision, advice and insight helped what was a simple conversation about gauging stations issues develop into this thesis.

Thanks to Terry Ridgway, the most resourceful person I'll likely ever meet. I started this project knowing one thing: that I didn't know the first thing about field work, but I could count on Terry being there for me to bother and ask questions to. I learned most things I know about field work and most importantly, I learned the joys of field work from him. He also protected me from dangerous hogweed plants on multiple occasions.

I must acknowledge the help I received from the members of the Eco-Hydraulics group, Ben, Cailey, Jeff, Chris, Logan, Jimmy, Brad and Luca. All of them helped me with field work, research questions, paper reviews and almost never made fun of my mis-pronunciations of the English idiom. I share a lot of fond memories with all of them and I consider myself lucky to call them my friends.

Thanks also to the multitude of agency people that I met during these years and helped me fulfill the goals of this project. Among them, surely Tom Arsenault deserves a special mention. Nonetheless, many Environment Canada and Maitland Valley Conservation personnel, provided instrumental advice and data over these years.

This project wouldn't have been possible without the funding secured by my advisor, Bill Annable and other sources such as NSERC, JTB Environmental Systems Inc., R&M construction and the University of Waterloo international graduate student scholarship. I would like to thank these people and institutions for providing crucial financial help.

Finally, I would like to thank my family (both "biological" and "extended") for their constant support in all these years and for leading by example every day.

Dedication

This thesis is dedicated to my wife Cailey, without whom I would not have made it this far.

Table of contents

List of Figures

List of Tables

List of Equations

List of Abbreviations

7Q20: 7-day, 20 year low flow

BDT: Board Drop Test

MVCA: Maitland Valley Conservation Authority

NCS*:* Normalized cross-sectional spacing

PPTW: Permit to take water

RTK-GPS: Real Time Kinematic GPS (Global Positioning System)

RMSD: Root mean square deviation

RMSE: Root mean square error

SBT: Settling Board Test

SD: Standard Deviation

SE: Standard Error

UAV: Unmanned Aerial Vehicle

WSC: Water Survey of Canada

VDC: Vegetation Distribution Curve

List of Symbols

A: Cross-sectional area (m^2)

A_i: Portion of reach occupied by vegetation (m^2)

A_T: Total area of reach (m^2)

A_R: Reference area (m^2)

B_A: Aerial cover (dimensionless)

b_X: Blockage factor at a single cross-section (dimensionless)

B_X: Reach-averaged blockage factor (dimensionless)

$B_{X,p}$: p-th percentile of b_X on a given vegetation distribution curve (dimensionless)

BH: Board height from board-drop test or settling board test (m)

CS_X: Spacing between two consecutive cross-sections (m)

d_i: Distance of a point from bank (m)

d_{max}: maximum flow depth (m)

D_j: Distance between $(j)^{th}$ and $(j+1)^{th}$ cross section (m)

E: Vegetation modulus of elasticity (N/m^2)

E_m: Error in the estimation of L_A using m cross-sections (%)

$E_{m,p}$: Error in the estimation of the p-th percentile of B_X using m cross-sections (%)

E_Q: Error in the estimation of Q due to vegetative flow resistance (%)

$E_{Q,S}$: Systematic error in the estimation of Q, unrelated to vegetation (%)

f: Darcy-Weisbach friction factor

h: length of a single vegetation stem (m)

I: second moment of inertia of plant stem (m^4)

k: vegetation bent height (m)

K: Normalized water level increase ($m^{3/2}s^{-1/2}$)

L_A: Reach-averaged blockage width (dimensionless)

l_A: blockage width at a single cross-section (dimensionless)

M: Vegetation spatial density (m^{-2})

n: Manning's n ($sm^{-1/3}$)

n_b: Manning's n component due to grain and bedform roughness ($sm^{-1/3}$)

n_v: Manning's n component due to vegetative resistance ($sm^{-1/3}$)

NCS: Normalized cross-sectional spacing (dimensionless)

Q: Discharge or flow rate (m^3/s)

R: Hydraulic radius (m)

R^2: coefficient of determination – correlation score (dimensionless)

Pix_D: Pixel density (m^{-2})

S: Reach slope (dimensionless)

S_W: Reach water surface slope (dimensionless)

S_F: Reach friction slope (dimensionless)

t: Time (hrs)

t_s: artificial plant stem thickness (m)

T_W: Cross-sectional top width (m)

u^*: shear velocity (m/s)

V: water velocity (m/s)

w_s: artificial plant stem width (m)

$WL(Q)$: Water level at flow rate Q under vegetative conditions

$WL_b(Q)$: Water level at flow rate Q under non-vegetative conditions

$\Delta WL(Q)$: Difference in Water level between a vegetative and non-vegetative condition under flow rate Q

y: local water depth (m)

“Quod potui feci, faciant meliora potentes.”

J. Boswell, An Account of Corsica (1768)

Chapter 1: Introduction

River discharge data is of crucial importance for multiple engineering and scientific applications. It is used to assess the severity of hazards or environmental conditions as well as to define policies and regulations for water use. Specific examples of these practices include: the estimation of flood elevations (Quick, 1991), the assessment of habitat conditions, (Bradford and Heinonen, 2007), water allocation decisions (Smakthin, 2001) and the evaluation of climate change impacts (Quilbe et al., 2008). In order for any of these analyses to achieve reliable results it is paramount that the discharge data used is accurate. In most of the world, it is common practice to estimate flow rates at gauging stations. Here, direct, continuous measurements of water level (or stage) are converted into discharge estimates using empirical relationships, commonly referred to as rating curves. These curves are generated by collecting discrete measurements of stage and discharge (Herschy, 1995) and are unique for each gauging station.

Unfortunately, several factors may cause errors in discharge-stage relationships, which lead to errors in flow estimates. These require rating curve adjustments (shifts) or even, in some instances, the interruption of data reporting to avoid publishing erroneous results. In Canada, these issues are commonly caused by the presence of beaver dams, ice jams, or vegetation growth (Pellettier, 1988; 1989; Hamilton and Moore, 2011). In the latter case, seasonal growth of instream vegetation can temporally increase channel resistance resulting in increased stage and thus overestimations of discharge (Gurnell and Midgley, 1994, Figure 1-1). This effect is well-known and can be annually anticipated (Gurnell and Midgley, 1994; Cassan et al., 2015). However, quantifying the impact that macrophytes have on discharge estimated at gauging stations is prone to difficulties, related to the temporal nature of this issue. In fact, as plants grow and decay, their effects on water levels change throughout the season, and are often different from year to year.

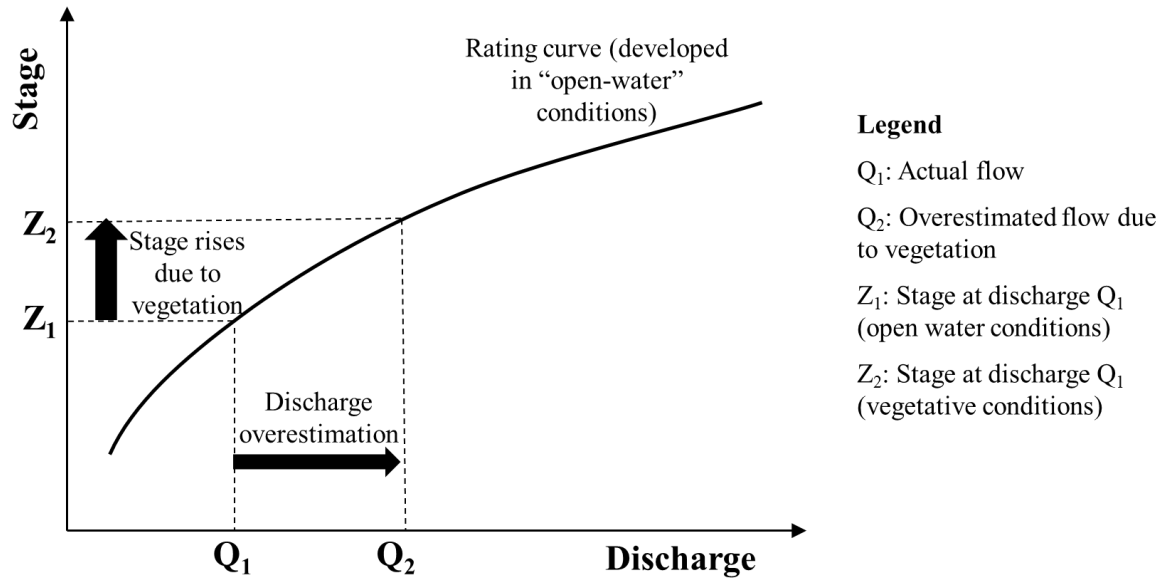

Figure 1-1: Conceptual representation of discharge estimation errors resulting from vegetation growth (Gurnell and Midgley, 1994; Hamilton and Moore, 2011).

Issues related to vegetative flow resistance have been investigated for almost a century. Most research divides plants interacting with streamflow into two categories: riparian plants, commonly associated with floodplain conveyance, and aquatic plants, which grow within the bankfull channel (Gurnell, 2014). Arguably previous research placed a larger focus on riparian vegetation to improve the accuracy of flood risk assessments (Darby and Thorne, 1996; Darby, 1999; Sellin and Van Beesten, 2004; Nikora et al., 2006). Nevertheless, historically, the first studies were undertaken in artificial canals, to quantify the conveyance potential of grass-channel linings for agricultural purposes (e.g. Ree 1939, 1941, 1949, 1958; Cox, 1942; Palmer, 1945, 1946; Kouwen et al., 1969, 1973; Temple, 1980). In later years, research transitioned to laboratory studies, using artificial plants first (Kouwen et al., 1969, 1973, 1980, 1981) and eventually natural vegetation to assess their effects on flow resistance (Jarvela, 2002, 2005; Sand-Jensen, 2003; Carollo et al., 2005; Bal et al., 2011). Most of these studies found flow resistance to be related with spatial density and flexural stiffness (Folkard, 2011; Nepf, 2012; Luhar and Nepf, 2013) and these findings affected both channel maintenance and design practices. For instance, plants were often removed from canals to enhance conveyance (Kouwen, 1970; Armitage et al. 1994), while procedures for the design of erosion-resistant grass-lined channels were created (Kouwen, 1992, United States Department of Agriculture, 2007).

In contrast to the large amount of laboratory-based research on flow-vegetation interaction, few studies have been undertaken in natural channels to estimate flow resistance at the reach-scale. Furthermore, some of the documented approaches are also disruptive (Bal and Meire, 2009; O'Hare et al., 2010), limiting the desired use of the methods. Similar to laboratory study findings, flow resistance was found

related to the spatial distribution of plants (Abdelsalam et al., 1992; Huntington and Whitehead, 1992; Green, 2005a; 2005b; 2006; Nikora et al., 2008; Bal and Meire, 2009; Old et al., 2014).

To date, none of the previous results has been applied to correct rating curves affected by vegetative flow resistance. The reason for this missing linkage between research results and their practical application relates to the variety of approaches used. This in turn led to a multitude of formulae and methods being proposed, to quantify both flow resistance and vegetation spatial distribution. These are based on results from the above-mentioned field studies (Green, 2005a; Nikora et al., 2008; Old et al., 2014), laboratory observations (Kouwen et al., 1980, 1981; Stone and Shen, 2002; Jarvela, 2004; Carollo et al., 2005) and also from analytical procedures (Petryk and Bosmaijan, 1975, Darby, 1999; Baptist et al., 2007). However, no method or equation is generally being preferred to others.

This lack of a unified approach has hindered the possibility of applying this knowledge consistently in a multitude of practical applications, including the correction of rating curves. In turn, this can lead to flows being incorrectly estimated at gauging stations which can have detrimental effects for water resources management. Further, as macrophyte growth often coincides with the occurrence of low flow periods, errors arising from vegetative flow resistance can significantly impact low-flow regulations and decisions. These include: drought prevention protocols, water allocations as well as aquatic habitat protection and rehabilitation (Smakthin, 2001). Consequently, use of incorrect low flow records may result in several negative effects for both the environment and communities relying on water (Rolls et al, 2012). For instance, design flows for fish passage are directly related to the knowledge of low flow indices (e.g. the Q_{95}, the 95^{th} percentile on a flow duration curve, or the 7Q20, the 7-day, 20-year low flow) which is in turn related to the accuracy of low flow estimations (Bradford and Heinonen, 2008; Bradford, 2008). Incorrect low flow records may also allow excessive surface water takings, which can trigger long-lasting changes on ecosystem dynamics (Scheffer and Carpenter 2003). Some of these variations can be particularly detrimental as they may lead to algal blooms (Biggs and Stokseth, 1996), or loss of species richness (Haxton and Findlay 2008; Rolls et al, 2012). Effects are not limited to aquatic species as avian fauna has been proven to be affected by artificially reduced low flows (Nebel et al., 2008). Furthermore, water allocation agreements between provinces or countries (for instance, the Master Agreement on Apportionment between Canadian Provinces and American States) rely on accurate knowledge of streamflow for agricultural and potable use. In these cases, incorrect flow ratings may cause disproportionate water divisions amongst different communities and yield drought conditions. These will not only exacerbate the aforementioned environmental consequences, but also affect the public directly. Finally, data obtained through hydrologic models, which may be used in any of the applications mentioned above, may also be affected as model calibration relies upon accurate

low flow data. As a result, methodologies to quantify aquatic vegetation and its impacts upon the estimation of low flow rates to allow for reliable flow records are warranted.

1.1 Objectives

The objectives of this research are to develop methods and quantify the effects of instream vegetation on flow resistance under low-flow conditions. Further, an overarching objective is, based upon the research conducted, to develop tools and techniques to aid water managers in more accurately estimating discharge rates at gauging stations. Specifically, this research addresses the following objectives:

1. To assess the capabilities of innovative techniques to determine vegetation spatial distribution at the reach scale,
2. To develop non-disruptive methods to assess plants density and stiffness,
3. To determine metrics able to quantify reach scale flow resistance caused by aquatic plants and the necessary resolution,
4. To employ the above objectives to efficiently correct flow rates incorrectly estimated due to vegetation growth at gauged sites.

This work directly contributes to topics that are relevant within water resources engineering such as stream gauging and estimation of flow resistance. Communication with Environment Canada staff have suggested that techniques arising from this thesis could constitute an improvement to their current practices. Discharge data released by the Water Survey of Canada, as well as other agencies, is invaluable to designers, researchers and regulators in the fields of water resources and river science. Specifically, the findings from this work can improve the accuracy of low flow data which, as discussed in the previous section, has important management applications. Improved low flow records are necessary to determine water apportionments that are fair to the stakeholders in need, while not causing damage to aquatic ecosystems. Further, accurate estimates of flow rates can help evaluate whether aquatic flora and fauna may be impacted negatively by surface water takings.

1.2 Thesis organization

This thesis is organized into three main chapters which were written in research article format in order to be submitted to scientific journals for publications. While the three chapters can be read

independently from each other, they all contribute to the same overall research objective, thus a certain degree of overlap in the background sections should be expected.

Chapter 2 mainly addresses objective one. Here an aerial photogrammetry method to inventory planometric in-channel vegetation was developed. Data from an unmanned aerial vehicle (UAV) was post-processed with mathematical methods to assess vegetation spatial distribution and then applied to field measured discharge rates and stage to offer a technique for rapid and reliable data acquisition of vegetation.

Chapter 3 addresses objective two. It focuses on the development of a tool to evaluate the biomechanical properties of instream vegetation which can be related to relative roughness used in the determination of channel velocities. The temporal changes on vegetative biomechanical properties are also evaluated to further assess how vegetative flow resistance varies temporally.

Chapter 4 directly addresses objectives three and four. An extensive 3-year investigation was aimed at quantifying vegetative flow resistance at the reach scale, to improve the accuracy of flow records, with a focus on low flows. To achieve the desired objectives, repeatable field protocols to sample vegetation spatial distribution were also created and implemented. This Chapter also builds on the results from the previous two sections. It uses similar methods and theory as Chapter 2 to inventory aquatic vegetation and assess their accuracy. Further, it assesses temporal changes in vegetation distribution, enhancing the findings of Chapter 3.

Chapter 5 provides an overall conclusion section to the thesis by combining the major findings from each of the three chapters and discussing their significance for engineering and water management practices in further detail.

Chapter 2: Assessing the accuracy of vegetative roughness estimates using unmanned aerial vehicles [UAVs]

Brignoli, L., W. K. Annable and B. D. Plumb (2018) Assessing the accuracy of vegetative roughness estimates using unmanned aerial vehicles [UAVs], *Ecological Engineering (118) Pages 73-83*

2.1 Introduction

Accurate measurement of stream discharge under low-flow conditions is of utmost importance to many water resources practitioners. Methods of estimating discharge commonly occur at gauging stations using rating curves which relate observed water stage (z) to field measured discharge (Q) in the general form $Q = f(z)$ (Herschy, 1995). Often in low-gradient environments, water stage is seasonally affected by in-stream vegetation which can confound the unique stage vs discharge relationship (Gurnell and Midgley, 1994). Seasonal coincidence between vegetative growth and low-flow conditions can often result in large overestimates of discharge to the extent that many reporting agencies identify accuracy caveats or discontinue data reporting entirely during these periods (Chapter 4).

Laboratory and field scale studies have shown that vegetation considerably increases resistance to flow (e.g. Green, 2005a; Kouwen et al., 1973; 1980; 1981; Nikora et al. 2008; Ree and Palmer, 1949). Consequently, under these conditions, stage may be a function of many parameters:

$$z = f(Q, S, T_W, B_A, B_X, M, EI)_{t=1,\dots d} \tag{2-1}$$

where S denotes the channel slope, T_W the flowing top width, B_X and B_A are the cross-sectional blockage factor (Green, 2005a) and surface area blockage factor (Green, 2005a), respectively, M denotes vegetation stem density, and EI denotes flexural rigidity. Equation (2-1) can be further confounded as all parameters can vary temporally (t) throughout the growing season until eventual dislodgement ($t = d$) and because the spatial heterogeneity in plant growth has been shown to affect flow resistance (e.g. Bal et al., 2011).

The principle objective is then to find the most predictive, repeatable and readily attainable parameters that can be quantified in the field to estimate low flow resistance and thus discharge. Both B_A and B_X have been used to estimate flow resistance (e.g Green, 2005a; Huntington and Whitehead, 1992; Nikora et al., 2008). B_X, or cross-sectional blockage factor (Green, 2005a) is defined as the sum of submerged areas occupied by vegetation for a given cross section divided by the total cross-sectional area. Aerial cover (B_A) is defined as the planform area covered by plants divided by the total channel planform area.

As the intent of this study was to use aerial imagery to map aquatic vegetation, B_A was chosen as the parameter of interest between the two with the definition:

$$B_A = \frac{\sum_{q=1}^{N} A_q}{A_T} \tag{2-2}$$

where A_q is the planform area of the q^{th} patch of vegetation (Figure 2-1a) contained within the study reach planform area (A_T).

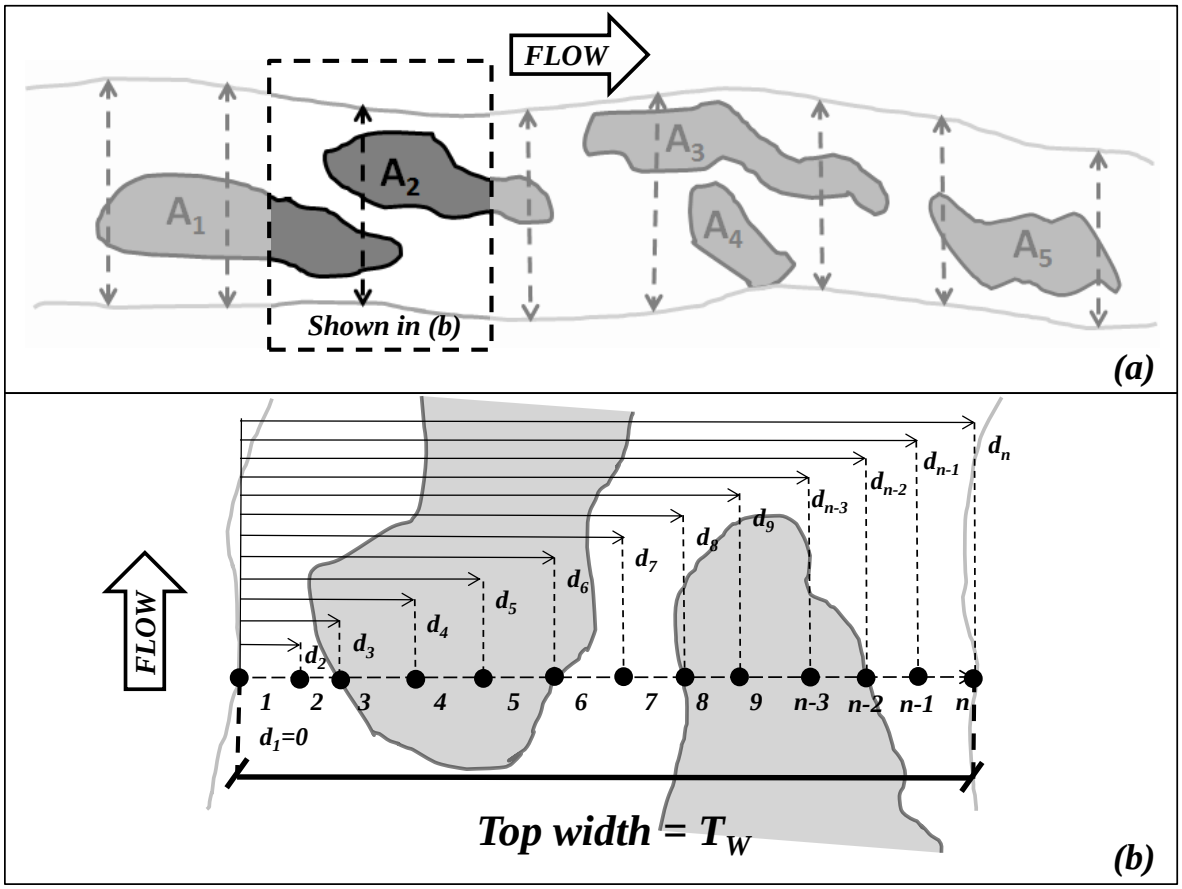

Figure 2-1: (a) Schematic representation of macrophyte cover (gray patches) in a vegetated channel for the calculation of B_A. The detailed frame (b) illustrates the field survey discretization used in the calculation of the blockage width at the cross-sectional scale $l_{A,j}$.

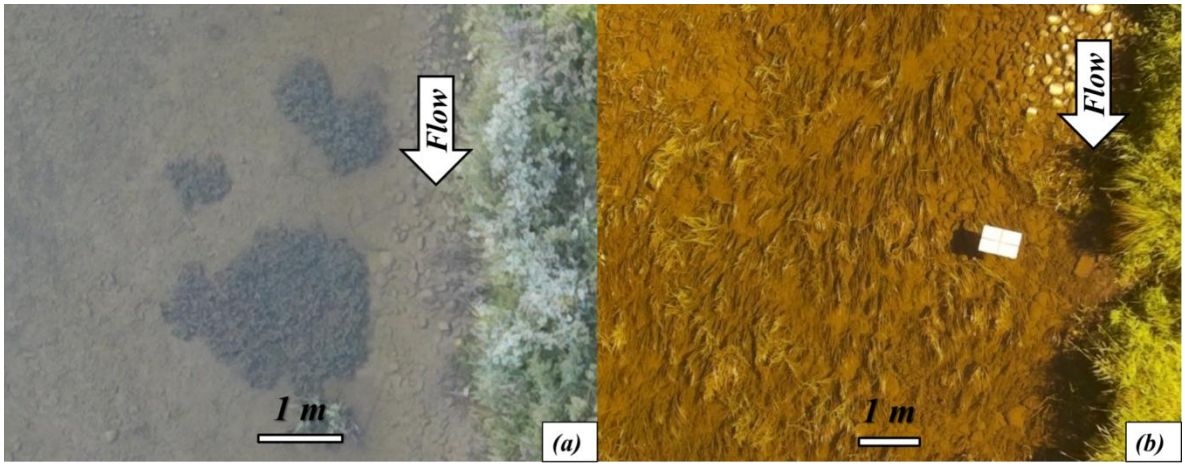

Figure 2-2: (a) *Potamogeton* plants (North Maitland River, Ontario, Canada) and (b) *Sparganium americanum* plants (Moorefield Creek, Ontario, Canada).

It is noteworthy that for proper calculation of B_A using Equation (2-2), clear boundaries to field identify each A_q (Figure 2-2a) must exist (e.g. Huntington and Whitehead, 1992; Sand-Jensen and Pedersen, 2008). In natural channels, where ill-defined plant boundaries exist (Figure 2-2b), defining each A_i patch, and thus the calculation of B_A becomes increasingly prone to error. Current techniques either estimate B_A qualitatively with visual techniques (e.g. Mean Trophic Rank by Holmes et al., 1999) or quantitatively using field survey methods at a series of cross-sections (e.g. Baatrup-Pedersen, 2002; Green, 2005a; Champion and Tanner, 2000; Nikora et al., 2008; O'Hare et al., 2010). Following the quantitative methods for the j^{th} cross-section, a blockage width $l_A(j)$ can be obtained in the form (cf. Green, 2005a):

$$l_A(j) = \frac{\sum_{i=2}^{n} \frac{1}{2}(d_i - d_{i-1})(F_i + F_{i-1})}{d_n} \qquad (2\text{-}3)$$

$$where \quad \begin{matrix} F_i = 0 \; if \; aquatic \; vegetation \; is \; not \; present \\ F_i = 1 \; if \; aquatic \; vegetation \; is \; present \end{matrix}$$

where i is the survey point of interest, d_i is the point distance from the bank and F_i is a binary function as defined in Equation (2-3). Spacing between points can either be constant or varied depending on the heterogeneity of plants or bathymetry. If patch edges are sampled, spacing in the vicinity should be kept small to avoid overestimating $l_A(j)$. The denominator in Equation (2-3) is equivalent to T_W (Figure 2-1b). The value of B_A is assumed equal to L_A (the weighted average of $l_A(j)$ values) which accounts for changes in width and distance amongst cross sections, as defined by:

$$B_A \approx L_A = \frac{1}{A_T}\sum_{j=1}^{m} T_{W,j} D_j l_A(j) = \frac{1}{A_T}\sum_{j=1}^{m} T_{W,j} D_j \left(\frac{\sum_{i=2}^{n} \frac{1}{2}(d_i - d_{i-1})(F_i + F_{i-1})}{d_n} \right)_j \quad (2\text{-}4)$$

to account for changes in channel shape and uneven spacing, L_A should be calculated as a weighted average using both D_j (distance between j^{th} and $[j+1]^{th}$ cross-sections) and $T_{W,j}$ as a weighting factor. This field method is potentially adaptable to any patch shape. However, Equation (2-4) assumes that L_A is equal to B_A, which is theoretically true when:

$$NCS = \frac{CS_X}{T_W} \rightarrow 0 \quad (2\text{-}5)$$

where *NCS* is the normalized cross section spacing and CS_X is the average distance between cross-sections (loosely based on Samuels, 1990). *NCS* calculated for previous studies ranged between 7.76 (Champion and Tanner, 2000) and 0.28[1] (Green, 2005a). Therefore, for Equation (2-4) to be valid, patch discretization must increase as vegetative anisotropy increases to achieve equivalent accuracy in the estimate of L_A. Axiomatically, this condition requires increased field efforts and resources with increasing instream vegetation anisotropy. To date, no study has demonstrated what cross section spacing is required to achieve consistent, repeatable results in L_A. Further roughness metrics, such as Manning's *n*, can be determined from L_A (e.g. Green, 2005a), however, it is unknown whether these equations were produced from data with sufficient resolution.

Employment of remote controlled unmanned aerial vehicles (UAVs) to inventory several metrics along watercourses has remarkably increased in the past decade (e.g. Markus and Fonstad, 2010; Shahbazi et al., 2014; Palmer et al., 2015). Although the vast majority of UAV applications are directed towards agricultural applications (Shahbazi e al., 2014), noteworthy studies by Detert and Weitbrecht (2015) and by Tamminga et al. (2015) have deployed UAVs to estimate river velocity profiles and to analyze geomorphic changes after large floods, respectively. Other studies have deployed UAVs to map: aquatic plants (Husson et al., 2014; 2016; Visser et al., 2016; Verschoren et al., 2017), invasive species growth (Göktoğan et al., 2010), biodiversity (Getzin et al., 2012), algal cover (Flynn and Chapra, 2014), and to classify riparian vegetation and canopy mortality (Dunford et al., 2009). Huntington and Whitehead (1992) is the only known published study that attempted to estimate B_A from aerial photographs acquired from a helicopter and a remote-controlled plane (predating recent UAV technological advancements) which produced unsatisfactory results due to lack of contrast and poor image resolution. UAVs may then be able to improve the planometric discretization of vegetative

[1] Note 1: *NCS*=0.28 was calculated for Green's data assuming greatest XS density for the greatest channel width (i.e. best case scenario – 9 cross sections for a 25 m reach that is approximately 10 m wide).

patches while removing field survey bias in the estimation of L_A. This may be especially true where strongly anisotropic instream vegetative conditions exist.

This paper presents an innovative, non-invasive approach to map the spatial extent of both submerged and emergent aquatic vegetation using UAVs. Two separate image processing techniques were tested, using GIS software and an algorithm combining edge detection (Sobel and Feldman, 1968), morphological dilation and image filtering (Serra, 1983). Five different tests were undertaken on three separate reaches. Results were then compared against detailed field measurements to validate the post processing methods and to assess the accuracy of Equation (2-4) in estimating B_A.

2.2 Materials and methods

2.2.1 Data collection

Aerial surveys were undertaken during the summers of 2015 and 2016 at three study reaches located in Southern Ontario, Canada. The reaches are seasonally affected by aquatic vegetation growth causing overestimates in discharge approaching twice the field measured discharge values (this issue is discussed in detail in Chapter 4). Both submerged and emergent aquatic plants were found.

Photogrammetry data were acquired using a 3D Robotics™ IRIS+ quadcopter equipped with an onboard GPS system (±2.5 m) and a 12 Megapixel visible light camera (Peau Productions™) fixed to the bottom of the quadcopter. The camera was also outfitted with a polarized lens to ensure greater visibility through water regardless of the light conditions which varied as flights were taken both in the morning and the afternoon. The UAV can be navigated by either remote control line-of-sight or autonomously via predefined way-points. In total, five different cases were evaluated, summarized in Table 2-1. One flight (Case 3, Table 2-1) resulted in a mostly shaded aerial photo as the flight was undertaken in the early morning.

Table 2-1: Summary of flights. *Notes: (a) Areas covered by riparian vegetation, or shaded, are excluded. (b) Calculated as Planform area/Reach length.

Case #	**1**	**2**	**3**	**4**	**5**
Sunlit/shaded	Sunlit	Sunlit	Shaded	Sunlit	Sunlit
Pixel density *(Pix_D)* (m^{-2})	26,776	1,469	9,266	17,148	13,101
Planform area[(a)] (m^2)	332	357	359	518	863
Reach length[(a)] (m)	49	53	69	81	135
Average width[(b)] (m)	6.8	6.7	5.2	6.4	6.4
Average depth (m)	0.27	0.26	0.22	0.26	0.30
Most common *macrophyte* species present on site	*Sparganium americanum Potamogeton*	*Sparganium americanum Potamogeton*	*Sparganium americanum*	*Sparganium americanum Elodea, Potamogeton*	*Nymphaea Potamogeton Nasturtium*

Ground-truthing surveys were undertaken by wading each reach and recording vegetation characteristics using a SOKKIA® RTK-GPS unit (±0.01 m in horizontal accuracy). At each surveyed position either presence or absence of vegetation was recorded. Spacing between points averaged 0.69 m with increased resolution where vegetation boundaries or changes in channel bathymetry were observed (Figure 2-1b).

Image stitching was achieved using the free software Microsoft® ICE. Then imagery was geo-rectified to ground control points surveyed prior to each flight with the same SOKKIA® RTK-GPS unit. To achieve geo-rectification, at least two ground control points (GCPs) must be present, although at least three are recommended (Paine and Kiser, 2003). Thus, for each flight, between 4 and 16 GCPs were positioned along the banks and within the channel (depending on overhanging vegetation coverage and other environmental factors). Geo-referencing of raster images was performed using ArcMap® by ESRI software. In order to reduce distortion, an affine transformation (first order polynomial) was chosen. This transformation only allows the aerial picture to be shifted, scaled or rotated, as specified in the software manual, and was found to yield the lowest residual errors.

Geo-referencing residual errors (computed as the root mean square error – *RMSE*) were calculated with ArcMap® and represent the average distance between the location of the control points in the geo-rectified raster (i.e. on the map) and their true location (measured by GPS). Resulting *RMSE*s ranged $0.02\ m \leq RMSE \leq 0.47\ m$ and were found to vary as a function of flight elevation and, consequently,

pixel density. *RSMEs* could have been reduced if more expensive equipment and software were used, as discussed in Section 2.2.1.1.

2.2.1.1 Limitations due to low-cost equipment

As many different photogrammetry equipment and software are available depending on available budgets, differences in the final image quality should be expected. For instance, using an RTK-GPS equipped UAV, a gimbal and state-of-the-art image stitching software will most likely yield a lower *RMSE* in the georeferenced image. Correspondingly, this would also result in increased project costs.

In this study, it was not possible to use a gimbal due to incompatibility with the camera used in this study; however, it is recommended that other researchers use one when possible. Here, UAV speed was kept to a minimum and flights were undertaken in minimal to no wind, to account for the lack of a gimbal. Furthermore, to compensate for the limitations of both the image stitching software and the UAVs onboard GPS accuracy, a higher density of GCPs was used.

2.2.2 Data analysis

Geo-corrected orthophotos were imported into ArcMap® with cases 1, 2, 4 and 5 having overhanging riparian vegetation and shaded areas visually identified and excluded from the picture before the image analysis took place (Figure 2-3). Conversely, in Case 3, sunlit areas were visually identified and excluded in ArcMap® and the shaded portions of the channel analyzed as these accounted for 88% of the planform area. Two different image analysis techniques were developed and evaluated in order to estimate vegetation cover: manual GIS post-processing and automated MATLAB® post-processing. In the former case, vegetation boundaries were visually identified and digitized as polygons in ArcMAP® (Figure 2-5b), similarly to the technique used by Husson et al. (2014) and Verschoren et al. (2017). This post-processing technique was developed to assess whether vegetation presence could be detected without the aid of expensive image-processing software.

Figure 2-3: Manual detection of shaded areas (bordered in black) and overhanging riparian vegetation (bordered with white dotted line) to be excluded before image analysis took place.

For the automated technique, an edge detection operator was developed in MATLAB® based on Sobel and Feldman (1968) to analyze aerial photogrammetry data. Edge detection is an image processing technique directed at identifying object boundaries by comparing adjacent pixels and evaluating user defined differences in image intensity (Marr and Hildreth, 1980). The edge detection operator was coupled with a morphological dilation operator to further isolate vegetation limits (Serra, 1983; The Mathworks, 2018). Post-processed images resulted in binary black and white images representing the non-vegetated and vegetated portions of the channel, respectively (Figure 2-5c). A flow-chart of this procedure is shown in Figure 2-4.

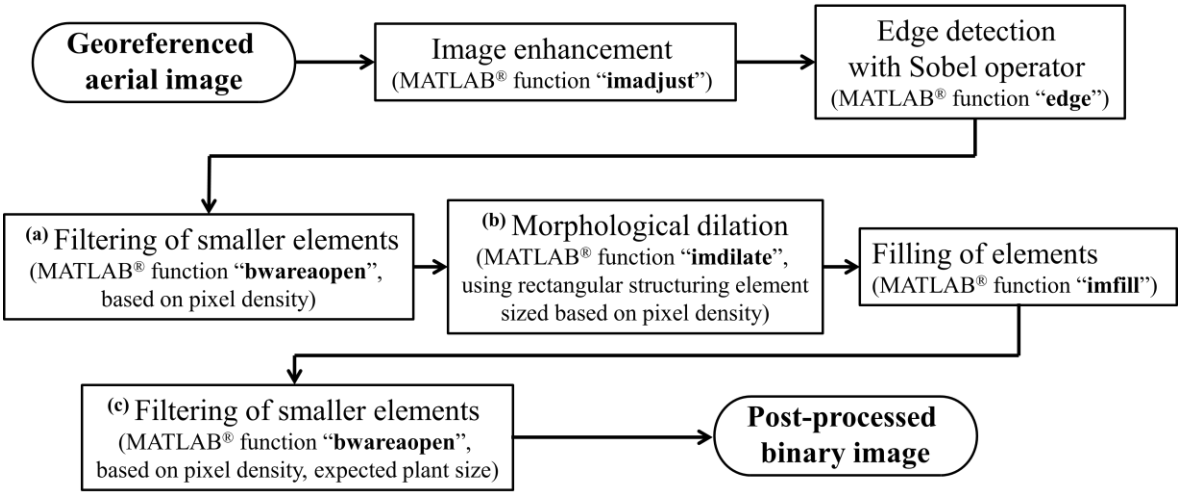

Inputs based on pixel density (Pix_D) expressed in pixels/m^{-2}		
(a) Filtered element size (in pixels) – 1st filter	**(b) Structuring element size (in pixels)**	**(c) Filtered element size (in pixels) – 2nd filter**
$\begin{cases} 0 & if\ Pix_D < 10{,}000 \\ 0.014e^{0.0468\sqrt{Pix_D}} & if\ Pix_D \geq 10{,}000 \end{cases}$	$S_E x\ S_E$ *where:* $S_E = 0.49 + 0.11\sqrt{Pix_D}$	Manually estimated smallest plant patch area on aerial image expressed in pixels

Figure 2-4: Flowchart summarizing the MATLAB® algorithm. Equations to calculate the inputs provided were empirically derived. The "smallest plant patch area" was manually determined in ArcMAP®, its value ranged between 12 and 27 cm^2.

Accuracy of the post-processing methodology was evaluated by comparing results with those obtained from ground-truthing as calculated from each surveyed cross-section. To account for errors associated with geo-rectifying or systematic ground surveying instrument errors, blockage width of the post-processed image, $l_A(j)_{,calc}$, at each cross-section was calculated over a specific reference area (A_R). A_R equalled the product of the distance between the two farthest points in a given cross-section by the largest value between the GPS-RTK horizontal accuracy (±0.01 m) and the *RMSE* (gray area in Figure 2-5a). This was done as part of the cross-section may have shortened due to the exclusion of shaded areas or those covered by overhanging vegetation. For the manual technique, $l_A(j)_{,calc}$ was evaluated in AutoCAD® whereas for the automated technique, $l_A(j)_{,calc}$ was calculated in MATLAB® as the ratio between white pixels (vegetated) and A_R. Field measured values of $l_A(j)_{,meas}$ were calculated using Equation (2-3), on the surveyed points comprised within A_R.

Values of $l_A(j)_{meas}$ and $l_A(j)_{calc}$ were compared following the procedure suggested by Piñeiro et al. (2008) by plotting $l_A(j)_{,meas}$ versus $l_A(j)_{\ calc}$ and testing their 1:1 significance for slope and intercept at the 95% confidence interval. Thus, B_A for each reach could be calculated with the post-processed data using Equation (2-2). Following Piñeiro et al. (2008), the root mean square deviation (*RMSD*) was also determined at each cross-section which measures the average difference between observed and

measured values of $l_A(j)$. These values were compared to the standard deviation (*SD*) of $l_A(j)_{meas}$ which represents the natural variations in l_A values. In reference, a homogeneous aquatic vegetation distribution would produce a low *SD* and thus small deviations between calculated and observed values whereas *SD* values would increase with increasing vegetation heterogeneity or anisotropic conditions.

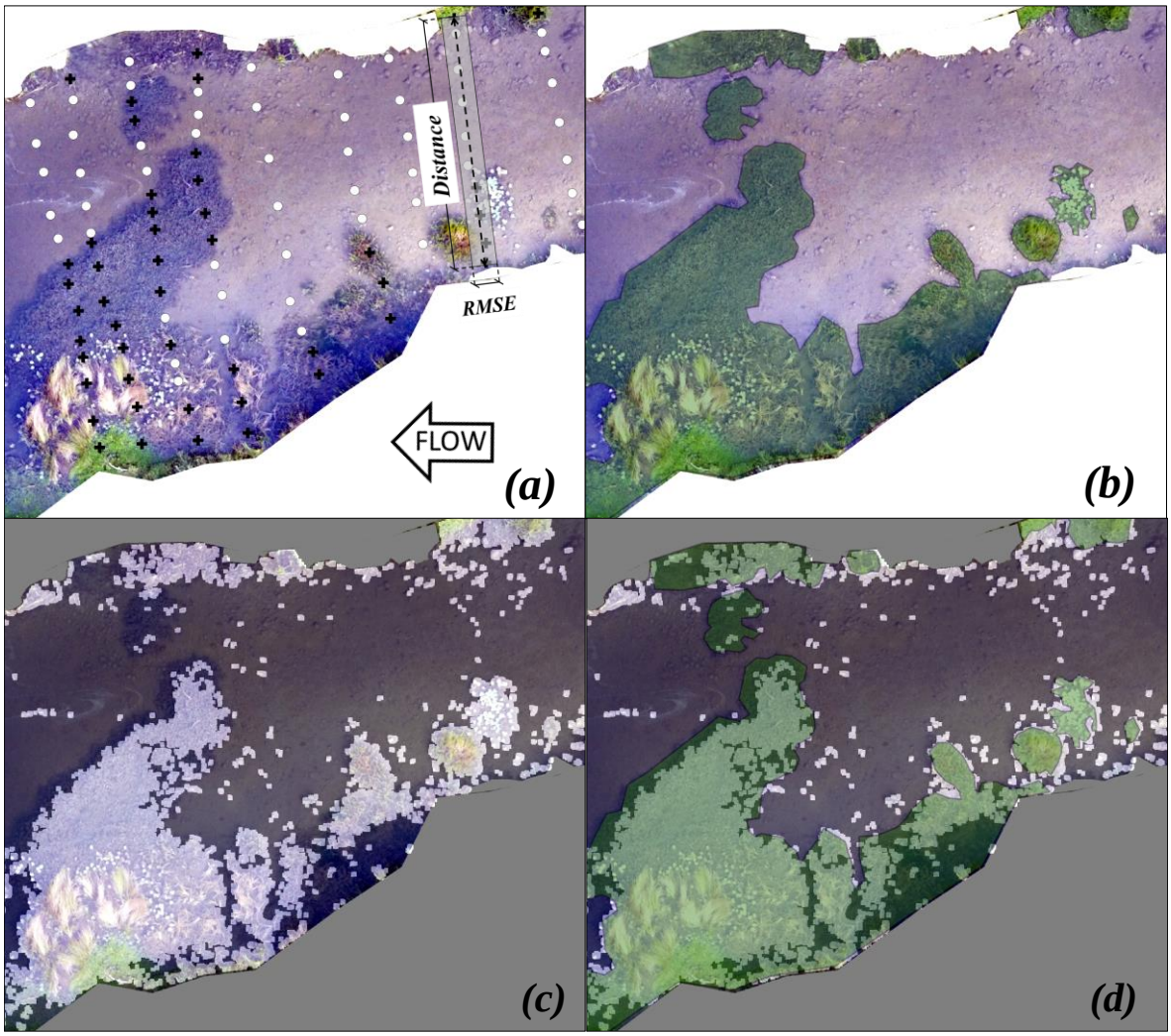

Figure 2-5: (a) Original airborne image (Case 5) with field survey data superimposed (crosses represent vegetated points, dots non vegetated points); Area over which l_A is evaluated, A_R is shown, (*RMSE* is exaggerated for visual purposes) (b) manually post-processed picture, green areas represent vegetated areas (c) resulting binary image after processing with edge detection technique superimposed on the original picture (black pixels are made 50% transparent to allow superimposition) (d) resulting images from both techniques superimposed on the original picture.

2.2.3 Estimating the sensitivity of Q from L_A data resolution

To understand the importance of how data resolution (i.e., *NCS*) affects discharge estimates, a sensitivity analysis of a published formula (Green, 2005a) was undertaken and presented in Section 2.3.2.

In order to estimate how *NCS* affects the error between L_A and B_A, the error between $(L_A)_m$, the blockage width calculated with Equation (2-4) using a sub-set of *m* cross-sections and B_A, was calculated in terms of the number of cross-sections (which is proportional to *NCS*) as:

$$E_m = 100 \left| \frac{(L_A)_m - B_A}{B_A} \right| \tag{2-6}$$

This was only calculated for data where an accurate estimation of B_A could be obtained from aerial image post-processing. For the purposes of this analysis, B_A was assessed over an area bound by the cross-sections that were surveyed in the field, which closely resembled to the planform area. To assess how *Q* estimates are affected by L_A accuracy, Manning's *n* was calculated using published data and an equation provided by Green (2005a, Figure 4c), which was re-arranged as follows:

$$n = n_b + n_v = n_b + (0.0035(100L_A) - 0.0857) \tag{2-7}$$

where n_v is the roughness due to vegetation and n_b accounts for all remaining roughness (bed and form), which was determined using the procedure outlined by Green (2005a). As this requires characterizing grain sizes, the pebble count technique offered by Wolman (1954) was used to sample the bed material[2]. More details of this procedure are available in Task Force for friction in open channels (1963).

Using Equation (2-7), discharge can be estimated using Manning's formula (e.g. Chow, 1959) in the form:

$$Q = \frac{\theta A R^{2/3} \sqrt{S_F}}{n} = \frac{\theta A R^{2/3} \sqrt{S_F}}{n_b + 0.35L_A - 0.0857} \tag{2-8}$$

where, given a representative cross-section for the channel reach, *A* is its wetted cross-sectional area, and *R* is its hydraulic radius, S_F is the reach friction slope and θ is a constant ($\theta = 1$ or $\theta = 1.49$ for SI and imperial units, respectively). Then, errors in estimated *Q* resulting from discrepancies between B_A and L_A, can be quantified by calculating:

$$E_Q = 100 \left| \frac{(Q)_{B_A} - (Q)_{L_A}}{(Q)_{L_A}} \right| = 100 \left| \frac{(n)_{L_A} - (n)_{B_A}}{(n)_{L_A}} \right| \tag{2-9}$$

where $n(B_A)$ and $n(L_A)$ are values of *n* calculated with Equation (2-7) using B_A and L_A respectively. Similarly, $Q(B_A)$ and $Q(L_A)$ are discharge values calculated with Equation (2-8) using B_A and L_A respectively.

[2] Grain size distribution in Case 5 was assumed to be comparable to Cases 1 – 4 due to geomorphological similarities between the reaches, determined from field observations.

2.3 Results and discussion

2.3.1 Comparison between the two techniques

The manual technique was only able to successfully predict field-measured l_A values for Case 2. Amongst the five cases, R^2 between measured and calculated data ranged $0.62 < R^2 < 0.88$. In all other cases, either the slope or the intercept of the best fit line $l_A(j)_{meas}$ vs. $l_A(j)_{,calc}$ were found to significantly deviate from 1 and 0 respectively (Table 2-2) which indicates a significant difference with the 1:1 line at the 95% level. This also signifies systematic over or underestimations occurred using this method. The former is evident in Case 4 (especially for $l_A > 0.6$) while the latter occurred most notably for Cases 1 and 3 (Figure 2-6).

Edge detection of vegetated patches performed well in Cases 1, 4 and 5, where pixel resolutions were more than 13,000 pixels/m^2. In each case, both the slopes and intercept of the best fit line were not significantly different than 1 and 0, respectively with $0.54<R^2<0.82$ (Table 2-3). Moreover in each of these cases, the RMSD values remained lower than the standard deviation of $l_A(j)_{,meas}$. The automated technique did not perform well in Cases 2 and 3, where pixel densities were less than 13,000 m^{-2} (largely resulting from higher flight elevations). For Case 2, which had the lowest pixel density, vegetation cover was strongly underestimated (Figure 2-6). Moreover, the poor result in Case 3 was likely exacerbated by shading conditions where pixel contrast between vegetative patches decreased limiting the effectiveness of both visual and automated methods in vegetation patch edge detection.

Detection of aquatic vegetation at the individual pixel scale was relatively similar between the two techniques. Between 67% and 85% of pixels were identified with the same outcome both by manual and automated post-processing (Table 2-4**).** These results are in good agreement with those obtained at the cross-sectional scale (Figure 2-7). For example, in Case 2, disagreement between manual and automated techniques was largely caused by pixels estimated as "not vegetated" rather than "vegetated" by the former method (Table 2-4). This is then reflected by a systematic underestimation of $l_A(j)$ by the automated technique (Figure 2-6). The opposite outcome occurs in Case 4 where pixels are identified as "vegetated" for the manual method with the opposite classification occurring for the automated method (Table 2-4) and thus the systematic overestimation of $l_A(j)$ (Figure 2-6). When both techniques underestimated $l_A(j)$, such as in Case 3 (Figure 2-6), a large number of pixels were estimated to be non-vegetated using both methods (Table 2-4).

Table 2-2: Results of the comparison $l_A(j)_{,meas}$ vs. $l_A(j)_{,calc}$ for the manual technique; p-values not significantly different than 1 and 0 for slope and intercept are marked with an asterisk. Values of *RMSD* below the Standard deviation of $l_A(j)_{,meas}$ are marked with an asterisk.

	Regression results		Significance of test (p-value)		R^2	RMSD
	Slope	Intercept	Slope	Intercept		
Case 1	0.717	0.221	0.004	0.003	0.652	0.167*
Case 2	0.840*	0.095*	0.150	0.267	0.622	0.171*
Case 3	0.720	0.240	0.045	4.36E-05	0.624	0.208
Case 4	0.787	0.048*	8.47E-05	0.198	0.892	0.161*
Case 5	0.961*	0.032	0.520	0.038	0.854	0.080*

Table 2-3: Results of the comparison $l_A(j)_{,meas}$ vs. $l_A(j)_{,calc}$ for the automated technique; p-values not significantly different than 1 and 0 for slope and intercept are marked with an asterisk. Values of *RMSD* below the Standard deviation of $l_A(j)_{,meas}$ are marked with an asterisk

	Regression results		Significance of test (p-value)		R^2	RMSD
	Slope	Intercept	Slope	Intercept		
Case 1	0.921*	-0.003*	0.569	0.981	0.577	0.175*
Case 2	0.394	0.475	2.63E-05	1.81E-06	0.214	0.328
Case 3	0.573*	0.2903	0.093	0.001	0.228	0.249
Case 4	0.938*	0.073*	0.478	0.180	0.782	0.149*
Case 5	0.977*	-0.003*	0.799	0.901	0.732	0.102*

Table 2-4: Comparison between the manual and automated techniques at the pixel scale

	Percentage of pixels computed as:				**Pixels evaluated the same by both techniques**
	Vegetated by both techniques	*Not vegetated by both techniques*	*Not vegetated by manual, vegetated by automated*	*Not vegetated by automated, vegetated by manual*	
Case 1	64%	11%	15%	11%	75%
Case 2	50%	17%	12%	21%	67%
Case 3	11%	73%	11%	4%	85%
Case 4	53%	20%	8%	19%	73%
Case 5	14%	69%	11%	6%	83%

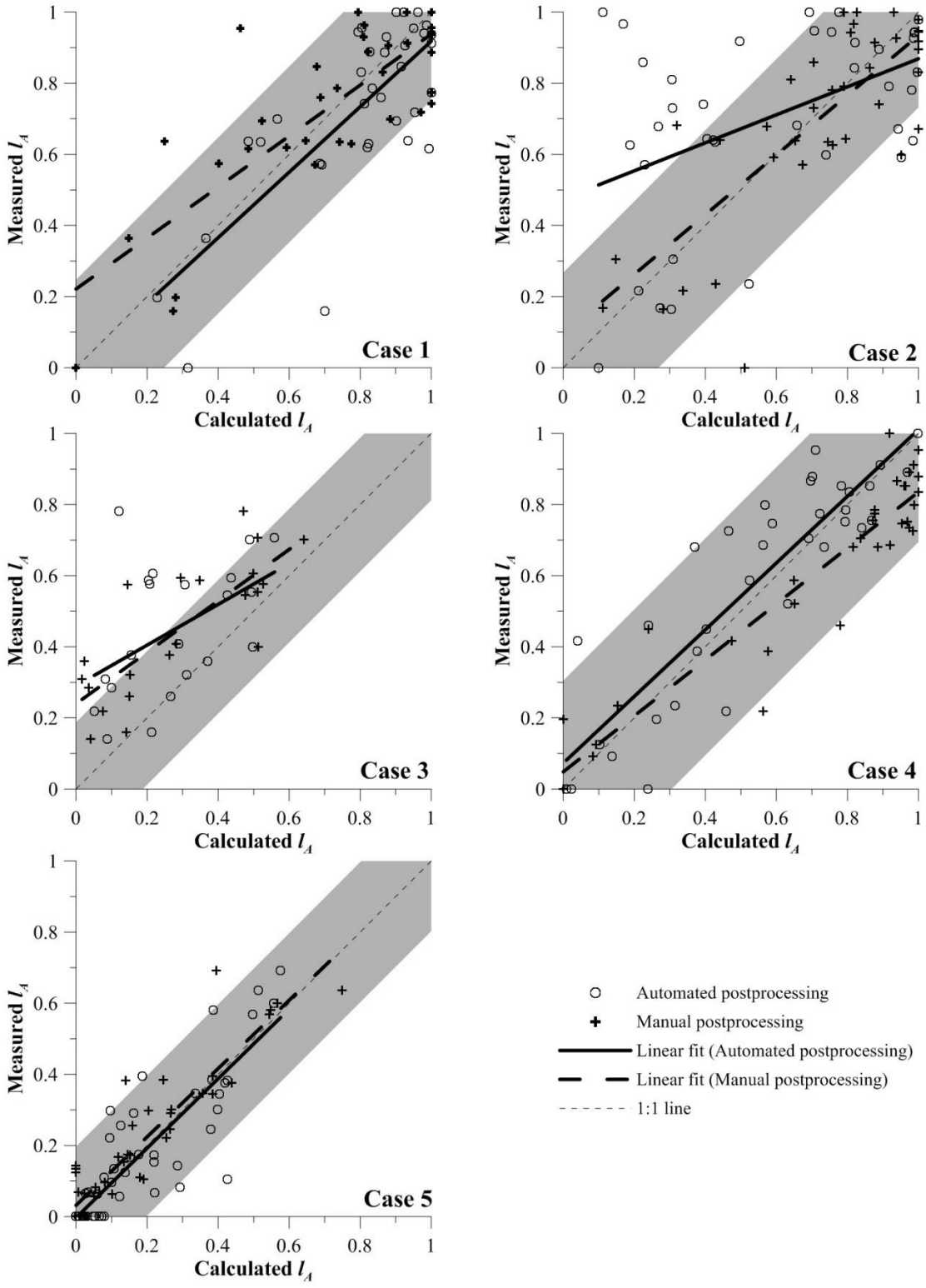

Figure 2-6: Plots of $l_A(j)_{,\,meas}$ vs. $l_A(j)_{\,calc}$ for both techniques for Cases 1 through 5. Shading represents ±1 Standard Deviation of $l_A(j)_{,\,meas}$

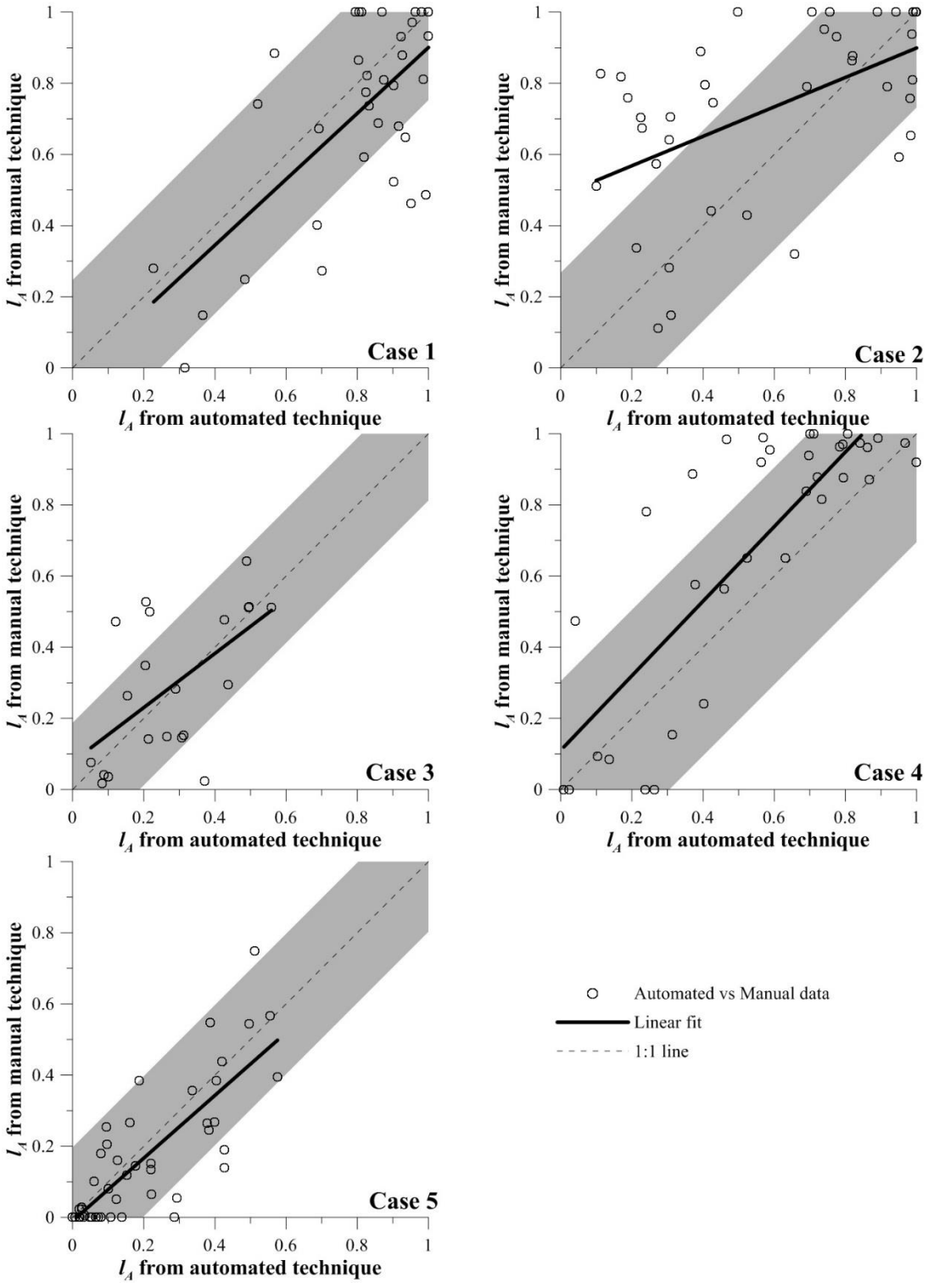

Figure 2-7: Plots of $l_A(j)_{,calc}$ (automated) vs. $l_A(j)_{,calc}$ (manual) comparing the agreement between techniques for Cases 1 through 5. Shading represents ±1 Standard Deviation of $l_A(j)_{,meas}$

For the cases where calculated and measured $l_A(j)$ values were in strong agreement (Case 2 for the manual technique, Cases 1, 4 and 5 for the automated technique), values of L_A and B_A were found to be approximately equal, with a maximum difference between B_A and L_A values of 0.037 (Table 2-4).

These results support the equivalency assumption in Equation (2-4) that reasonably accurate estimates of B_A can be obtained from estimates of L_A. However, this observation does not quantify at what level of resolution the condition when $B_A = L_A$ is achieved or to what extent differences in B_A and L_A may affect Q estimates. To evaluate this, values of B_A determined from Cases 1, 4 and 5 were compared against calculated values of L_A on the automated post-processed images. Resulting errors (E_m) were determined using Equation (2-6) for decreasing *NCS*, thus resolution was gradually increased to reproduce the convergence condition expressed in Equation (2-5).

Table 2-5: Comparison between L_A computed using ground data and B_A computed with Equation (2-2) using post-processed data. Values of B_A obtained from post-processed data not significantly different from ground data (Table 2-2 and Table 2-3) are marked with an asterisk.

	B_A (Manual)	B_A (Automated)	L_A (ground data)
Case 1	0.743	0.785*	0.748
Case 2	0.707*	0.622	0.721
Case 3	0.155	0.223	0.430
Case 4	0.723	0.610*	0.627
Case 5	0.198	0.245*	0.216

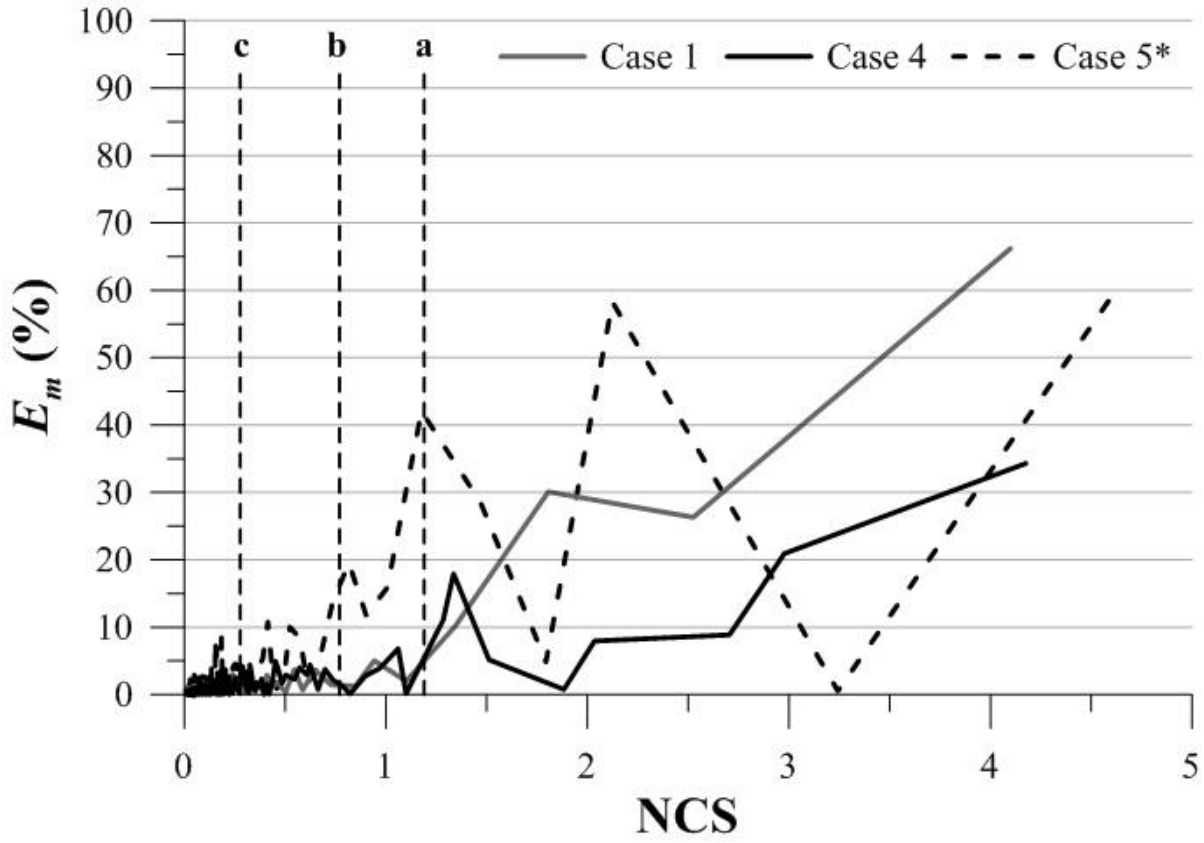

Figure 2-8: Absolute error in reach-averaged blockage width (L_A) with decreasing Normalized cross-sectional spacing *NCS* with respect to B_A. Vertical dash lines represent data resolution from (a) Nikora et al. (2008) (b) Baatrup-Pedersen (2002) and (c) Green (2005a, best case scenario). *Note: only data from cases in which $l_A(j)_{,meas}$ and $l_A(j)_{,calc}$ were not significantly different were used (Table 2-3). Case 5 was shortened to achieve a total channel length comparable to Cases 1 and 4.

Based on this study's results, L_A estimates B_A within ±5% error when $NCS < 0.15$ (Figure 2-8). Using the cross-section resolution in studies by Baatrup-Pedersen (2002) and Green (2005a) where *NCS* ranged between $0.15 < NCS < 1$, the B_A estimates from this study produced errors less than ±20%. In cases where $NCS > 1$ the B_A estimates from this study produced errors that were often over ±20%.

It is noted that a high *NCS* value (i.e. coarse cross-section spacing) may yield an accurate estimate of L_A which would be especially true for the case of a grass-lined artificial canal with homogenous vegetation cover. However, this condition is unlikely to consistently occur in natural channels with heterogeneous or anisotropic vegetation. For instance, E_m for Case 5 shown in Figure 2-8 decreases at $NCS \approx 3.2$ and then quickly rises again, indicating that the combination of data used for $NCS \approx 3.2$ yielded L_A close to the real value fortuitously.

2.3.2 *Impact of inaccurate L_A assessments on flow parameters*

In this section, the sensitivity of Q in relation to the accuracy of B_A is assessed, following the procedure outlined in Section 2.2.2. Errors in discharge estimates arising from using L_A instead of B_A (Table 2-5) were quantified using Equation (2-9) and illustrated in Table 2-6.

Table 2-6: values of Manning's n obtained with Equation (2-7) using B_A and L_A (Table 2-5) and resulting E_Q computed with Equation (2-9)

	n_b	Using B_A			Using L_A			E_Q
		n_v	n	Q	n_v	n	Q	
Case 1	0.062	0.189	0.251	0.063	0.176	0.238	0.066	5%
Case 4	0.06	0.128	0.188	0.064	0.134	0.194	0.062	3%
Case 5	0.061	5E-05	0.061	0.263	-0.01	0.051	0.315	20%

Discrepancies between B_A and L_A resulted in differences in estimated discharge, especially in in Case 5. However, this is not because of large differences between B_A and L_A (0.03, Table 2-5) rather it is a consequence of a limitation of Green's equation (2005) which yields an implausible negative value of n_v (i.e. plants cause a decrease in flow resistance) for B_A<0.24.

Using L_A values obtained as a function of cross-sectional spacing (Equation (2-6)), it can be determined at what resolution L_A should be determined to achieve E_Q < 5%.

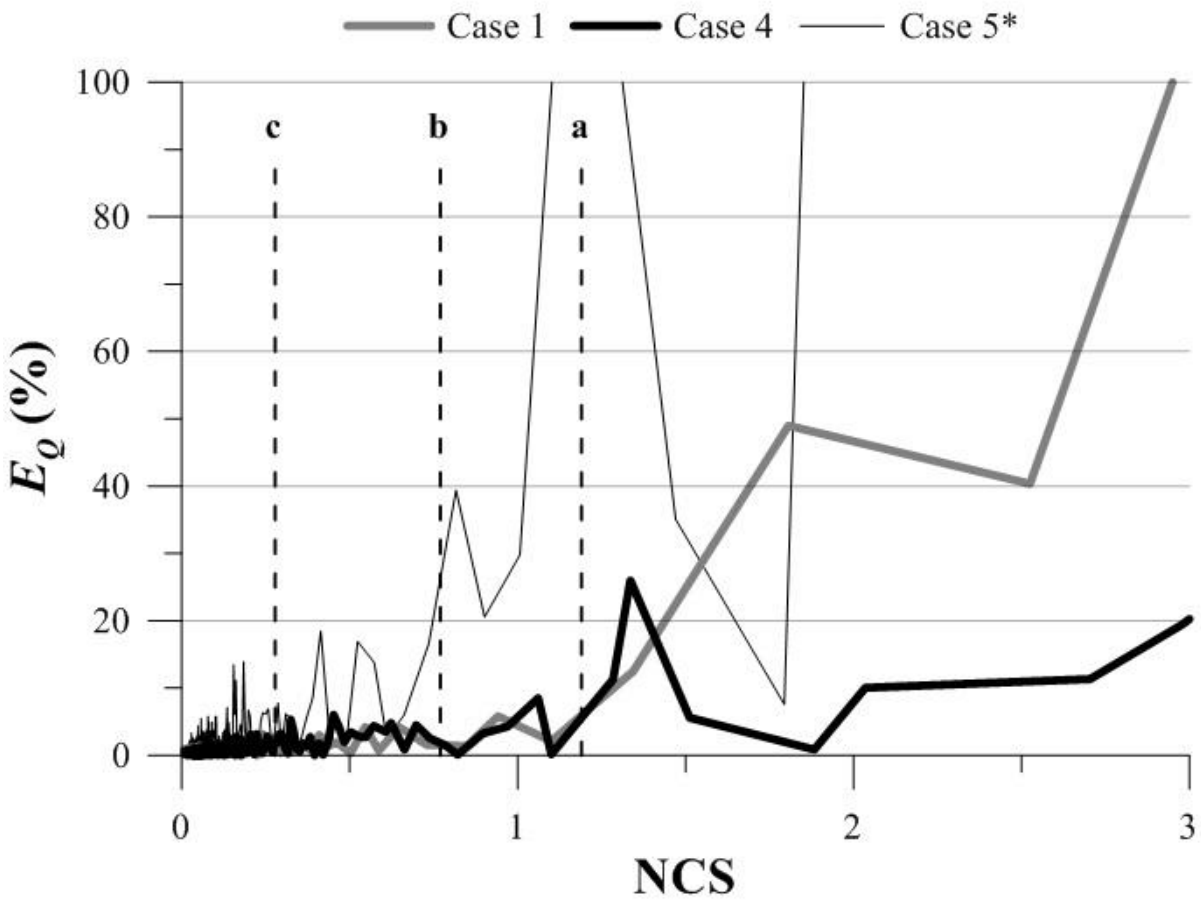

Figure 2-9: Absolute error in *Q* estimates with decreasing Normalized cross-sectional spacing, *NCS*. Vertical dash lines represent data resolution from (a) Nikora et al. (2008) (b) Baatrup-Pedersen (2002) and (c) Green (2005a, best case scenario). Note: only data from cases in which $l_A(j)_{,meas}$ and $l_A(j)_{,calc}$ were not significantly different were used (Table 2-3). Case 5 was shortened to achieve a total channel length comparable to Cases 1 and 4.

From this study, for conditions where channels are affected by seasonal vegetation, the spatial resolution of cross-sections (*NCS*) required to accurately estimate L_A (and thus discharge) should remain $NCS \leq 0.15$ to maintain a discrepancy between *Q* estimated with B_A and L_A below 5% for Case 5. In cases 1 and 4, where values of B_A are notably greater, this condition is achieved at *NCS*~1.

Here we estimate using Case 5 (which required approximately 4.5 hours of field survey time to achieve *NCS = 0.32)* that approximately 9 hours of field survey time would be required to achieve $NCS \approx 0.15$ and a corresponding discharge estimate error of ±5% with Equation (2-8). Conversely, acquisition of aerial photogrammetry data with the UAV (including setup) took less than 45 minutes.

Insufficient spatial and temporal resolution has been one of the main reasons why quantification of flow resistance in vegetated channels remains a significant field challenge (Nepf, 2012). Using techniques highlighted in this study, vegetation cover can be quantified, while significantly improving data collection time efficiency. Thus, the techniques presented here can be used to calculate flow resistance parameters with relationships relating L_A or B_A to Manning's n such as those proposed by Huntington and Whitehead (1992), Green (2005a) amongst other approaches. Moreover, scale and spatial distribution of plants have been shown to affect flow resistance (Nepf, 2012) by laboratory studies (Bal et al., 2011) and theoretical analyses (Luhar and Nepf, 2013). By capturing the spatial heterogeneity of instream vegetative patches using the non-invasive methods presented here, flow resistance caused by aquatic plants can be assessed with significant improvement in resolution and therefore result in more accurate estimates of flow rates.

2.4 Conclusions

The planometric spatial distribution of aquatic vegetation has been successfully quantified by analyzing aerial photogrammetry data acquired using a UAV. Automated methods of vegetation patch detection developed here outperformed manual digitization methods when compared to ground-truthing measurements. The automated methods worked well for sunlit reaches and for conditions when image resolution exceeded 13,000 pixels/m^2. Accuracy in identifying the limits of vegetated patches notably decreased if the two above conditions were not met. For low image resolution, manual detection worked well, although it is unknown how operator biases may affect these results as noted by Verschoren et al. (2017).

Data from this study also showed that macrophyte aerial cover, B_A, can be estimated along pre-determined cross-sections only if sufficient discretization is achieved such that $L_A \approx B_A$ can be assumed. In this study, $NCS < 0.15$ is required to achieve discharge estimates calculated from either L_A or B_A within a ±5% error.

Finally, airborne methods presented here were demonstrated to be an efficient method of acquiring the spatial distributions of instream vegetation non-disruptively. This was achieved in a significantly shorter time span (minutes) than previous field instream survey methods (hours). The field and software post-processing methods presented here can easily be employed by technical field staff and to adjust discharge estimates.

Chapter 3: A non-destructive method to estimate the biomechanical properties of aquatic vegetation in-situ

Brignoli, L., W. K. Annable and T. P. Ridgway (*in review*) A non-destructive method to estimate the biomechanical properties of aquatic vegetation in-situ. *Journal of Ecohydraulics*

3.1 Introduction

Careful and temporally representative estimates of flow resistance imparted by vegetation can have significant effects upon the accuracy of estimating flood elevations and environmental low-flows (e.g. Gurnell and Midgley, 1994; Neary, 2003). Estimating these roughness factors is complicated by the inherent heterogeneity in vegetation arising from species richness and caliper (Nepf, 2012; Miler et al., 2012; 2014). Unlike grain-form roughness (e.g. Millar, 1999) which remains relatively constant between stream-bed mobilizing events (Langbein and Leopold 1964), estimating vegetation roughness is further confounded by its temporal nature arising from seasonal and inter-annual growth (Gurnell and Midgley, 1994; Gurnell, 2014).

Laboratory and field scale studies over several decades have shown that vegetative resistance is related to the spatial distribution of plants and their biomechanical properties, with the former being more commonly measured (Kouwen et al. 1973, 1981; Carollo et al. 2005; Luhar and Nepf 2011, 2013). Accurate estimates of biomechanical properties commonly require large in-situ field sample sizes or harvesting of plant communities for subsequent testing and analysis (e.g. Sheldon and Boylen, 1978; Rodusky et al., 2005; Kenow et al., 2007; Johnson and Newman, 2011; Yin and Kreiling. 2011). Vegetation harvesting, however, is time-consuming, expensive, and can be detrimental to the environment as it may affect fauna that utilize plant communities for food and cover (Chubb and Liston, 1986; Dibble et al., 1996).

Relatively rapid non-disruptive techniques currently exist to measure the biomechanical properties of riparian vegetation which are infrequently inundated (e.g. Eastgate, 1966; Kouwen, 1988), however, none currently exist to measure similar properties of submerged and emergent instream vegetation. Such measurements are important in relating the biomechanical properties to flow resistance when considering environmental low flows, particularly where continuous discharge estimates are reliant upon rating curves.

Here, we present a new tool designed to estimate the in-situ biomechanical properties of aquatic vegetation in a non-destructive fashion. The method is easily deployed and inexpensive whilst leaving plant communities largely intact. The apparatus is an adaptation of the Board Drop Test (BDT) originally developed by Eastgate (1966) and re-adapted by Kouwen (1988). The current apparatus and technique was initially developed employing artificial vegetation with known biomechanical properties for calibration purposes and then deployed along field reaches with differing aquatic species for validation purposes. Temporal variations in biomechanics properties were also quantified through repeated field testing at each site over the growing season.

3.2 Background

Flow resistance arising from in-stream vegetation is commonly assumed to be a function of its spatial distribution (Huntington and Whitehead, 1992; Green, 2005a; Nikora et al., 2008). The cross-sectional blockage factor (b_X) quantifies the portion of the j-th channel cross sectional area (A) obstructed by vegetation (A_v) using the expression (Green, 2005a):

$$b_X(j) = \left(\frac{A_V}{A}\right)_j \tag{3-1}$$

as illustrated in Figure 3-1. Since b_X commonly varies spatially, a reach-based estimate of the blockage factor (B_X) over a reach length L can also be estimated as (Green, 2005a; Nikora et al., 2008):

$$B_X = \frac{1}{L}\sum_{j=1}^{m} D_j b_X(j) \tag{3-2}$$

where D_j is the spacing between consecutive cross-sections, which is employed as a weighting factor.

While field measurements yielding values of B_X are relatively commonplace and easy to obtain in determining flow resistance estimates, other studies have found plant stiffness to be a significant contributing factor. Ree (1939, 1958), Cox (1942) and Palmer (1945, 1946), for example, found that greener and stronger species yielded higher roughness coefficients than dormant or weaker ones. Kouwen et al. (1969, 1973, 1980 and 1981) through a series of laboratory experiments demonstrated how flow resistance in vegetated channels is related to both the spatial distribution and flexural stiffness of plant species through the following expression (re-adapted from Carollo et al., 2005):

$$\frac{V}{u_*} = a + b\ log\left(\frac{k}{y}\right) \tag{3-3}$$

where V is the average flow velocity, u^* is the shear velocity and a and b are constants dependent upon plant stiffness and density. Relative roughness (k/y) is the ratio between roughness height (k) and flow

depth (y) where the former is the plant height after being bent by flow (Figure 3-1b). Kouwen and Unny (1973) found k/y to be a function of both plant community density and flexural rigidity.

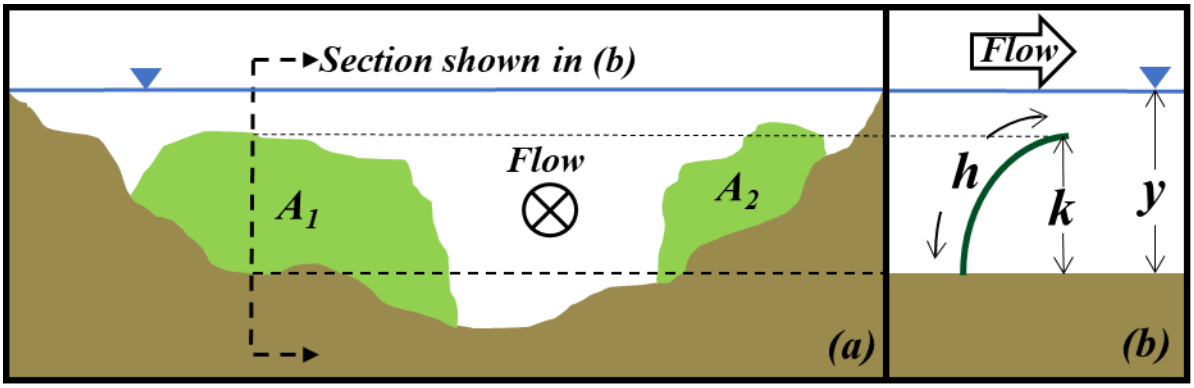

Figure 3-1(a) Cross-sectional channel view with in-stream vegetation patches (A1 and A2) and, (b) longitudinal channel profile detailing local water depth and bent plant height. Note: the symbol in (a) represents flow directed into the page.

Flow resistance formulae similar to Equation (3-3) are often used in gravel bed rivers (e.g. Bray, 1979) where k represents a characteristic grain size (e.g. Millar, 1999) which, as long as the channel particle size distribution does not change, is a temporally constant value. However, in vegetated channels, k, being the plant bent height (Figure 3-1b), can be subject to significant seasonal changes. Such changes occur due to plant growth/decay, which may be triggered by water temperature as warmer water is known to enhance plant growth (Madsen and Brix, 1997; Hussner et al., 2014) while colder trending temperatures commonly lead to seasonal macrophyte decay (Hill and Webster, 1982; Trepel and Holsten, 2003). Variations in k may also be induced by changes in velocity which affect the bending characteristics of plants and their spatial distribution (Sand-Jensen, 2003; O'Hare et al., 2007; Verschoren et al, 2016).

Changes in relative roughness (k/y) directly translate to changes in B_X as the two are inter-related (Figure 3-1). Thus, estimating both B_X and (k/y) are subject to the same conditions of drag, buoyancy, and stiffness (Kouwen et al., 1973, 1981; Sand-Jensen, 2003; Statzner et al., 2006; Nikora, 2010; Nepf, 2012; Luhar and Nepf, 2011; 2013). Plant shape and frontal flow area (Sand-Jensen, 2003; Nepf, 2012) further affect drag and generate additional feedback effects upon buoyancy and stiffness which also vary temporally and as a function of the flow field distribution. Similar to Kouwen et al. (1973, 1981) it is assumed in this study that the reach-averaged biomechanical properties of plants and their spatial distribution can be interrelated.

Kouwen and Unny (1973) found that stem density (M) and flexural stiffness (EI) experienced inter-dependent effects upon k/y and thus estimates of flow resistance. EI is defined as the product of the

modulus of elasticity (*E*) and the second moment of inertia (*I)*. They proposed a composite metric of aggregate stiffness (*MEI)* to account for the combined effects of stem density and flexural stiffness (*MEI*). Specifically, Kouwen and Li (1980), proposed the equation:

$$MEI = \left[3.4h\left(\frac{k}{h}\right)^{0.63}\right]^4 (\gamma y S) \tag{3-4}$$

where, *S* is the channel slope, γ is the specific weight of water and *h* is the plant height before bending forces (i.e. flow) are applied. Chen et al. (2014) undertook a mechanical analysis of stems assuming a cantilever beam-like behaviour and demonstrated that the relationship between *k/y* and flow was governed by plant stiffness and density. Although Equations (3-3) and (3-4) were developed and verified employing artificial plants with known biomechanical properties, they were later demonstrated by Carollo et al. (2005) in laboratory studies to be valid for natural vegetation, albeit with some modifications to values of *a* and *b* due to different densities used. Luhar and Nepf (2013) further demonstrated that flow resistance in a vegetated channel can be estimated by determining the drag and buoyancy forces arising from vegetation patches.

Regardless of the studies or equations mentioned above, representative estimates of in-channel biomechanical properties for *E* and *I* and for plant densities (*M*) remain challenging to obtain due to the large variations in vegetative communities found in nature. Studies by both Bradley and Houser (2009) and Stone et al. (2013) found that their respective modulus of elasticities (*E*) varied by more than an order of magnitude within the same species. Variability can further increase at the single stem scale, as noted by Miler et al. (2012, 2014), who found significant variations in both *E* and *I* of individual stems ranging from their root bases to tips. Seasonal variations in daily solar radiation and corresponding water temperature changes can also vary the biomechanical properties leading to greater growth rates in warmer seasons and decay and dislodgement in winter seasons (Barko et al., 1982; Hill and Webster, 1982; Madsen and Brix, 1997; Trepel and Holsten, 2003; Hussner et al., 2014; Dallas, 2008).

When considering large patches of vegetation, which has been noted to commonly control vegetative flow resistance at the reach scale in both floodplain (Kuta et al., 2010) and main channel flows (Luhar and Nepf, 2013), the stem densities of plants (*M*) also need to be accounted for. However, given the innate heterogeneity and anisotropic growth patterns of instream vegetation, field measurements of *M* are not commonly obtained. Eastgate (1966) developed the Board Drop Test (BDT), to determine the vegetation cover class according to the Soil Conservation Service (SCS) classification system. The test was subsequently re-adapted by Kouwen (1988), to estimate the composite responses of an applied force on plant stiffness and flexural rigidity (*MEI*, product of *M*, *E* and *I)*. The BDT consists of

vertically standing a board (of fixed dimensions and weight) on one end and allowing it to freely rotate about its fulcrum in contact with the ground surface coming to rest on the vegetated surface (Figure 3-2). The resulting height of the fallen board resting above the ground surface is then measured - referred to as the 'Board Height' (*BH*), and used to calculate *MEI* ($R^2 = 0.97$) with the empirical formula offered by Kouwen (1988) of the form:

$$MEI = 3122(BH)^{2.82} \tag{3-5}$$

Kouwen (1988) notes that *BH* must be expressed in metres. The BDT is capable of measuring the biomechanical properties of vegetation in a non-disruptive and cost-effective manner, however, it can only be used in non-submerged conditions and thus it is not applicable to aquatic vegetation.

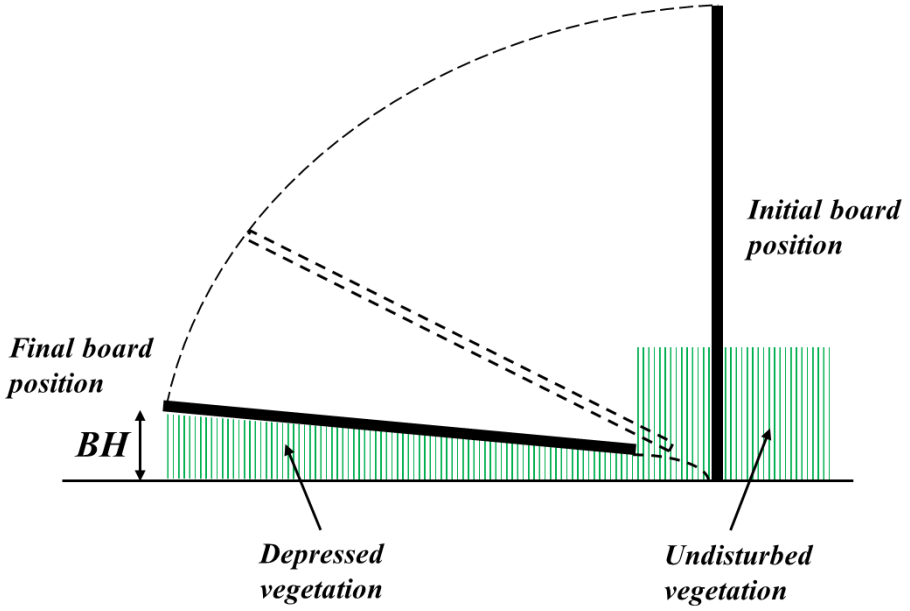

Figure 3-2: Schematic of the board drop test (re-drawn from Kouwen, 1988)

3.3 Experimental apparatus and testing

The tool presented here is an adaptation of the BDT by Eastgate (1966) and Kouwen (1988) to assess the biomechanical properties of submerged and emergent in-channel aquatic vegetation - subsequently referred to as the Settling Board Test (SBT). The settling board, consists of a 762 mm (30") long by 508 mm (20") wide 6.35 mm thick PVC board (ρ = 1,350 Kg/m^3) weighing 3.26 Kg (Figure 3-3a). It is outfitted with a series of 12.5 mm holes spaced 100 mm on centre to promote settling of the board through the water column. Four 170 mm long PVC sealable pipes (Ø = 37 mm) were adhered to each corner of the board to assist with positioning of the board above the desired sample areas.

The SBT method was designed to evaluate the biomechanical properties of submerged vegetation, which is similar in many ways to the BDT developed by Eastgate (1966) and Kouwen (1988), but here modified for submerged conditions. The test consists of hovering the plane of the board at the water surface (affixed pipes pointed upward) and then allowing it to freely settle over a visually identified patch of vegetation (Figure 3-3c). Once the fall of the board has been arrested by the plants, the resting vertical distances from each board corner to the channel bed (*BH*) are measured and an average height of the four corners calculated. Similar to the BDT, the SBT induces bending of the plant strands. As such, resulting *BH* values are assumed to be a function of the bulk vegetation stiffness and density, since plant bending is caused by pressure forces arising from a rigid plain body and thus their values reflect the stiffness and density characteristics of the plants themselves (Eastgate, 1966; Kouwen, 1988).

3.4 Laboratory calibration

Calibration of the SBT to the biomechanical properties of vegetation was determined using artificial vegetation (Figure 3-3b) made of Lexan®, as its tensile properties were known, and plant densities, lengths and spatial patterns could be varied in a controlled manner. Calibration tests were conducted in a stationary pool of water with varying water depths between 0.2 m and 0.37 m (a depth range commonly observed during field validation testing – Section 3.5). Following the model and methods of Kouwen and Unny (1973), *BH* values were assumed to be related to plant stiffness and density in addition to plant strand lengths. Values of *M*, *I* and *h* were varied throughout the laboratory calibration process to account for differences in plant geometry.

The Lexan® modulus of elasticity (*E*) was specified to be E = 2.35 GPa by the manufacturer. Flexural rigidity (*EI*) ranged between 1.31×10^{-5} and 2.96×10^{-5} Nm^2 since *I* was varied between 0.0056 and 0.0126 mm^4 which resulted from both stem thickness (t_s) and width (w_s) being varied amongst tests. The second moment of inertia (*I*) was determined by the relationship (Serway, 1986):

$$I = \frac{w_s t_s^3}{12} \tag{3-6}$$

Artificial vegetation densities (*M*) ranged between 659 and 3976 stems/m^2, whereas to limit experimental costs, only two stem lengths (*h*) were tested: 0.1 m and 0.15 m. Calibration results showed that for equal *MEI* values, longer plant lengths yielded higher values of *BH*. This result was attributed to the fact that longer plants constitute a denser medium able to support the board more effectively as its weight is distributed across a larger surface area. Thus, a composite metric (*MEIh*) is introduced

here which is the product of the plant density, modulus of elasticity, second moment of inertia (analogous to Kouwen et al., 1969, 1973), and plant length.

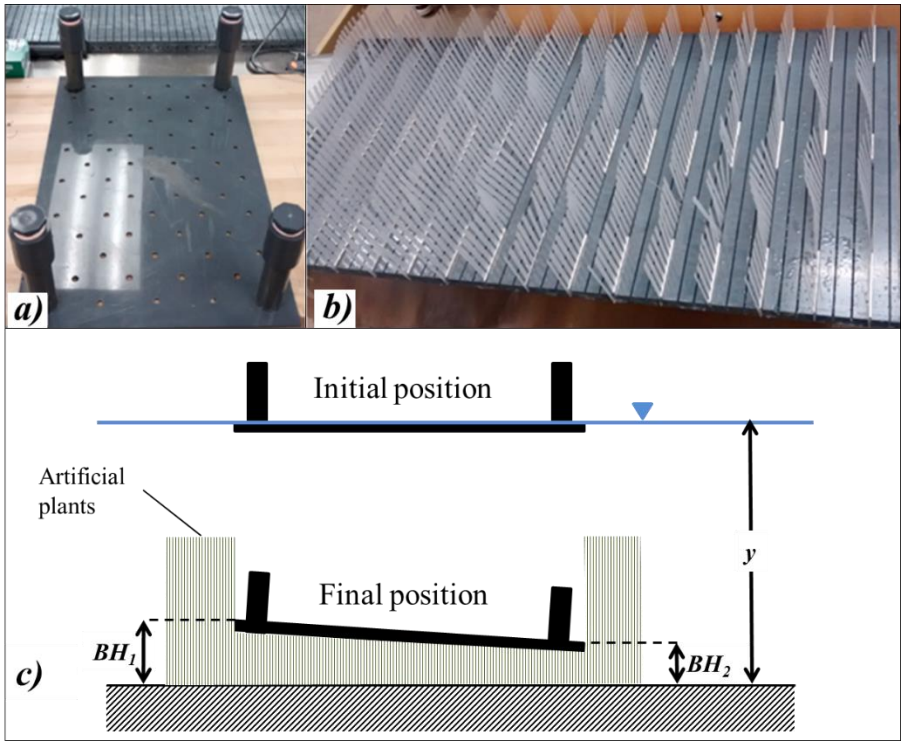

Figure 3-3 (a) The Settling Board' (b) artificial vegetation used in calibration testing and, (c) a cross-sectional schematic of the initial and final testing positions of the apparatus.

The Settling Board was observed to decelerate while sinking and therefore impacted plants with a force inversely proportional to flow depth *y*. Consequently, for the same *MEIh* value, resulting *BH* was always greater with increasing water depths (Figure 3-4).

An empirical relationship to calculate *MEIh* as a function of *BH* and *y* was determined (R^2=0.96; p<0.001):

$$MEIh = \frac{(0.018BH - 0.0003)}{y^{1.5}} \tag{3-7}$$

It is noted that both *BH* and *y* must be expressed in metres which results in *MEIh* expressed in Nm. This relationship was considered to be valid for conditions when *BH* > 0.02 m (median bed material grain size (d_{50}) found while undertaking field tests). Observations during field validation noted that not all corners of the Settling Board came to rest on vegetation in all test cases. In some instances, a varying number of the Settling Board corners came to rest on the channel bed. Therefore, an additional series of Settling Board calibration experiments were conducted to address these conditions by varying *M*, *I* and *h* in a similar fashion to those discussed above. Results of these findings are listed in Table 3-1.

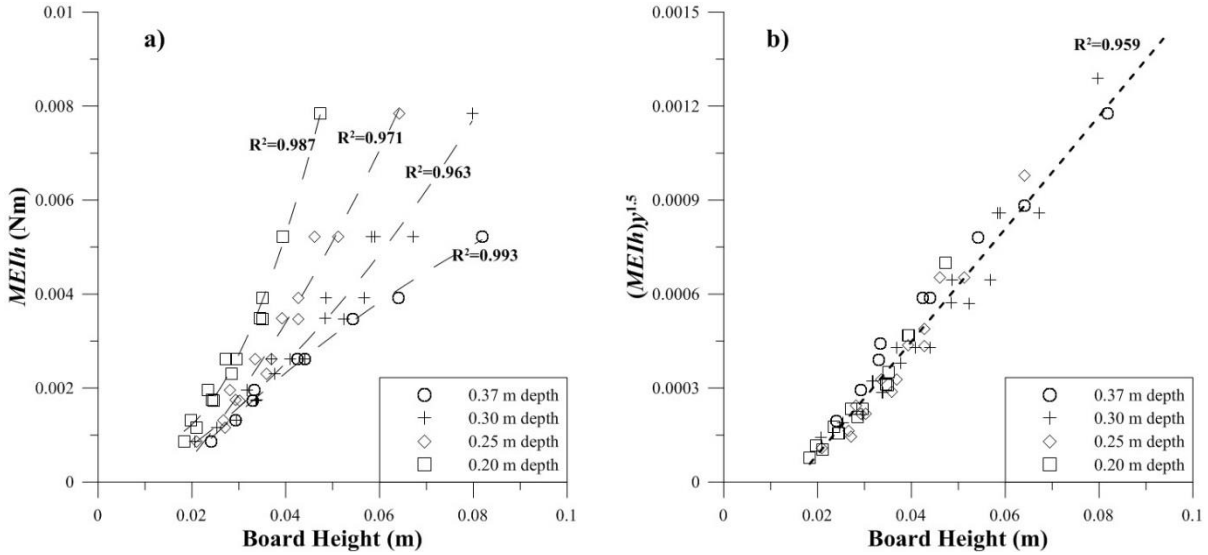

Figure 3-4(a) Laboratory calibration results with different depths shown (b) Results normalized by depth to obtain Equation (3-7)

Table 3-1: Limit values of *MEIh* to be assigned when parts of the Settling Board rest on the channel bed.

Field Scenario	**Resulting *MEIh***
No plants present	$MEIh = 0^{(a)}$
One corner touches channel bottom	$MEIh = 0.0023 - 0.0046y^{(b)}$
More than one corner touches channel bottom	$MEIh = 0.001 - 0.0023y^{(b)}$

(a) Assumed, since if no plants are present M=0, thus $MEIh$=0; (b) From laboratory tests, y (flow depth) is in metres, resulting *MEIh* is in Nm

3.5 Field testing

Field validation tests were undertaken over two summers along two different reaches of Moorefield Creek in Southern Ontario, Canada. Different species of aquatic plants were tested: *Sparganium americanum* (Figure 3-5a) at both reaches, *Elodea canadensis* (Figure 3-5b) at Reach 1 and *Potamogeton natans* at Reach 2. As *S. americanum* plants may emerge from the water surface, both submerged and emergent plants of this species were tested. This was not possible for *P. natans* and *E. canadensis* since only submerged plants were found.

All test locations were geo-referenced using a SOKKIA® RTK-GPS (±0.01 m) so that they could be repeated at the same locations during different seasonal growth stages to evaluate temporal changes in *MEIh*. The testing procedure here follows closely that described in the calibration phase. In cases where the Settling Board came to rest on the channel bed, *MEIh* values were assigned based upon the criteria

listed in Table 3-1. Discharge (Q) was estimated at-a-station by employing the velocity area method (e.g. Herschy, 1995) using a SONTEK Flow Tracker (±0.001 m/s). Average velocity was calculated as the ratio Q/A where A is the average cross-sectional area measured with the same RTK-GPS unit. Tests were repeated throughout the summer, with an average frequency of 14 days.

The spatial distribution of instream vegetation was determined by inventorying k and y at a series of points along each given cross-section (within the channel top width) using the same RTK-GPS unit. Spacing between each inventory point averaged 0.68 m, while spacing between successive cross sections averaged 2.68 m. Both point and cross-sectional sample spacing were varied based upon field observations of plant heterogeneity. In areas where GPS coverage was interrupted (typically under overhanging riparian vegetation), missing data points were interpolated based upon field observations. For each cross-section, blockage factor b_X was calculated as a weighted average of k/y values (Table 3-1; note: if $k \geq y$ then $k/y = 1$) using the distance among points as a weighting factor. The average blockage factor B_X was computed by averaging b_X values using Equation (3-2). Furthermore, for each SBT, a k/y value corresponding to each test location was obtained by averaging k/y values within 0.762 m (the side of the settling board) of the test location.

Field tests were undertaken in flow depths ranging between 0.15 m and 0.51 m. Approximately 93% of the field tests were undertaken in flow depths ranging between 0.2 m and 0.37 m (corresponding to the depths used in the calibration testing). While field tests were conducted under flowing conditions (calibration tests were conducted in standing water), the highest velocity observed at the field site was relatively low (0.04 m/s) which did not cause the board to deviate from its vertical path during settling. It is not recommended to undertake SBT's under flow conditions other than very low velocities to minimize settling paths that deviate from those normal to the water surface.

As water temperature has been documented to affect plant growth (Madsen and Brix, 1997; Hussner et al., 2014) and decay (Hill and Webster, 1982; Trepel and Holsten, 2003), it was measured from April to November of each sampling year using ONSET® pressure and temperature sensors (±0.1ºC) at five minutes intervals.

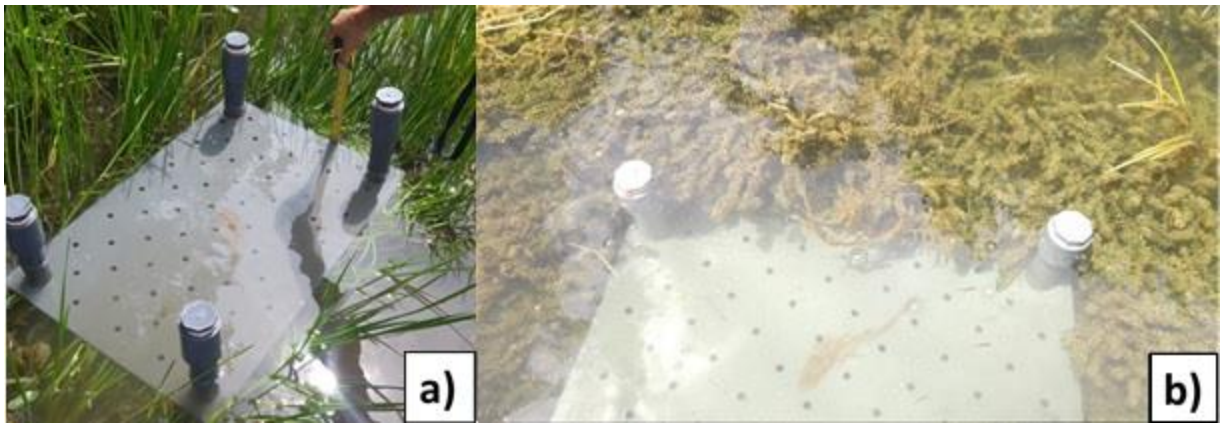

Figure 3-5 Field Settling Board test on: (a) *Sparganium americanum* and, (b) *Elodea canadensis*

3.5.1 Field testing results and discussion

A statistically significant relationship (R^2=0.58, p<0.001) was found between field-measured *MEIh* values and corresponding *k/y* values for the combined validation reaches (Figure 3-6). Similar relationships were obtained at each test reach where different instream species were observed: Reach 1 (R^2=0.40, p=0.001), Reach 2 (R^2=0.85, p<0.001). These results agree with observations by Kouwen *et al.* (1973, 1981) who showed *k/y* to be directly related to *EI* for artificial plants. At both sites, emergent vegetation (*Sparganium americanum*) was present and it was noted that emerging stems arched in the general direction of channel flow rather than protruding vertically. In these cases, resulting stem heights were measured from the channel bed to the maximum height that the vegetation floated at (as opposed to the net stem length that may be greater in several cases). As such, *k* is assumed to be a function of *EI* for emergent plants. Naturally, *k* is also directly proportional to *h*, consequently a proportionality between *k* and *MEIh* also exists.

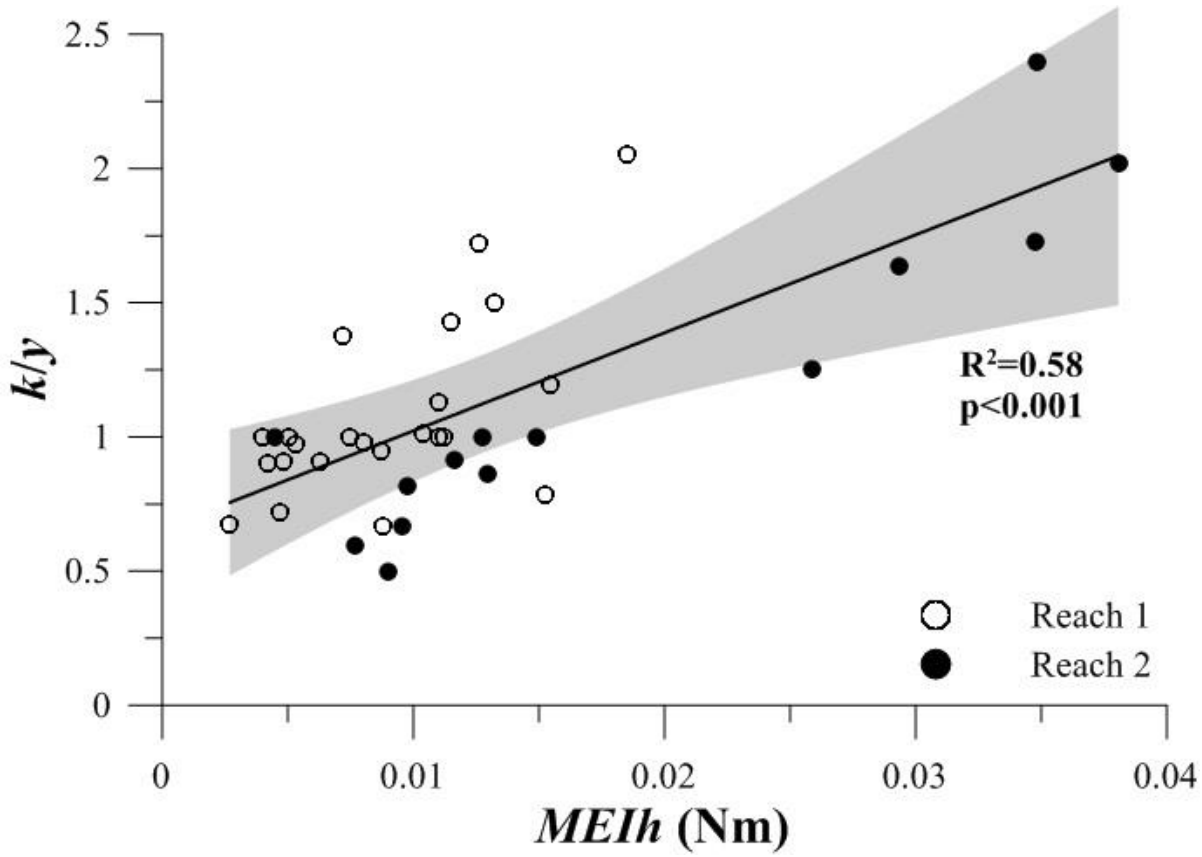

Figure 3-6 Relationship between *MEIh* and *k/y* for *S. americanum* plants. For Reach 1, n=23; Reach 2, n=14. No data are shown for other species as sample sizes were too small to obtain statistically significant results and lack of *k/y* data.

During each annual series of SBT's, no high flow events (i.e. exceeding the mean annual flow of the stream) occurred. These observations combined with the relatively small changes in mean velocities during each SBT (Reach 1: 0.01 – 0.025 m/s, Reach 2: 0.019 – 0.042 m/s) infer that the correlations between *MEIh* and *k/y* result from plant growth rather than either reconstitution of the channel bed or reconfiguration of vegetative patches (i.e. plant bending due to flow, Sand-Jensen, 2003) which would require higher velocities.

Average *MEIh* values for each reach were compared to the reach-averaged B_X value and a statistically significant relationship (p<0.05) was found at Reach 1 but not at Reach 2 (Figure 3-7), where a weaker correlation and statistical significance were found (p=0.14). Denser and stiffer plants tended to occupy more of the cross-section (Kouwen and Unny, 1973; Luhar and Nepf, 2013) thus yielding higher B_X values. Since B_X is related to *k/y*, some degree of correlation with reach-averaged *MEIh* values were also to be expected. The density of vegetation at Reach 2 was not as prominent as Reach 1 which may explain the lack of correlation at Reach 2.

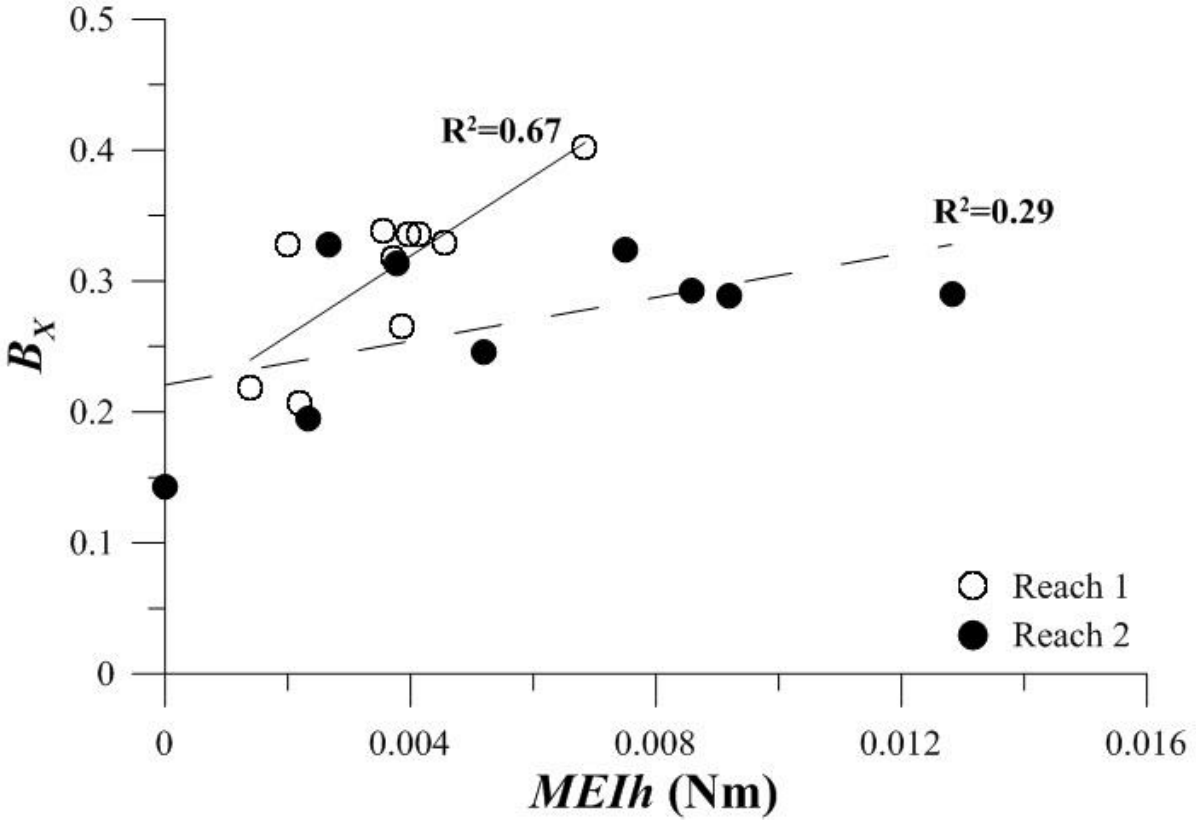

Figure 3-7: B_X versus reach-averaged *MEIh*

It is also plausible that *MEIh* data collected from each SBT could be used to predict changes in *k/y* and subsequently B_X due to reconfiguration (Green, 2005a; Nikora et al., 2008; Luhar and Nepf, 2013). To test this hypothesis, measurements of *k/y* and B_X needed to be obtained at similar growth stages (to avoid changes in *MEIh* because of growth/decay) under different flow conditions to assess different bending forces. Unfortunately, in the present study, this could not be assessed due to the lack of higher velocities (maximum velocity observed during field test was 0.042 m/s) capable of producing noticeable differences in plant bending throughout the study duration.

3.5.2 Temporal changes in plants biomechanical properties

At Reaches 1 and 2, *MEIh* increased for *E. canadensis*, *P. natans* and *S. americanum* as water temperatures seasonally increased above 15 ºC and decreased when water began to seasonally decrease (Figure 3-8). Seasonal decreases result from biomass losses and consequent loss in plant density (*M*) which can be triggered by colder temperatures. For aquatic plants typical of temperate regions, decreases in *h*, *E* and *I* have also been observed to occur seasonally (Miler et al., 2014; Łoboda, 2017). Hill and Webster (1982) found *E. canadensis* biomasses began to decay when river temperatures decreased below 14 ºC, a threshold similar to the current study. Similarly, Trepel and Holsten (2003)

observed that the biomass of *S. emersum* (a species similar to *S. americanum*) markedly decreased when water temperatures fell below 10 ºC. The threshold observed here for *S. americanum* are approximately 5 ºC higher than the previous study - which may be related to the difference in biomechanical properties of different species in the same genus. For *S. americanum* plants, greater *MEIh* values were found at Reach 2, than at Reach 1. This is likely related to differences in temperatures between the two reaches: Reach 2 was characterized by warmer water (Figure 3-8) which may have enhanced plant growth, thus specimen biomechanical properties and density. Reasons for differences in temperatures between the two reaches are attributed to possible different volumes of groundwater infiltration (Conant, 2004) and shading due to riparian cover (Johnson, 1971; Beschta, 1997) along Reach 1. Findings from this study demonstrate that the inter-seasonal biomechanical properties of macrophytes can be captured over their entire growth period by deploying the SBT at approximate three to four-week intervals.

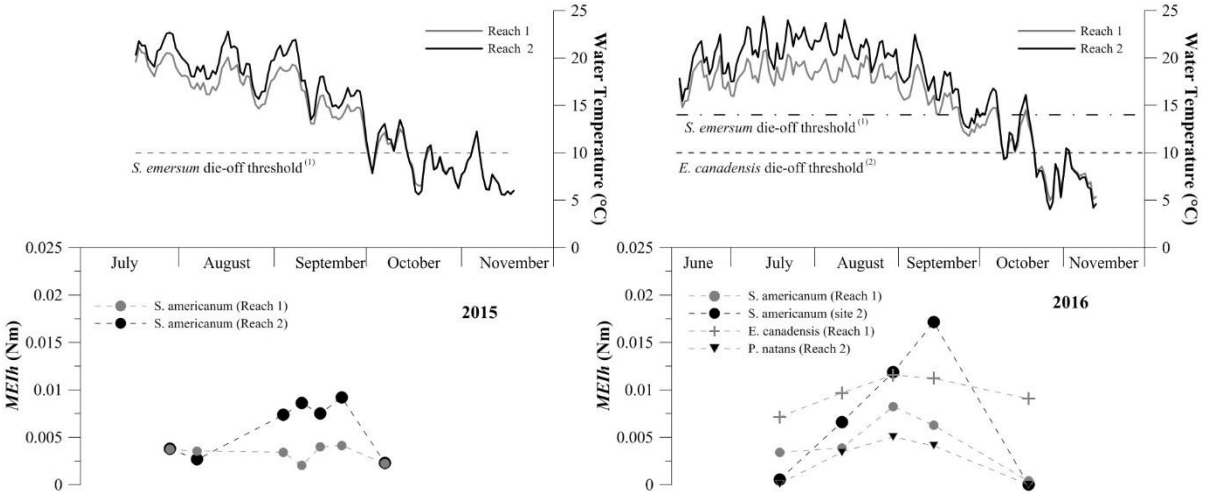

Figure 3-8: Water temperature variations and changes in *MEIh* for 2015 data and 2016 data.

3.6 Conclusions

A simple method has been developed (SBT) to evaluate the biomechanical properties of in-stream vegetation and relate them to the relative roughness metric (*k/y*) in a non-destructive fashion. Laboratory calibration of the SB showed its ability to detect differences in plant densities and stiffnesses whereas field tests confirmed that the SBT can be used to detect temporal changes in the biomechanics properties of submerged species and successfully relate them to relative roughness. The biomechanical properties have been documented in other studies to be related to flow resistance caused by aquatic plants but had not been previously sampled or quantified in a systematic fashion such that they could

be directly related to relative roughness. Measurements obtained through the use of the SBT can then be used to aid in the successful estimation of vegetative flow resistance and thus improved discharge estimates at-a-station – particularly under environmental low-flow conditions.

Applications of the SBT are not limited to estimating flow resistance but can also be used to map submerged plant densities at finer scales than previously studied. Tests can be used to distinguish patches with higher density and rigidity from lower density ones if repeated on different plants of the same species. Plant density is related to turbulence intensity (Nepf, 2012) and also controls water retention time among plant communities (Nikora, 2010). Thus, *M* is related to reach scale roughness, which in turn affects the ability to estimate discharge.

Chapter 4: Improving flow records affected by in-stream vegetation during low-flow conditions

4.1 Introduction

Many water resources management applications, ranging from engineering to biology, rely on accurate, continuous flow records. Examples include environmental assessments, water supply management and planning as well as infrastructure design (Kiang et al., 2009). Continuous records exist at gauging stations where river levels are continuously measured and converted into discharge using rating curves. Employment of rating curves assume that a unique relationship exists between flow rate (Q) and water level (WL), where the latter is often called stage and measured with respect to a datum. The general formula of a rating curve is (Herschy, 1995):

$$Q = f_n(WL) \tag{4-1}$$

Equation (4-1) is reliable if the channel boundary conditions, relative to when the curve was originally developed, do not vary. However, external factors can alter the boundary conditions and, if these are not accounted for, errors in discharge estimates can arise. Causes of these errors include: abrupt changes in channel morphology (Reitan and Petersen-Øverleir 2011; Guerrero et al., 2012), localized erosion/deposition (Quick, 1991; Magnuszewski and Moran, 2015), backwater from beaver dams (Hamilton and Moore, 2011), presence of ice (Pelletier, 1988, 1989) or aquatic vegetation (Gurnell and Midgley, 1994; Hamilton and Moore, 2011; Cassan et al., 2015).

Erroneous flow estimates resulting from aquatic vegetation are often temporally variable, due to seasonal growth and decay cycles of plants (Gurnell and Midgley, 1994). Correction of these errors has historically been undertaken by shifting a given rating curve, using empirical "*a posteriori*" methods. These, however, require instantaneous on-site measurements of discharge and often lead to the introduction of systematic errors (Schmidt, 2004).

In most of the temperate regions of the world, aquatic plant growth occurs in the summer months when low flow conditions are common (De Doncker, 2009). During this period, water management decisions are critical as they are made to prevent water scarcity from affecting farming and potable use. Furthermore, some water allocation regulations are made to protect aquatic habitats asexcessive water takings cause long-term negative effects on ecosystems (Scheffer and Carpenter, 2003). This is especially important at the present time, as climate change is expected to increase the severity of low flows and droughts (Whitfield and Hendrata, 2006). Consequently, skewed water apportionments resulting from incorrect low flow estimates can lead to detrimental impacts on the public as well as the

environment. Finally, the sustainability of aquatic habitats, such as fish passage requirements, is usually determined from flow estimates (Suren and Jowett, 2006; Bradford and Heinonen, 2008, Dunbar et al., 2010). In summary, methods to improve the accuracy of discharge records, especially at low flow, are needed.

This chapter presents a simple, accurate method to correct flow rates erroneously calculated at gauging stations due to the added flow resistance by aquatic vegetation at the reach-scale. The proposed methodology uses non-disruptive measurements of vegetation spatial distribution (i.e. not requiring harvesting of plants) and can be applied to both discrete and continuous flow estimates, the ultimate goal being to improve the estimation of low flow metrics at gauged sites. A sensitivity analysis to address the effect of sample size (number of samples and monitoring temporal frequency) is also shown for application purposes.

4.2 Background

Vegetative flow resistance (i.e. vegetative roughness) has been studied for approximately eight decades. To estimate it, several parameters have been used (Fentzl, 1964; Baptist et al., 2007; Nepf, 2012), some of which are not easily obtained, thus making it a challenging issue to solve. The first studies in this field involved assessments of flow conveyance in irrigation canals by Ree (1939, 1941, 1949, and 1958), Cox (1942), and Palmer (1945 and 1946). These works found that vegetative flow resistance was affected by plant density (*M*), stem length (*h*), cross-sectional blockage, and crop conditions. Kouwen et al., (1969, 1973, 1980, and 1981) later estimated flow resistance of artificial plants in a flume, offering the formula:

$$\frac{V}{u_*} = C_1 + C_2 log\left(\frac{k}{y}\right) \tag{4-2}$$

where, V is flow mean velocity, u_* is the bed shear velocity, y is flow depth, k is roughness height or vegetation bent height (*i.e.*: the height that the plant stem assumes after it is bent over by flow) and C_1, C_2 are constants indirectly dependent on stem density (M) and stiffness (EI). While Equation (4-2) was developed for artificial plants, later experiments with natural grass species confirmed that relative roughness (k/y) is proportional to flow resistance (notably, Wilson and Horritt, 2002; Järvelä, 2002; Carollo et al., 2005). Other studies have found that the spatial distribution, stiffness and density of vegetation were also contributing factors to flow resistance (James and Birkhead, 2004, and Wilson, 2007).

The majority of the aforementioned studies was based on laboratory experiments, as few field-based studies have been undertaken on this topic. Generally, at the reach scale, vegetative roughness is separated from other sources of flow resistance in the following form (e.g. Huntington and Whitehead, 1992; Green, 2005a; 2005b; Nikora et al., 2008):

$$n = f_n(n_b, n_v) \tag{4-3}$$

where n_b is the base roughness value of Manning's n, due to combined grain and form roughness (Millar, 1999) and n_v is the Manning's n resistance factor arising from vegetation. Consequently, when vegetation is not present, $n = n_b$.

Although there is a sound theoretical and empirical basis for this approach (Cowan, 1956; Arcement and Schneider, 1989; Millar, 1999), Equation (4-3) is often applied inconsistently (Table 4-1). Specifically, while n is generally calculated directly from flow data using Manning's equation (e.g.: Chow, 1959), n_b is often estimated indirectly from grain size data (Green, 2005a), and, in some instances, assumed constant with Q (Huntington and Whitehead, 1992, Nikora et al., 2008). The latter scenario is possible, however, correlation between n_b and Q is common in natural channels, especially at low flows (Hicks and Mason, 1991; Ferguson, 2010; 2013).

Conversely, calculations of n_v are usually related to the sizes, spatial distributions and densities of vegetation patches at the reach scale, which relates well to results from laboratory observations by Kouwen et al., (1969, 1970, 1973, 1981, 1988), James and Birkhead (2004), Carollo et al., (2005) and Wilson (2007). However, as different metrics and methods to quantify the spatial distribution of vegetation exist, different approaches and formulations are available for n_v as well. This variety of approaches frequently causes estimations of vegetative flow resistance and resulting discharge estimates to differ markedly amongst studies.

For the purposes of estimating n_v, the reach-scale spatial distribution of vegetation has been quantified in various ways. One common method is to quantify the portion of the channel bed covered by vegetation, also called aerial cover, defined as:

$$B_A = \frac{\sum_{q=1}^{N} A_q}{A_T} \tag{4-4}$$

where B_A is aerial cover A_i is the surface area of the q-th vegetated patch (Sand-Jensen 2002), N is the total number of patches and A_T is the study reach total surface area. Huntington and Whitehead (1992), Green (2005a) and Old et al., (2014) found B_A and flow resistance (expressed as Manning's n) to be correlated. Different methods can be used to quantify the latter; however, the spatial distribution of plants can often be heterogeneous and boundaries between channel bed and vegetation may not be as

clearly defined as illustrated in Figure 4-1a. Thus, within a reach B_A is often estimated through a discretization approach by measuring plants at m cross-sections and applying the following relationship to estimate B_A (e.g.: Green, 2005a; Nikora et al., 2008):

$$B_A \approx L_A = \frac{1}{A_T}\sum_{j=1}^{m} T_{W,j} D_j l_A(j) = \frac{1}{A_T}\sum_{j=1}^{m} T_{W,j} D_j \left(\frac{\sum_{i=2}^{n} \frac{1}{2}(d_i - d_{i-1})(F_i + F_{i-1})}{T_W} \right)_j \quad (4\text{-}5)$$

$$F_i = 0 \; if \; no \; vegetation \; is \; present \; at \; point \; i$$
$$F_i = 1 \; if \; vegetation \; is \; present \; at \; point \; i$$

where, at the j-th cross-section, $l_A(j)$ is the blockage width, i is the surveying point of interest, d_i is its distance from the bank (Figure 4-1b), F_i is a binary function and T_W is the channel top width. L_A represents the average of $l_A(j)$ values and, in most studies, it is assumed that $B_A \approx L_A$. The accuracy of this assumption, is discussed in detail in Chapter 2.

The spatial distribution of vegetation has also been quantified at the cross-sectional scale using the cross-sectional blockage factor (b_X, Green, 2005a). This is defined as the ratio between the proportion of a given cross-section containing vegetation to the total cross-sectional area (Green, 2005a, Nepf 2012). Increases in flow resistance were found related to the blockage factor in field studies by Champion and Tanner (2000), Green (2005a), and Nikora et al. (2008). At the j-th cross-section, b_X can be calculated with a weighted sum to account for uneven spacing between points sampled as defined by:

$$b_X(j) = \frac{1}{2}\sum_{i}^{n} (d_i - d_{i+1}) \left(\frac{k_i}{h_i} + \frac{k_{i+1}}{h_{i+1}} \right) \quad (4\text{-}6)$$

in which, i is the measurement point of interest, d_i is its distance from the bank, h_i is local depth and k_i is local vegetation height (Figure 4-1c). When $k_i > h_i$ it is generally assumed that $k_i = h_i$ as the emergent part of the vegetation does not contribute to flow blockage.

To obtain a metric representing blockage for the whole reach, different statistical parameters have been used. These include a vegetation distribution curve (Green, 2006) or calculating the mean value of b_X, weighted according to cross-sectional spacing in the general form (Green, 2005a; Nikora et al., 2008):

$$B_X = \frac{1}{L}\sum_{j=1}^{m} D_j b_X(j) \quad (4\text{-}7)$$

Different reach delineation methods and cross-sectional spacings have been used to define B_X. Furthermore, the extent to which sample size affects the accuracy of vegetation distribution parameters remains unknown (Nepf, 2012). In summary, while different methods and metrics have been proposed,

there remains a lack of consensus on which methodology is most appropriate to quantify vegetation spatial distribution, and how vegetative resistance to flow should be calculated.

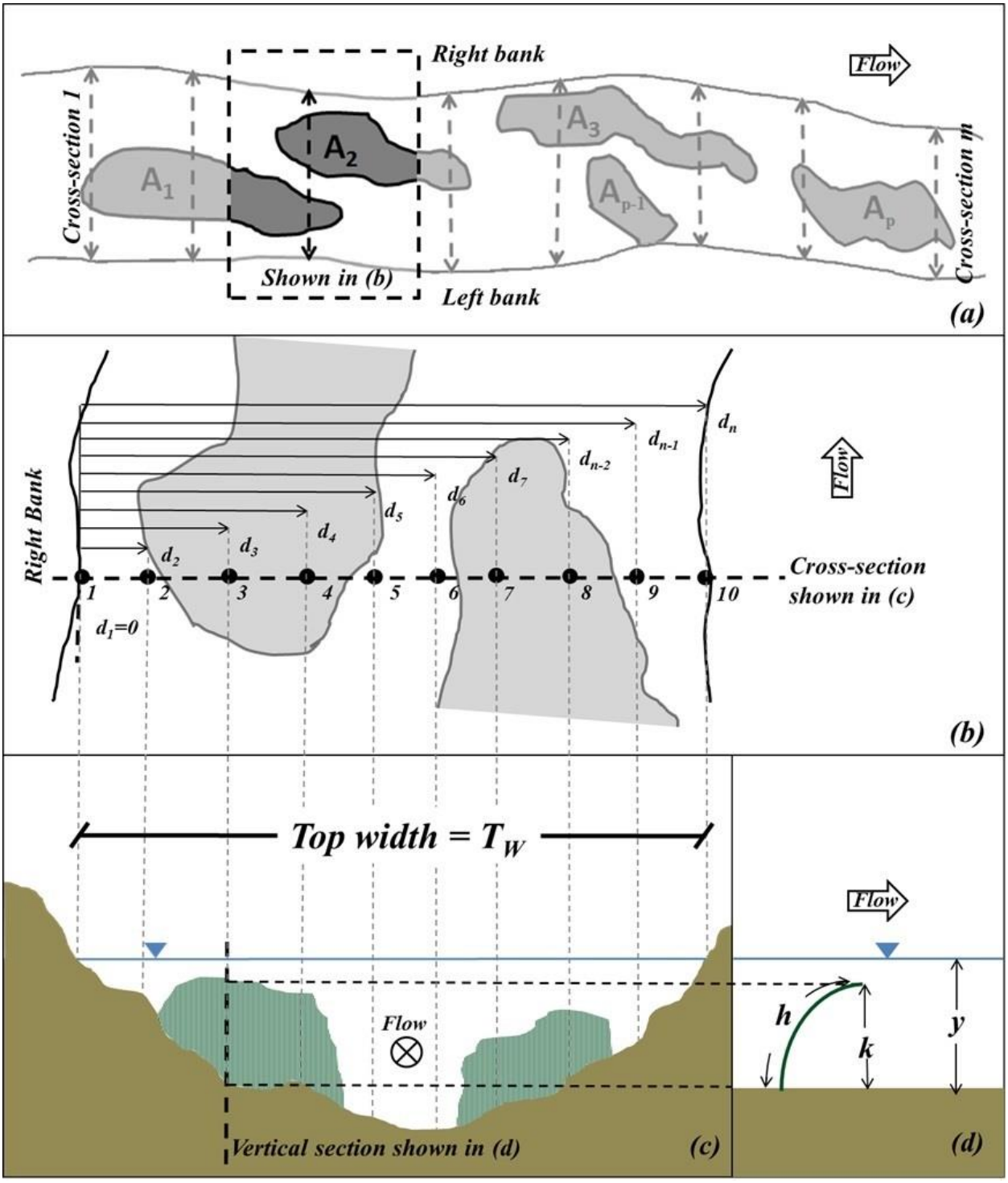

Figure 4-1: Simplified schematic of vegetation distribution at the longitudinal scale (a) detail of cross-section calculation (b) cross-sectional view (c) and vertical view (d)

Table 4-1: Expressions for $n=n_b+n_v$ in vegetated channels found in literature.

Study	Expression for n_b	Expression for n
Huntington and Whitehead (1992)	0.0337 (constant value)	$n_b + 0.0239\frac{L_A}{VR}$
Champion and Tanner (2000)	0.048 (constant value)	$n_b + 0.33B_X$
*Green (2005a) (1)	$\frac{R^{1/6}}{17.984\left(\log\frac{11.1R^{0.686}{d_{max}}^{0.314}}{k_s}\right)}$	$n_b + 0.35L_A - 0.0857$
*Green (2005a) (2)	$\frac{R^{1/6}}{17.984\left(\log\frac{11.1R^{0.686}{d_{max}}^{0.314}}{k_s}\right)}$	$n_b + 0.43B_X - 0.0497$
Nikora et al., (2008)	0.025 (constant value)	$n_b e^{3B_X}$

Notes: * - d_{max} is maximum flow depth (Hey, 1988) and $log(k_s)= -1.54+1.02log(Z^3/XY)_{91}$, where $(Z^3/XY)_{91}$ is the 91st percentile of Z^3/XY where X, Y, and Z are long, intermediate and short axes of a particle respectively (in mm).

4.3 Methodology

4.3.1 Study sites

Five river reaches affected by aquatic vegetation were selected for this investigation (Figure 4-2, Table 4-2). Reaches 1 and 2 were selected as the study testing and method development reaches, while the remaining three were used for independent validation purposes. All reaches are gauged by the Water Survey of Canada (WSC) with the exception of Reach 3, which is gauged by the Maitland Valley Conservation Authority (MVCA). Summer flow rates for Reach 1 and 2 have not been published by WSC for over a decade. Streamflow data for Reaches 4 and 5 is subject to *a posteriori* seasonal shifts by WSC, which are based upon flow measurements, air temperature measurements and field observations of aquatic vegetation (Environment Canada, personal comm.). Flow records for Reach 3 are not subject to any shifts.

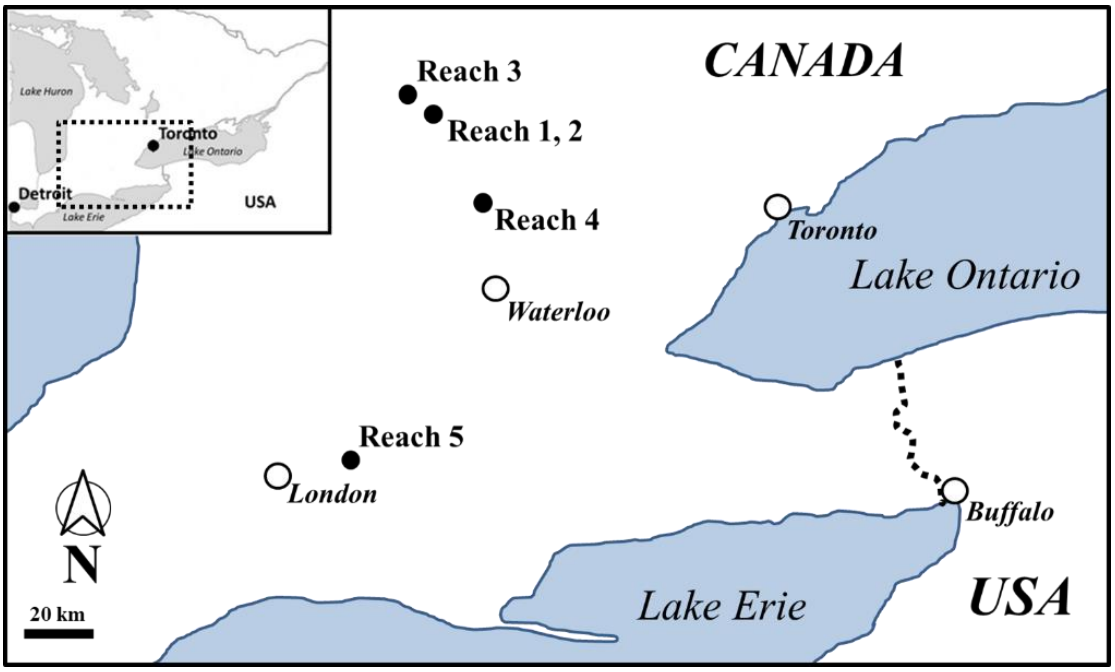

Figure 4-2: Location of study reaches

In previous studies that assessed vegetative flow resistance, reach lengths were kept either constant (Green, 2005a) or proportional to channel width (Nikora et al., 2008). Here, to isolate the backwater effects within a reach, the limits of each reach were defined at low flow hydraulic controls which were either man made or natural (Herschy, 1995). This resulted in different reach lengths (Table 4-2).

Table 4-2: Summary of study reaches main features; validation reaches are marked with (v).

Reach	Watercourse	[(a)]Drainage area (km^2)	Length (m)	Aquatic plants species	
				Scientific name	*Common name*
1	Moorefield Creek (02GA042)[(b)]	58	121	*Sparganium americanum Elodea canadensis*	*American bur-reed; Canadian waterweed*
2			106	*Sparganium americanum Potamogeton*	*American bur-reed; Pondweed;*
3 (v)	North Maitland River (MVCA)[(c)]	46	149	*Nymphaea spp. Potamogeton spp. Nasturtium spp.*	*Water lily; Pondweed; Watercress*
4 (v)	Canagagigue Creek (02GA023) [(c)]	114	140	*Potamogeton spp. Elodea canadensis*	*Pondweed; Canadian waterweed*
5 (v)	Reynolds Creek (02GD027) [(c)]	145	125	*Nasturtium spp. Elodea canadensis*	*Watercress; Canadian waterweed*

Notes: (a) Drainage areas for Reaches 1 – 3 were measured on ArcMap®, while those for Canagagigue and Reynolds Creek were provided by Water Survey of Canada (wateroffice.ec.gc.ca). (b) the gauge station is located approximately 360 m downstream of Reach 1 and 770 m upstream of Reach 2. (c) the gauge station is located in the middle of the study reach.

4.3.2 Hydraulic measurements

At Reaches 1 and 2, a rating curve was developed at a location not affected by seasonal backwater, but proximal enough to both reaches that spatial continuity in discharge could be assumed. Here, water levels were continuously recorded with HOBO® pressure transducers, (accuracy ± 3 mm). Flow velocities were measured with a SonTek® 2D Flow Tracker (accuracy ± 1 mm/s) and the velocity-area method applied to determine flow rates (Herschy, 1995). Thirty-four discharge measurements were obtained over a three-year period, ranging between 0.025 m^3/s and 0.410 m^3/s, (Figure 4-3). Discharge measurement error was determined by the instrument following the ISO Standard 748 (1997) and averaged 2.79%.

A continuous longitudinal water surface profile was obtained along Reaches 1 and 2 to measure the temporal effects of vegetation growth on flow depth at different flow rates. To achieve this, water levels were recorded using ONSET® pressure transducers (±3 mm) along twenty evenly spaced locations (12 at Reach 1 and 8 at Reach 2). Sampling frequency was defined at 5-minute intervals for approximately 200 days, between April/May and late November for each year.

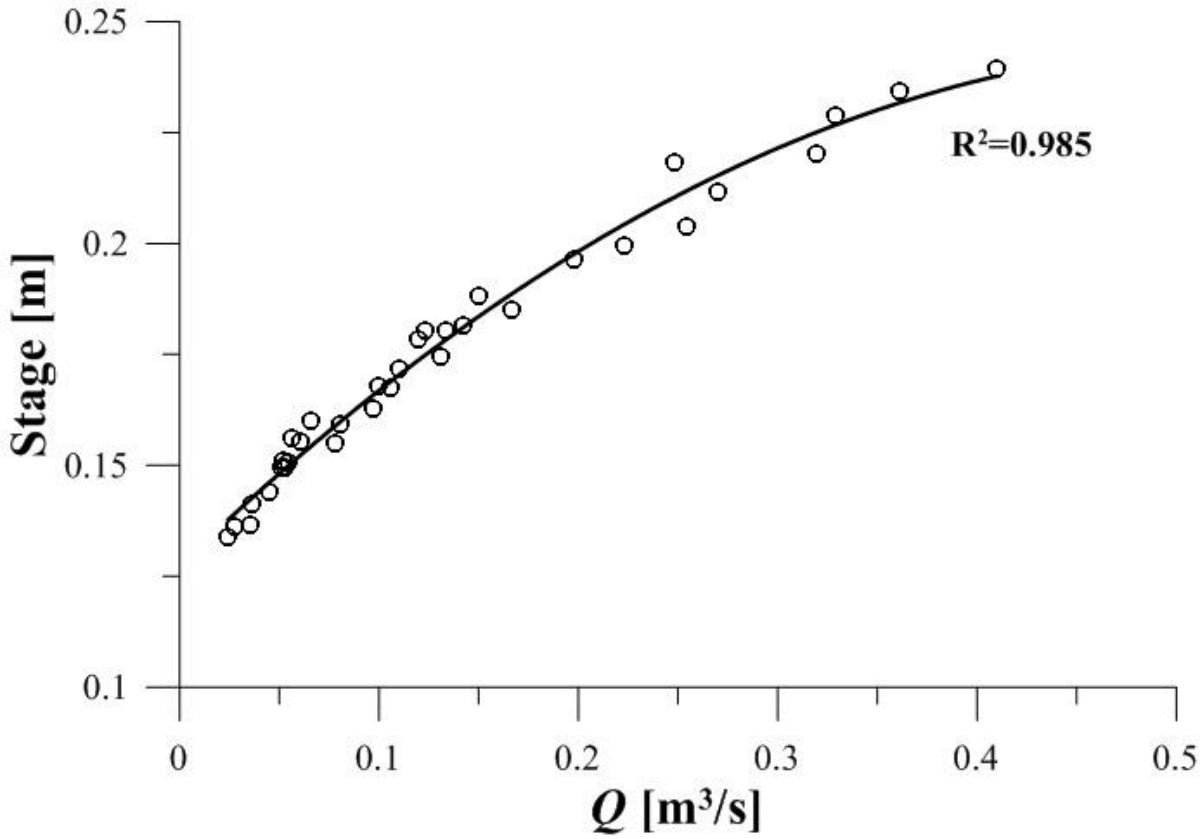

Figure 4-3: Rating curve for Reach 1 and 2, without vegetative backwater impairments

4.3.3 Flow resistance analysis

The effects of vegetation on flow resistance were quantified by comparing water levels recorded before vegetation growth with those obtained while plants were present in the channel. As water levels depend on discharge, the comparison was done at the same value of discharge as expressed by:

$$\Delta WL(Q) = WL(Q) - WL_b(Q) \tag{4-8}$$

where ΔWL is the increase in water level at flow rate Q caused by vegetation, WL is field-measured water level recorded when vegetation is present and WL_b is the field-measured water level for the base roughness (non-vegetated) condition. If an WL_b was not available for a specific Q, it was extrapolated based upon the value of water levels recorded at sections unaffected by vegetation (procedure is discussed in Appendix). No appreciable changes to other channel roughness elements (cross-sectional shape or grain size distribution) occurred during each in-stream growth season. Therefore, aside from instrument inaccuracy (which is discussed in Section 4.3.3.1), ΔWL values were attributed to increases in flow resistance caused by vegetation. Errors in Q estimates arising from vegetation growth (E_Q) were estimated as follows:

$$E_Q = \frac{Q(WL) - Q(WL_b)}{Q(WL_b)} \tag{4-9}$$

where $Q(WL)$ and $Q(WL_b)$ are discharges calculated using WL and WL_b respectively. As Q was estimated at a section unaffected by vegetative flow resistance (rating curve in Figure 4-3), $Q(WL_b)$ was assumed to be an accurate value of discharge.

Other factors, such as water surface slope, discharge, and channel width may have caused differences in ΔWL. Consequently, to compare ΔWL obtained under different flow rates and in different reaches, their values were standardized as follows:

$$K = \Delta WL \frac{(T_W)^{\alpha}}{(S_W Q)^{\beta}} \tag{4-10}$$

where K, the standardized increase in water level, expresses ΔWL for a given combination of discharge Q, water surface slope, S_W and top width, T_W. Alpha (α) and beta (β) are exponents equal to 2 and 0.5, respectively, and were determined through a best-fit approach in the data analysis phase. It should be noted that while K describes an increase in flow resistance it should not be interpreted as a roughness parameter, rather as a tool used to correct flow estimates and water levels (Section 4.5.2).

As Manning's n was found in other studies to be related to vegetative flow resistance, (Kouwen et al. 1981; Champion and Tanner, 2000; Nikora et al., 2008; Luhar and Nepf, 2013) it was calculated here to provide a direct comparison to expressions of the general form of Equation (4-3). Here n_v was calculated using:

$$n_v = n - n_b = \frac{AR^{2/3}\sqrt{S_f}}{Q} - n_b \tag{4-11}$$

where A is wetted area, R is hydraulic radius, S_f is friction slope. As the latter could not be measured directly, it was assumed equal to the surface water slope assuming that similar velocity distributions were present at the reach boundaries, due to observed morphological similarities at these locations. Manning's n for the base-roughness condition (n_b) is calculated using $WL_b(Q)$ and n using $WL(Q)$. In order to provide a comparison with other studies, n_b was also estimated using formulations found in literature (Table 4-1). As some of these require measures of grain size distributions (e.g.: Task force for friction in open channels, 1963), the pebble count technique offered by Wolman (1954) was employed.

4.3.3.1 Systematic discharge calculation errors

Errors in discharge estimates in the ±5% range are generally deemed acceptable by many agencies such as Water Survey of Canada (Hamilton and Moore, 2012). While this accuracy level is considered achievable most of the year, under low flow conditions it is common to incur large errors, as noted by Tomkins (2014). These errors are due to physical reasons including: an increased influence of the boundary layer, hyporheic exchanges, and measurement errors, which have a larger impact when Q is low (Hamilton, 2008).

It was then deemed necessary to quantify the aforementioned systematic discharge calculation errors to avoid attributing them to vegetative flow resistance. To achieve this, discharge calculated using water levels simultaneously measured at two locations not affected by aquatic vegetation was compared using Equation (4-9). As expected, errors in the measurement of discharge greater than ± 5% were present at lower flows while for Q>0.15 m^3/s discharge errors were in the ±5% range. While there was general agreement between field-measured E_Q (using Equation (4-9)) and calculated E_Q (which assumes errors are solely caused by pressure transducer inaccuracy), some divergence is present at low flow (Figure 4-4). Therefore, an empirical systematic error dependent on Q, encompassing 98% of E_Q values was determined from measured values and applied (solid lines on Figure 4-4). It should be noted that these limits are to be considered site-specific and should not be transferred to other rivers.

Due to the emphasis of this study on low flow rates, flow resistance analysis was focused on discharges below 0.5 m^3/s. Through a regional analysis (e.g.: Smakthin, 2001; Castellarin et al., 2004) it was estimated that this value is below the mean annual flow for Moorefield Creek (Q_{ma}~0.79 m^3/s) and well above percentiles commonly associated with low flow events such as Q_{90} or Q_{95} (Smakthin, 2001; Pyrce, 2004). This threshold was established to avoid extrapolating discharge values largely outside the range of field-measured flow rates (Figure 4-3) and to exclude the effects of bank vegetation on flow resistance which may affect higher flow rates (Darby and Thorne, 1996; Naden et al., 2006).

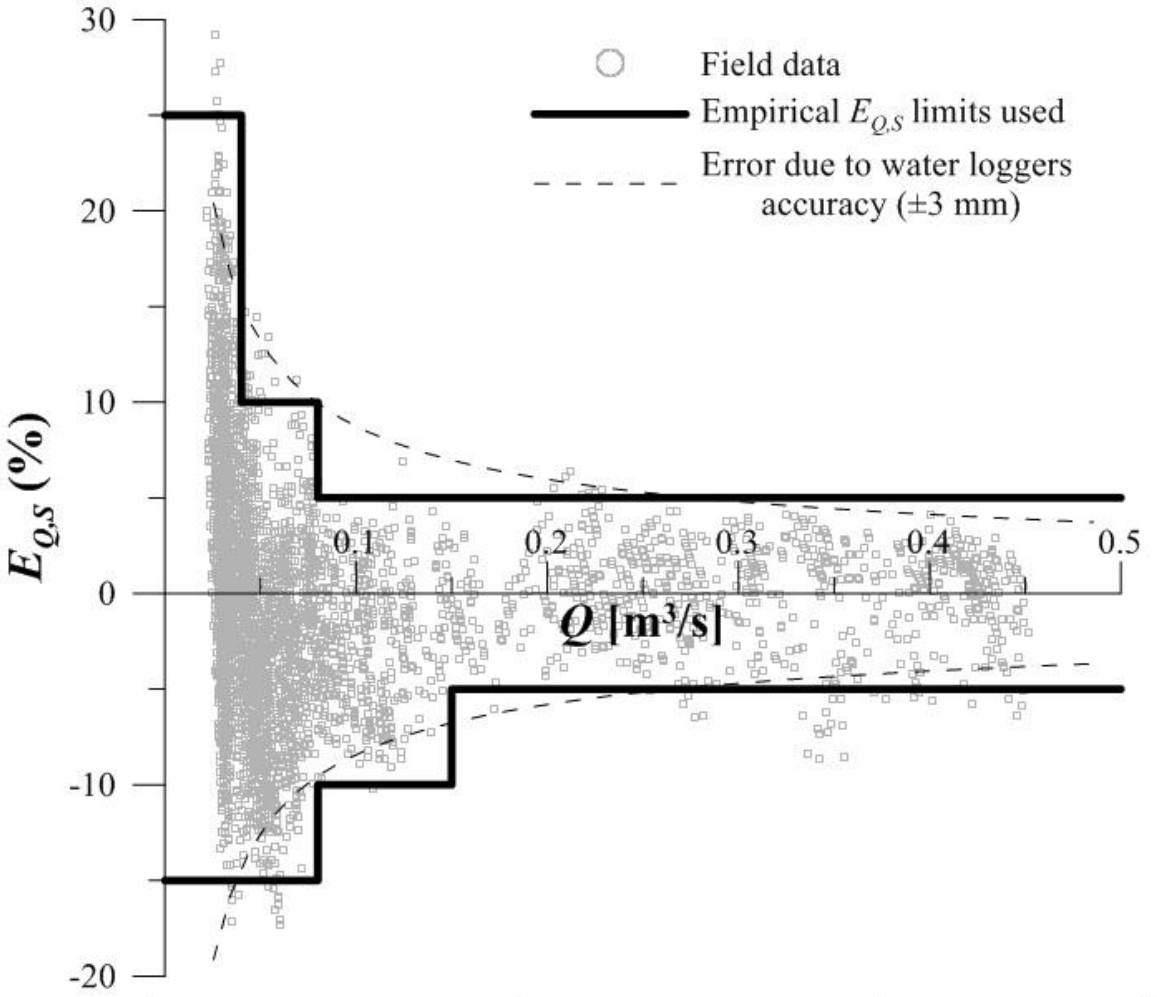

Flow rate range	Systematic err. range	% pts in range
$Q < 0.04$ m^3/s	$-15\% \leq E_{Q,S} \leq 25\%$	99%
0.04 m^3/s $\leq Q < 0.08$ m^3/s	$-10\% \leq E_{Q,S} \leq 15\%$	98%
0.08 m^3/s $\leq Q < 0.15$ m^3/s	$-10\% \leq E_{Q,S} \leq 5\%$	99%
$Q \geq 0.15$ m^3/s	$-5\% \leq E_{Q,S} \leq 5\%$	95%

Figure 4-4: Systematic error, $E_{Q,S}$ as a function of flow rate, specific values are shown in the inserted table. Dashed lines is $E_{Q,S}$ calculated assuming an error in water level equal to the accuracy of the loggers (±3 mm).

4.3.3.2 Duration of the non-vegetated period

Determining the duration of the non-vegetated period was required to discriminate between open water (non-vegetated) and vegetative flow-resistance and for the purposes of using Equations (4-8) to (4-11). These periods were established from both field observations and information concerning plant growth found in literature. In this study, increases in flow resistance were observed to occur when the mean daily water temperature was consistently above 10 °C for approximately 40 days (Figure 4-5), which

compares well to findings from other studies. Trepel and Holsten (2003) found *Sparganium* spp. plants (dominant genus at Reach 1 and 2) growth to commence when water temperatures were above 10 °C. While Trepel and Holsten's threshold was generally reached less than a week after the spring melt, plant growth was observed to start after water had been above 10 °C s for 15-20 days. However, in accordance with findings by De Doncker et al., (2009), plants had limited effects on flow resistance at these early growth stages.

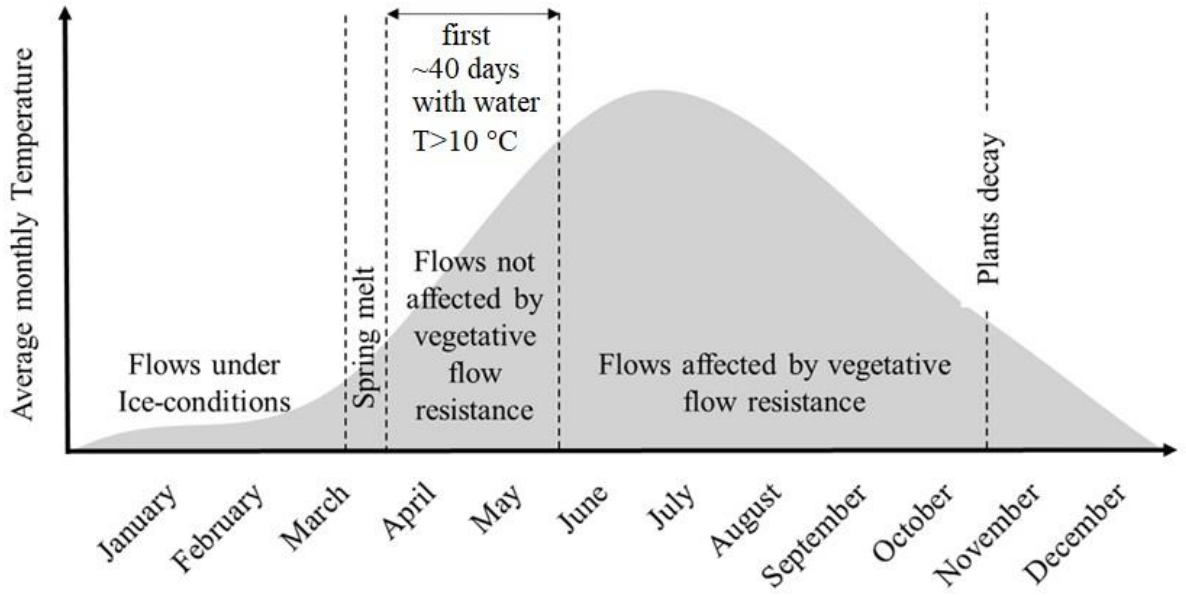

Figure 4-5: Conceptual representation of temperature variations and the different factors affecting flow resistance in a typical year at the study reaches.

4.3.4 Aquatic vegetation surveys

Non-disruptive plant surveys were undertaken over three years to spatially quantify the planform and cross-sectional distribution of aquatic macrophytes over each growing season. The surveying procedure entailed inventorying transects perpendicular to the flow direction. Along each transect, values of streambed elevation, water depth and vegetation height were recorded using a SOKKIA® RTK-GPS unit (±0.01 m). Due to occasional lack of GPS coverage, some points were interpolated based on field observations to infill the reach planform. Point spacing varied along each section according to the heterogeneity of the plants and bathymetry changes – averaging a 0.7 m discretization interval. At each cross-section, blockage width (l_A, Equation (4-5)) and cross-sectional blockage factor, (b_X, Equation (4-6)) were calculated. Equations (4-6) and (4-7) were then used to determine reach-averaged values for L_A and B_X.

A vegetation distribution curve (VDC) was developed for each survey following the procedure outlined by Green (2006). A VDC is a statistical distribution ranking the spatial density of plants measured at the cross-sectional scale. Analogous to a cumulative grain size distribution curve, each VDC has 100 $B_{X,p}$ percentiles where $B_{X,100}$ is the maximum b_X value recorded (i.e.: the cross-section with the highest blockage) and $B_{X,50}$ is the median value (i.e.: half of the cross-sections have higher blockage values). To produce a VDC, the reach length was divided into equally spaced 0.5 m segments. Each segment was assigned a value of b_X determined by linear interpolation from adjacent field-measured b_X values (similar to Green, 2006), and then $B_{X,p}$ values were calculated (Figure 4-6). A similar procedure was obtained for l_A. The standard error of each percentile on the VDC was quantified using a bootstrapping technique with replacement, following the procedures for grain size distribution curves by Rice and Church (1996) and Green (2003) and for VDC's by Green (2006). Results of this analysis are shown in Section 4.4.2.3.

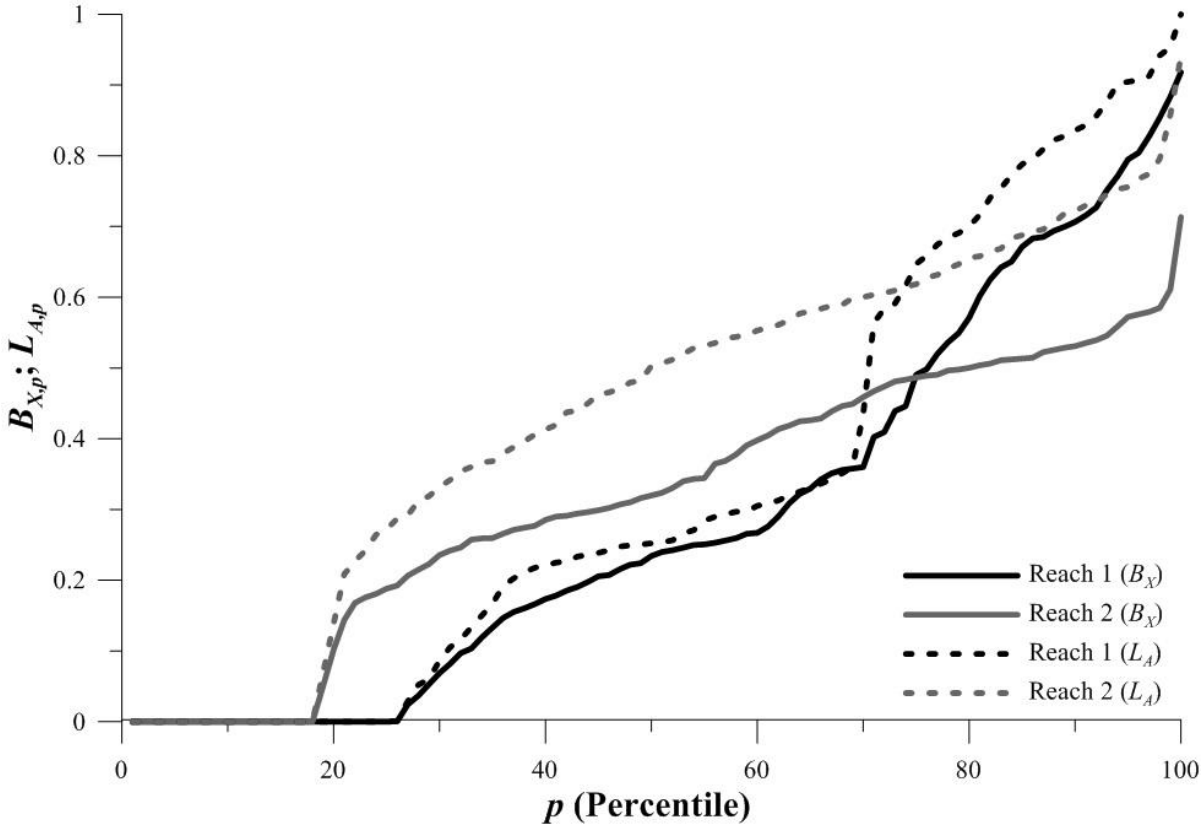

Figure 4-6: examples of vegetation distribution curves for Reaches 1 and 2 obtained using B_X or L_A values. Note: The Percentile was placed on the X-axis for consistency with Green (2006).

4.3.4.1 Temporal interpolation of vegetation spatial distribution metrics

To obtain daily values of B_X, L_A, and VDC percentiles, a 2nd degree polynomial function was fit to all vegetation distributions obtained in each year and at each reach (Figure 4-7). Resulting polynomial fits reflected temporal variations well as $0.75 < R^2 < 0.99$. The initial and final growth limits bounding Figure 4-7 were determined based upon the criteria defined in Section 4.3.3. While previous authors (Van der Heide et al., 2006) showed that plant growth can be exponential, this was not applied here as limited data was available at the beginning of each growing season. It was further assumed that vegetation did not contribute to flow resistance after December 1st of each year (confirmed through field observations) as plants decayed.

Due to the empirical, site-specific nature of these assumptions, these criteria need to be field validated if applied in different climatic regions or in streams where other species are present. It is further noted that these assumptions extrapolate plant growth and are only valid under low flow conditions where flow resistance effects are the greatest. The model does not account for plant bending which may occur under high flows and reduce B_X (e.g.: Sand-Jensen, 2003). As discussed in Section 4.3.3, in this study the analysis was focused on low flow rates and not high flows, which yield higher velocities capable of inducing substantial plant bending.

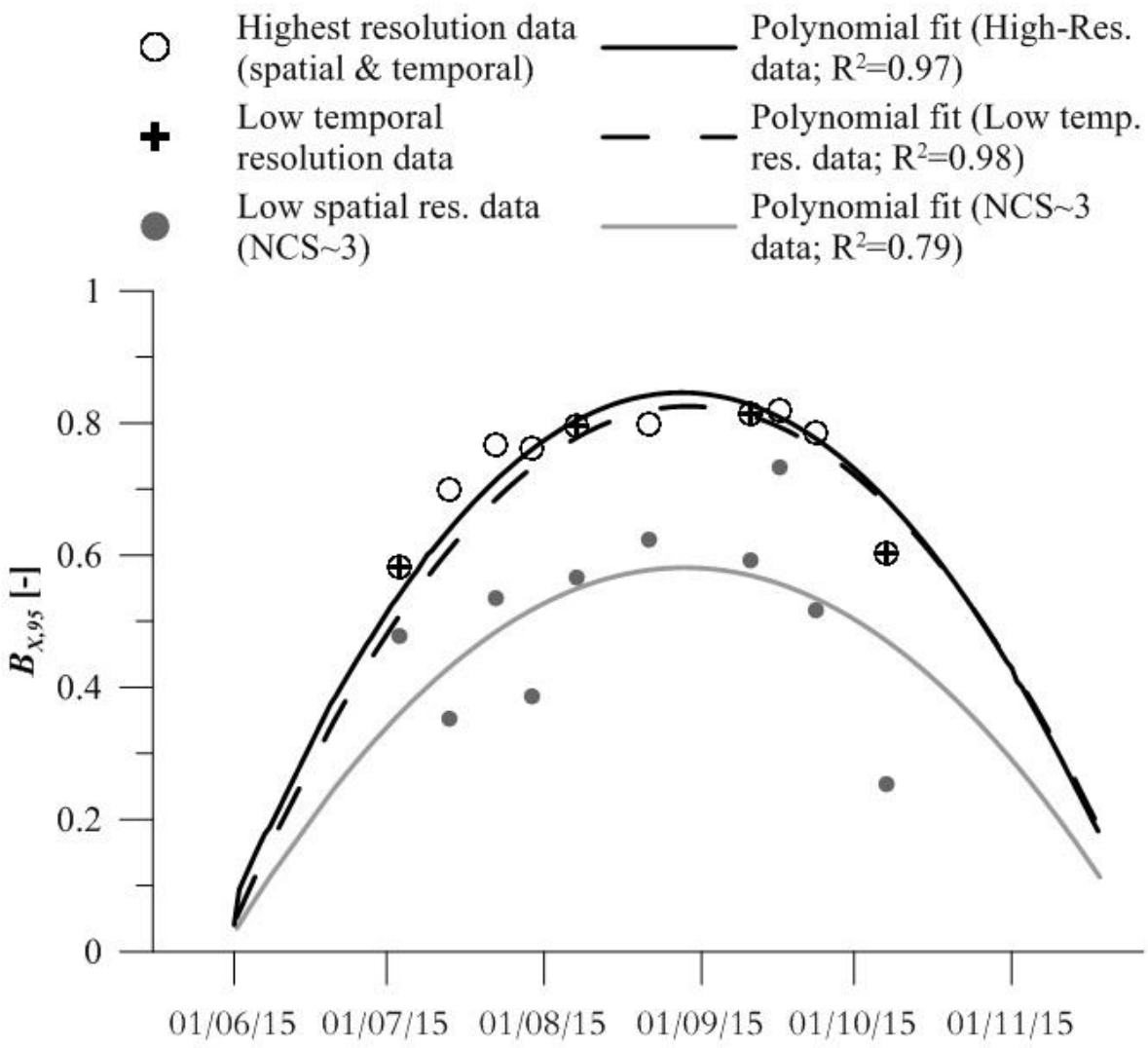

Figure 4-7: Example of polynomial model fit to vegetation metrics (example shown is the blockage factor 95th percentile)

4.3.4.2 Accuracy of vegetation parameters used

The accuracy of vegetation distribution metrics (i.e.: B_X, L_A, VDC percentiles) can be affected by the spatial and temporal sampling frequency (Nepf, 2012) which can be constrained by time and budget. Thus, to assess whether adopting a lower spatial or temporal resolution could affect the calculated values of B_X, L_A and VDC percentiles a sensitivity analysis was undertaken. This involved varying the number of cross-sections, to simulate different sample sizes as follows:

$$E_{p,m} = 100 \left| \frac{\left(B_{X,p}\right)_m - \left(B_{X,p}\right)_N}{\left(B_{X,p}\right)_N} \right| \quad (4\text{-}12)$$

where $E_{p,m}$ is the error of the p-th percentile on the *VDC* using a subset m of the total number of cross-sections available (N) and $(B_X)_{i,m}$ is its corresponding value on the *VDC*. For each subset, a "normalised cross-sectional spacing" (*NCS*) was calculated (roughly based on Samuels, 1990):

$$NCS = \frac{CS_X}{T_W} \quad (4\text{-}13)$$

where CS_x is the average distance between cross-sections, measured along the channel centre-line, and T_W is the channel average top width. Here, an average *NCS* ~ 1, 2 and 3 were used (compared to the average full resolution of *NCS* ~ 0.33). Using these spatial resolutions, $B_{X,p}$ values for each growing season were calculated using the techniques outlined in Section 4.3.4.1 and shown in Figure 4-7.

The temporal resolution was assessed by analyzing two scenarios: one with a reduced number of surveys per year, and one using the whole dataset. The former was achieved so that only one survey per month was present (Figure 4-7), resulting in an average 24-day frequency. Comparatively, the whole dataset had an average 12-day frequency between surveys.

4.4 Field Results

4.4.1 Seasonal effects of aquatic vegetation growth on discharge estimation

At Reaches 1 and 2, changes in water levels at coinciding discharge values (ΔWL) and resulting discharge calculation errors (E_Q) were calculated for the three years assessed, between April and November, following the procedure outlined in Section 4.3.3 (Figure 4-8, Figure 4-9). Increases in ΔWL clearly demonstrate the influence of vegetative resistance on water levels (Figure 4-8, Figure 4-9). At vegetated locations, ΔWL values were close to zero in April and May, as plants were either not present or in early growth stages. ΔWL began to increase in June, reaching its largest values (up to 35 mm) in late August and early September (Figure 4-8, Figure 4-9), when vegetation growth was at its peak and its effect on flow resistance the greatest. As illustrated in Figure 4-8 and Figure 4-9, autumnal plant decay caused ΔWL to decrease (October-November). However, if low flow events persisted into this period, dead plants often accumulated at the downstream end of Reach 1 adding to the backwater effects. This caused an increase in ΔWL as evidenced by the peak in early October 2015 and 2016 (Figure 4-8b, c). Conversely, if autumn flows were large (relative to low flow conditions), for instance in 2014, plants were washed downstream and ΔWL receded to pre-vegetation levels more quickly

(Figure 4-8a). This phenomenon was not observed at Reach 2, which was characterized by a higher water surface slope, allowing macrophytes to flow downstream.

Figure 4-8 and Figure 4-9 demonstrate that not accounting for ΔWL will cause notable errors in discharge estimation, E_Q. These errors were higher at lower flow rates, as a 20-30 mm increase in water level had larger impacts on flow calculation at low stages. This effect was evident when comparing E_Q values obtained within a single year and also between multiple years. For instance, 2014, where the minimum annual flow was 0.055 m^3/s resulted in lower E_Q values relative to 2015 and 2016 which had much lower minimum annual flows (0.016 m^3/s and 0.020 m^3/s, respectively). Therefore, not accounting for additional flow resistance by aquatic plants yielded errors in discharge estimations up to 100%, which generally coincides with the period of low flow.

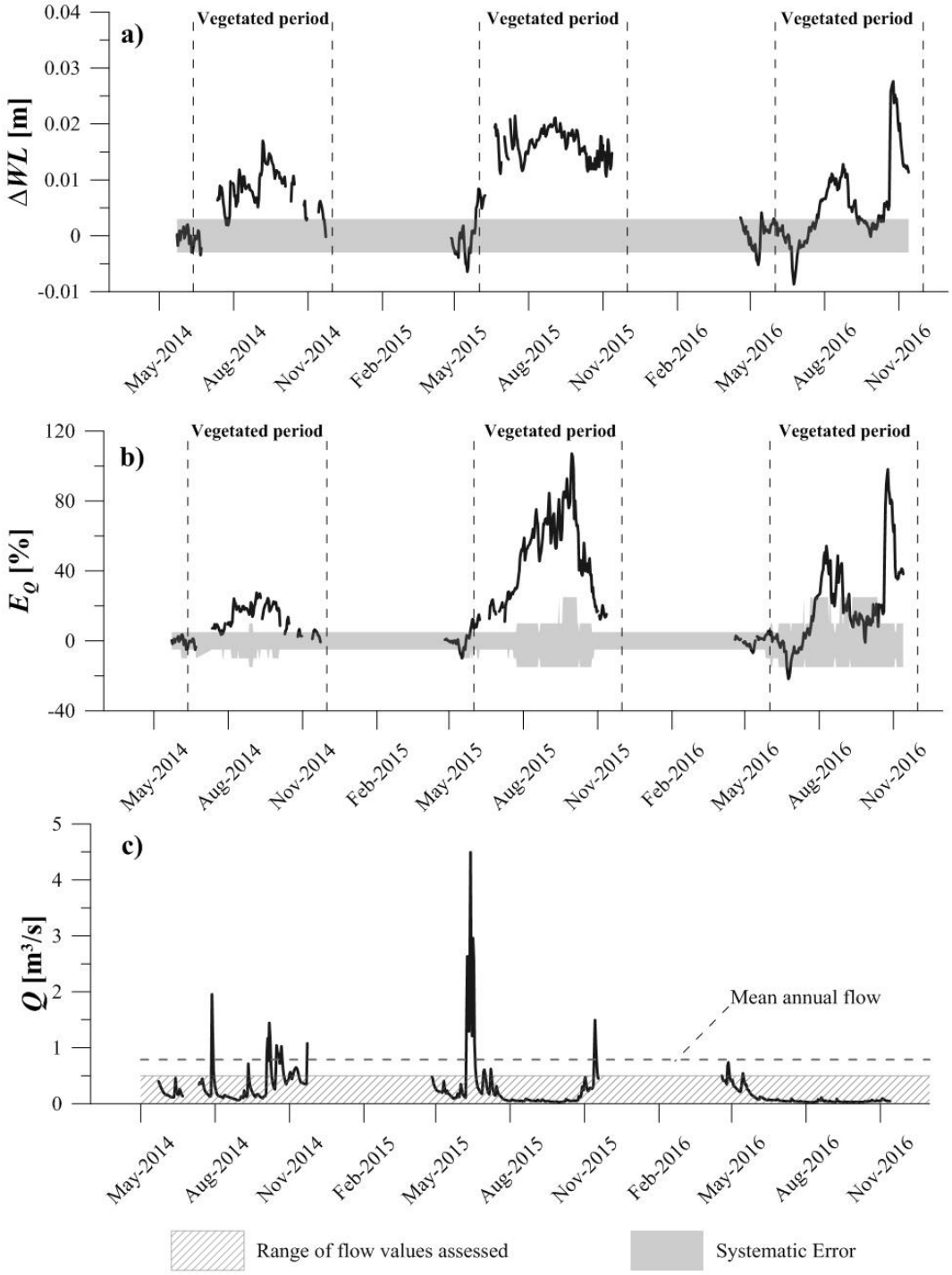

Figure 4-8: Daily values of (a) ΔWL, (b) E_Q and (c) Q at Reach 1 during the period of investigation. Discharge values shown are estimated at the non-vegetated section and as such assumed unaffected by vegetative resistance.

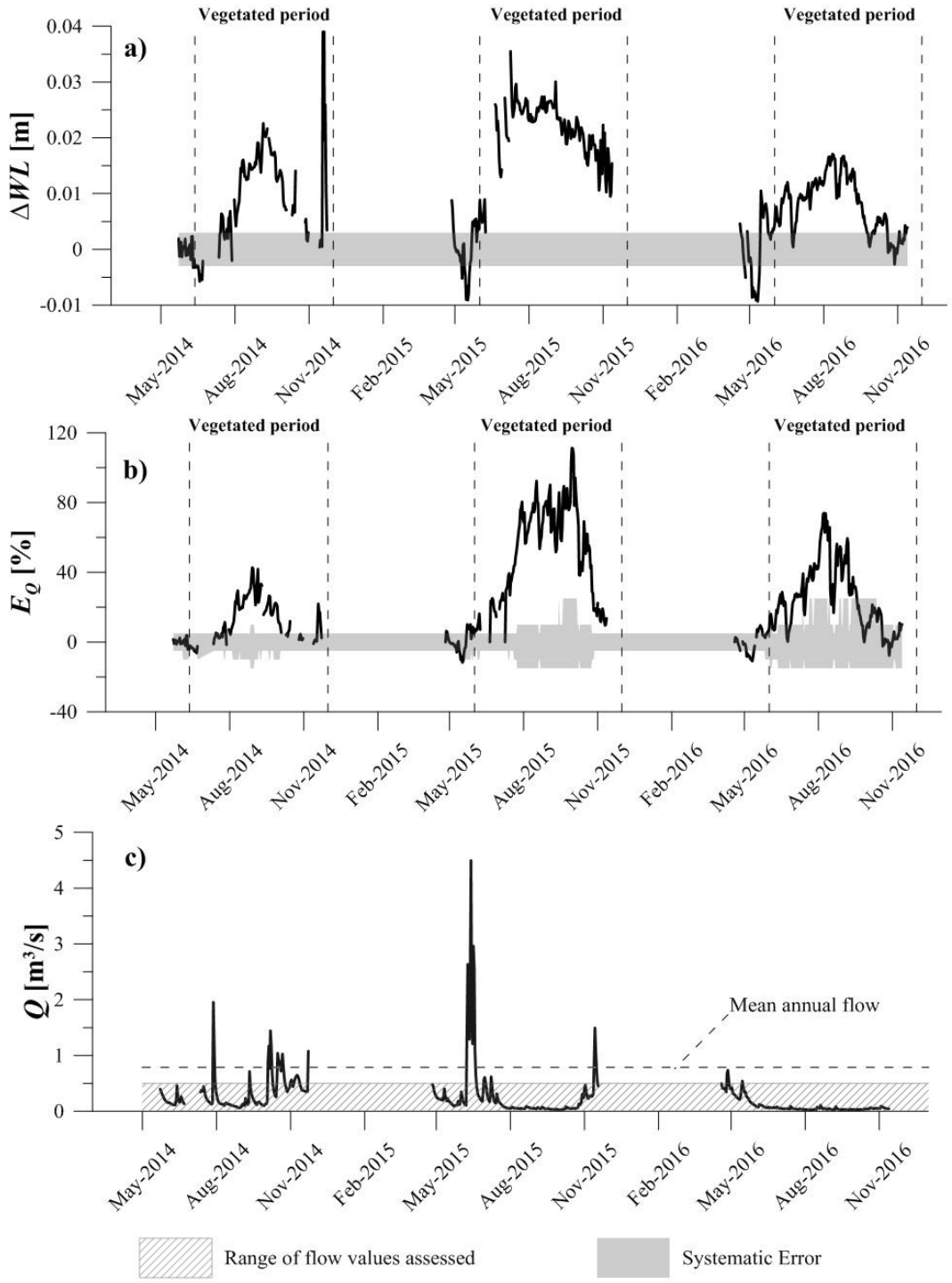

Figure 4-9: Daily values of (a) ΔWL, (b) E_Q and (c) Q at Reach 2 during the period of investigation (note, discharge time series is the same as in Figure 4-8). Discharge values shown are estimated at the non-vegetated section and as such assumed unaffected by vegetative resistance.

4.4.2 Quantifying vegetative flow resistance

4.4.2.1 Flow resistance and plants distribution at the cross-sectional scale

The goal of this section is to better understand the relationship between increases in flow resistance arising from aquatic vegetation and their spatial distribution. To achieve this, the standardized increase in water level (K) (Equation (4-10)) was compared to VDC percentiles calculated for each day when vegetation surveys were undertaken, following the procedure outlined in Section 4.3.4 was followed. Correlation scores between $B_{X,p}$ and K significantly increased for percentiles above 80%, while below this threshold, R^2 noticeably decreases, approaching zero for the median ($B_{X,50}$) value (Figure 4-11). Higher percentiles on the VDC represent a more densely vegetated cross-section in the reach. Thus, this result confirms observations by Green (2006): flow resistance is more strongly related to higher percentiles of VDC, just as in gravel bed rivers flow resistance is often found to be more related to higher percentiles on a grain distribution than the median (e.g.: Bray, 1982; Millar, 1999). Similar to a grain-based roughness scenario, low R^2 found between the bottom 50 percentiles on the VDC and K suggest that lower percentiles impart nominal effects upon flow resistance. Axiomatically, the results demonstrate that reach segments characterized by the highest blockage factors result in the greatest impacts on flow resistance and therefore, flow measurement accuracy, if stage-discharge techniques are employed.

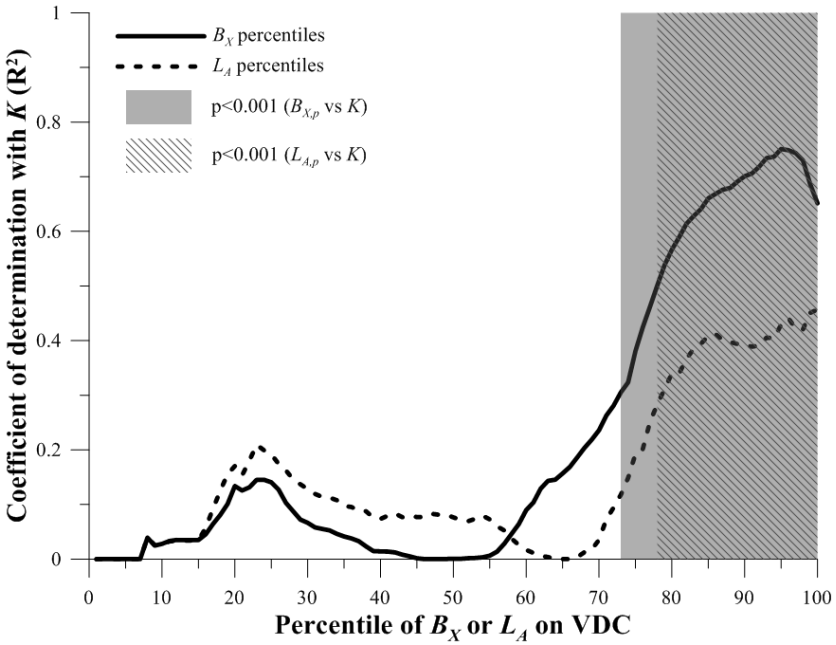

Figure 4-10: Coefficient of determination (R^2) between K and percentiles of B_X or L_A for relationships of the form $K=a[exp(bB_{X,p})]$ or $K=a[exp(bL_{A,p})]$. Statistically significant (99.9% level) relationships are highlighted.

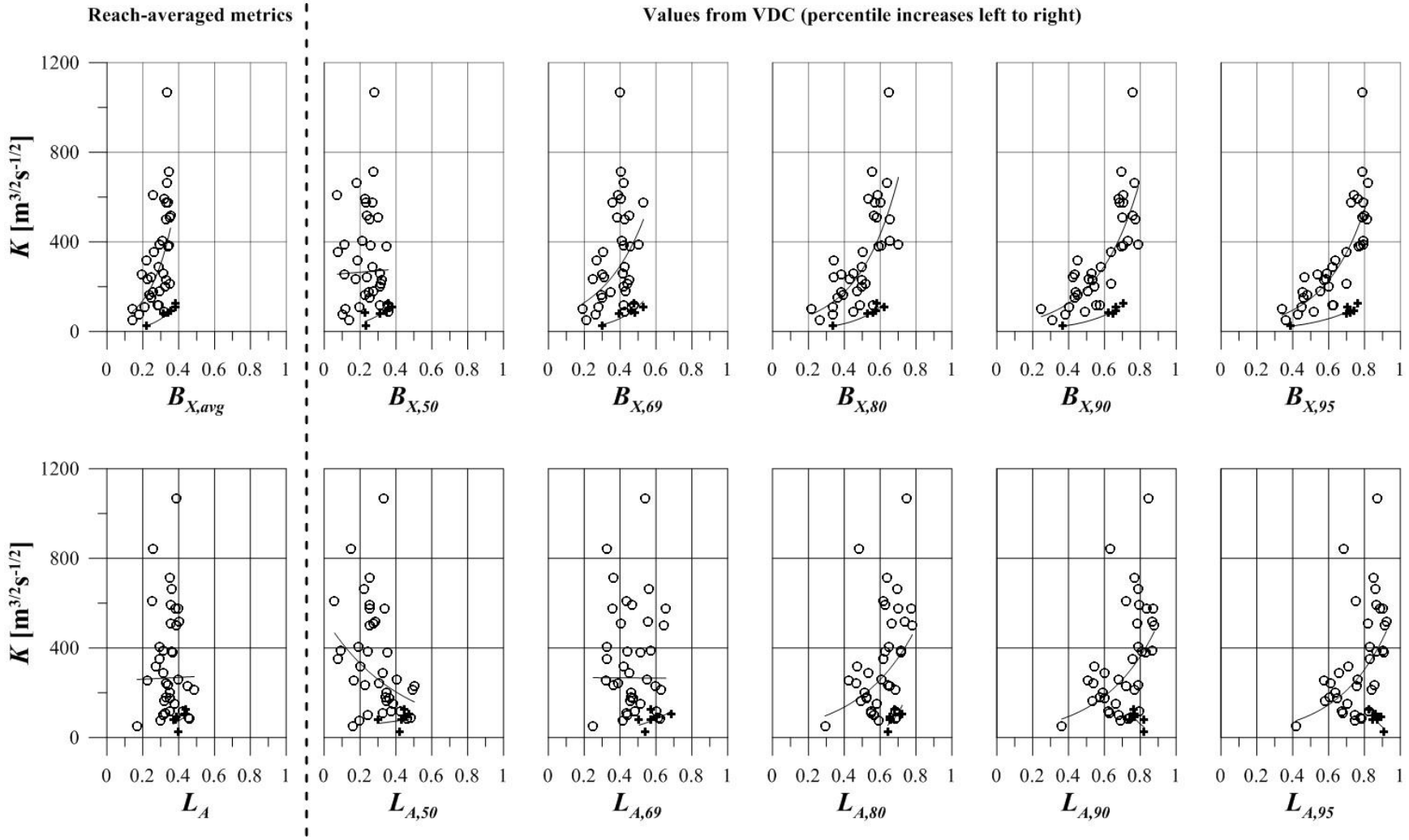

Figure 4-11: Relationship between K and different percentiles of b_X and l_A

The 95th percentile ($B_{X,95}$) of the VDC's (i.e. the cross-section with higher blockage than 95% of the remaining dataset) was found to have the highest correlation with K (as evidenced in Figure 4-10 and Figure 4-11). This result implies that flow resistance can be calculated from $B_{X,95}$, thus an exponential equation ($R^2 = 0.75$, $p < 0.001$) was fit to the dataset, resulting in:

$$K = 16.7e^{4.36B_{X95}} \quad (4\text{-}14)$$

A sub-set of the data obtained at Reaches 1 and 2 was found to trend differently than the rest of the dataset, especially for $80 < p < 100$ (crosses in Figure 4-11). In this case, the following equation was used:

$$K = 4.71e^{4.16B_{X95}} \quad (4\text{-}15)$$

All points in this sub-dataset were obtained within one single season at Reach 2. During this season the width of the hydraulic control section at the reach downstream limit was reduced due to the presence of a gravel bar colonized by riparian vegetation. At low flow, the riffle width and crest elevations define upstream water surface elevations by establishing a hydraulic control, (e.g. Herschy, 1995) and because of the presence of this feature the effects of vegetation on flow resistance were attenuated. This bedform was largely reduced in size in the following years and its effects upon flow resistance were not observed. Specifically, this finding implies that seasonal changes in cross-sectional width or presence of depositional features add further complications to the estimation of vegetative flow resistance as the width of the downstream hydraulic control, with respect of the average reach width, may impact how macrophytes affect the overall channel roughness. It should be noted that changes in cross-sectional width and presence of depositional features are common when aquatic and riparian plants are present as macrophytes are known to affect channel morphology (Corenblit et al., 2007; Gurnell 2014).

Cross-sectional blockage factor metrics employed in other studies such as $B_{X,50}$ and B_{X69} (Green, 2005a; 2006) were not found to be related to K in this study. The reach-average blockage factor B_X (Green, 2005a; Nikora et al., 2008) returned a significant correlation (R^2=0.42, p<0.001), although with lower R^2 than all percentiles above the 75th. It should be noted that $0.14 \leq B_X \leq 0.35$, while $0.34 \leq B_{X95} \leq 0.82$ as absence of vegetation in parts of the reach skewed B_X towards lower values. In such scenarios, it can be argued that a reach-averaged blockage factor can significantly underestimate the impact that vegetation blockage actually has on flow resistance. Indeed, if a highly-blocked cross-section is present, its effect on flow resistance outweighs the absence of vegetation in other parts of the reach. This result could be attributed to the use of different metrics (Section 4.3.3), however no correlation was found using n and B_X or n and any percentile on the VDC whether n was calculated with methods found in literature (Table 4-1) or measured data (Equation (4-11)).

While $B_{X,95}$ yielded the highest correlation with K, the scatter amongst data points increases when $B_{X,95}$ > 0.7 (Figure 4-11). Results are in agreement with a study by Luhar and Nepf (2013), which used data from Green (2005a) and Nikora et al., (2008) and hypothesized that for higher blockage (B_X > 0.8) flow resistance could not be expressed solely as a function of cross-sectional blockage as other factors affecting flow resistance arise. These were noted to relate to drag forces within individual plants and plant density, which act on a significantly smaller scale than drag forces caused by plant patches. In turn, these are directly related to the blockage factor. Moreover, flow through plants, likely to occur at high vegetation densities (Nepf, 2012) is similar to that found in wetlands where it may transition to the laminar regime (Kadlec, 1990). In these cases, accurate knowledge of plants hydrodynamics as well as quantification of flow patterns among plant patches is needed (Luhar and Nepf, 2013).

In this study, cross-sectional blockage was found to be well correlated to flow resistance, but when blockage was extremely high, secondary effects, related to drag at the individual plant scale, likely became additional contributing factors to flow resistance. Spacing between plants (or canopy porosity, as in Nepf, 2012), may also affect values of b_X as well as turbulence, however as the focus of this study was on large scale patches, canopy porosity was not measured and not believed to affect the results at the reach scale. In summary, findings from this study further reinforce the need for accurate knowledge of plant hydrodynamics in addition to spatial distribution to support more accurate estimates of vegetative flow resistance as noted by Luhar and Nepf (2013).

4.4.2.2 Flow resistance and plants distribution at the longitudinal scale

The relationship between blockage-width percentiles ($L_{A,p}$, Figure 4-6) and the normalized water level increase (K) was also evaluated. Similar to $B_{X,p}$, using data from each survey, the highest correlation scores were found between the highest percentiles of $L_{A,p}$ and K (Figure 4-10), although with overall lower R^2 values than those obtained for $B_{X,p}$. As differences between R^2 values for the five highest percentiles ($L_{A,95} - L_{A,100}$) were minimal, it was decided to use a relationship between $L_{A,95}$ and K (R^2 = 0.43; $p < 0.001$) as the former is directly related to $B_{X,95}$. The equation obtained is the following:

$$K = 13.3e^{3.92L_{A,95}} \quad (4\text{-}16)$$

This finding is, to some extent, comparable to the results by Green (2005a) and Nikora et al., (2008), who found L_A and flow resistance to be related although with lower R^2 values than B_X.

The correlation found between K and $L_{A,95}$ is related to the inherent relationship between values obtained at single cross sections (b_X and l_A) which were found to be strongly correlated with each other (R^2=0.82, p<0.001, Figure 4-12). Specifically, b_X and l_A are directly proportional and the latter is generally higher than the former, as most points plot to the left of the 1:1 line (Figure 4-12). The few

$b_X > l_A$ occurrences correspond to instances where vegetation was present only in the deepest part of the cross-section.

Despite the overall correlation, deviations between b_X and l_A were observed to be significant in some instances. For instance, a cross-section that has vegetation across its entire width yields l_A=1 while $0.4 \leq b_X \leq 1$ (Figure 4-12) as macrophytes have different degrees of submergence. By definition, l_A is insensitive to the degree of vegetation submergence as it only includes two-dimensional planometric information. As such, for the purposes of estimating flow resistance, the blockage width and its related metrics (L_A, L_{A95} etc.) are less suitable than the cross-sectional blockage factor and its related metrics (B_X, B_{X95} etc.). This happens because the former group is not capable of capturing the complexity of instream vegetation spatial distribution as thoroughly as the latter. Nepf (2012) noted that mechanisms that influence momentum balance and exchange between flow and plants are related to drag and therefore flow resistance. In vegetated channels, these phenomena act in three dimensions (Marjoribanks et al., 2014; 2017) and are affected by the shape and distribution of vegetation patches (Luhar and Nepf, 2013; Marion et al., 2014). In summary, the lower correlation score between l_A-related metrics and K found here confirms results obtained by Green (2005a) and Nikora et al., (2008). These results further reinforce that, where possible, plants cross-sectional distribution should be used instead of longitudinal distribution to evaluate flow resistance.

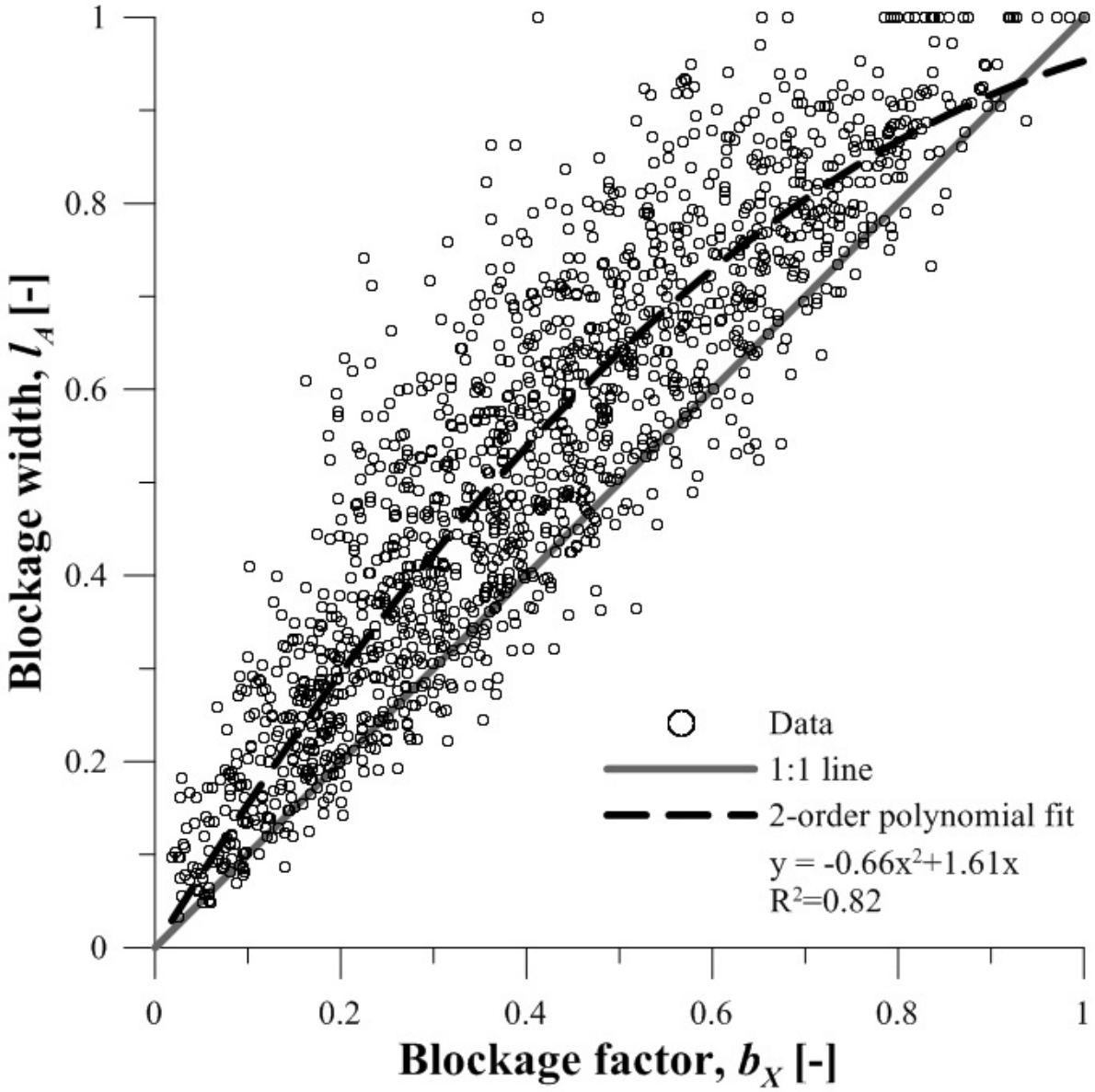

Figure 4-12: Relationship between blockage factor (b_x) and blockage width (l_A) for single cross-sections. Cross-sections with no vegetation were removed from the sample as it would have skewed R^2 value, however as for l_A=0, b_X=0, the best fit function was forced to pass through the axes origin.

4.4.2.3 Accuracy of vegetation spatial distribution metrics

As sampling errors (both in systematic and random forms) may have affected the correlations found between B_{Xp} and flow resistance, the accuracy of the former was assessed. This was achieved by calculating the standard error values (*SE*) of B_{Xp} (Figure 4-13) using a bootstrapping technique (Rice and Church, 1996). On average $0.015 \leq SE \leq 0.025$, except for percentiles below 20% where *SE* tended toward zero due to the small values of $B_{X,p}$ (Figure 4-13). In some instances, *SE* was noted to be affected by vegetation heterogeneity. Gradually varying vegetation distributions yield evenly sloped VDCs, and

thus, low *SE* (Figure 4-14a). Conversely, heterogeneous vegetation distributions yielded more abrupt slope changes along VDC's (Figure 4-14b) and higher *SE* values. If the latter case occurs, B_{Xp} values will be less accurate than those obtained for a gradually changing distribution and large sample sizes may be needed to adequately characterize vegetation distribution on a given study reach. Overall, these results are in agreement with those obtained by Green (2003) for grain size distribution curves.

In this study, changes in vegetation spatial distribution were mostly gradual, as evidenced by the large majority of B_{Xp} exhibiting low standard errors (Figure 4-13). Higher errors were observed in one instance, in early autumn, when vegetation was concentrated in a small part of Reach 1, yielding a higher sloped VDC (Figure 4-14b) generating larger *SE* values for the largest percentiles. In summary, the statistical analysis undertaken shows that sampling errors did not affect B_{Xp} data and consequently these are not expected to affect the accuracy of equations involving B_{Xp} percentiles presented earlier (e.g. Equations (4-14), (4-15), and (4-16)).

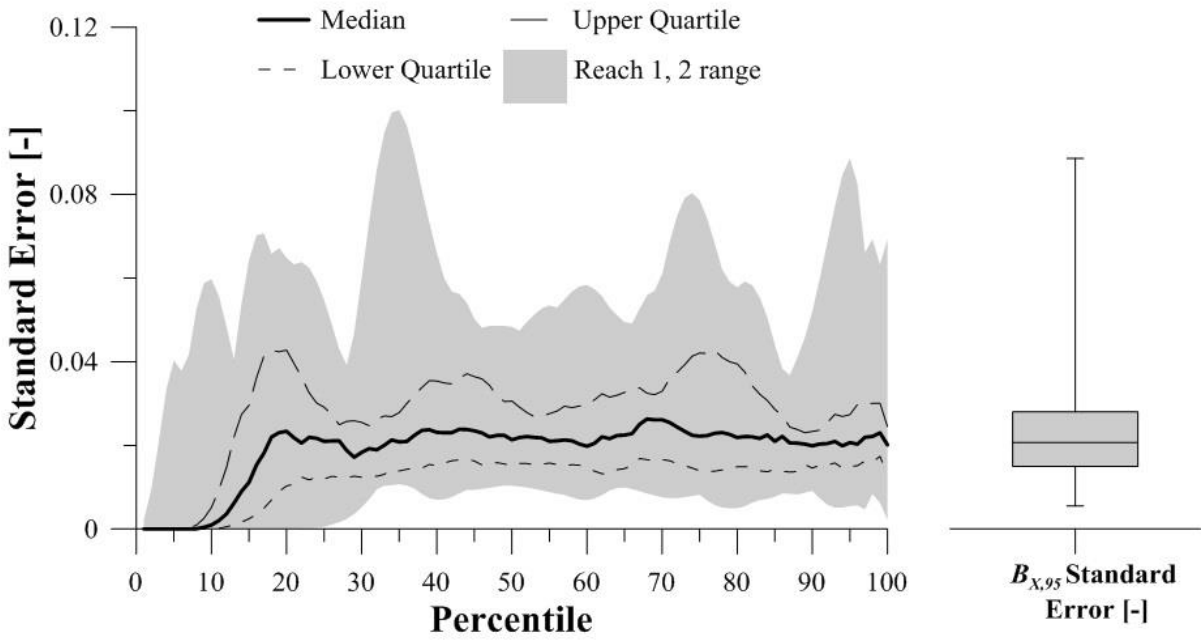

Figure 4-13: Standard error of $B_{X,p}$

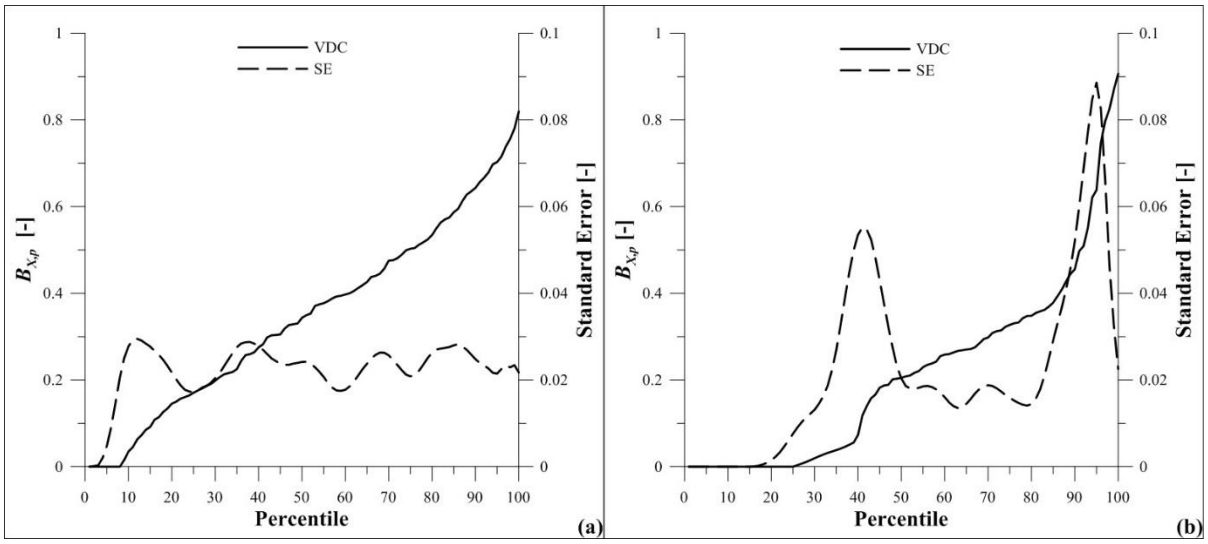

Figure 4-14: Variation of standard error of $B_{X,p}$ for two different VDC's.

4.5 Correction of discharge estimates

4.5.1 Using past approaches

For the purposes of comparison, Manning's *n* was calculated from vegetation and grain size data collected at Reaches 1 and 2 of the current study and compared to *n* calculated from previous approaches (Table 4-1). Large discrepancies were noted between calculated and observed *n* values and in most cases the former notably underestimated the latter (Figure 4-15). Huntington and Whitehead's (1992) method overestimated flow resistance as *n* in this case is indirectly proportional to the product of velocity and hydraulic radius, *VR* (Table 4-1), which decreases significantly under low flow conditions. Conversely, equations by Champion and Tanner (2000), Green (2005a) and Nikora et al., (2008) underestimated field-measured *n* values especially at low flows.

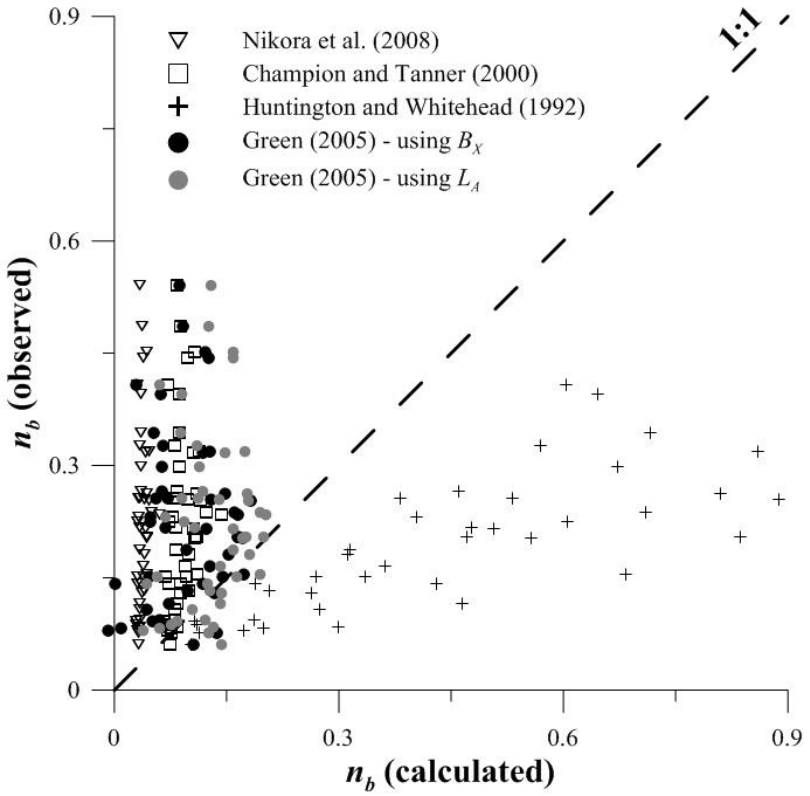

Figure 4-15: Comparison between calculated and measured values of *n* with equations using l_A (gray points) and with equations using b_X (black points)

This result was found related to the systematic underestimation of the base roughness conditions (Figure 4-16a) which was evident by comparing calculated n_b, using equations listed in Table 4-1 (i.e. grain size data) with observed n_b, determined using measured discharge and water level data (Equation 4-3). Large underestimations were obtained using constant values of n_b which do not account for the indirect

proportionality between n_b and Q shown in Figure 4-16b. The latter result is in agreement with results obtained by Bathurst (1985), Hicks and Mason (1991) and Ferguson (2010, 2013 and 2014) who showed how n values increase as Q decreases in various streams. Nevertheless, even variable base roughness formulae, such as Green (2005a) significantly underestimated flow resistance (Figure 4-16a) as their dependence on discharge is relatively minimal (Figure 4-16b). This result may be related to the different methods to delimit reaches used by Green (2005) and Nikora et al. (2008), compared to those presented in this study, or other site-specific factors. For instance, it is possible that the aforementioned studies did not target low flow conditions, and as such their roughness calculations may reflect higher flow scenarios. Given these discrepancies, and the lack of correlation between n_v and vegetation distribution metrics (Section 4.5.1), formulae listed in Table 4-1 were deemed not suitable to calculate discharge under vegetative flow roughness conditions at the study reaches and a new method was developed.

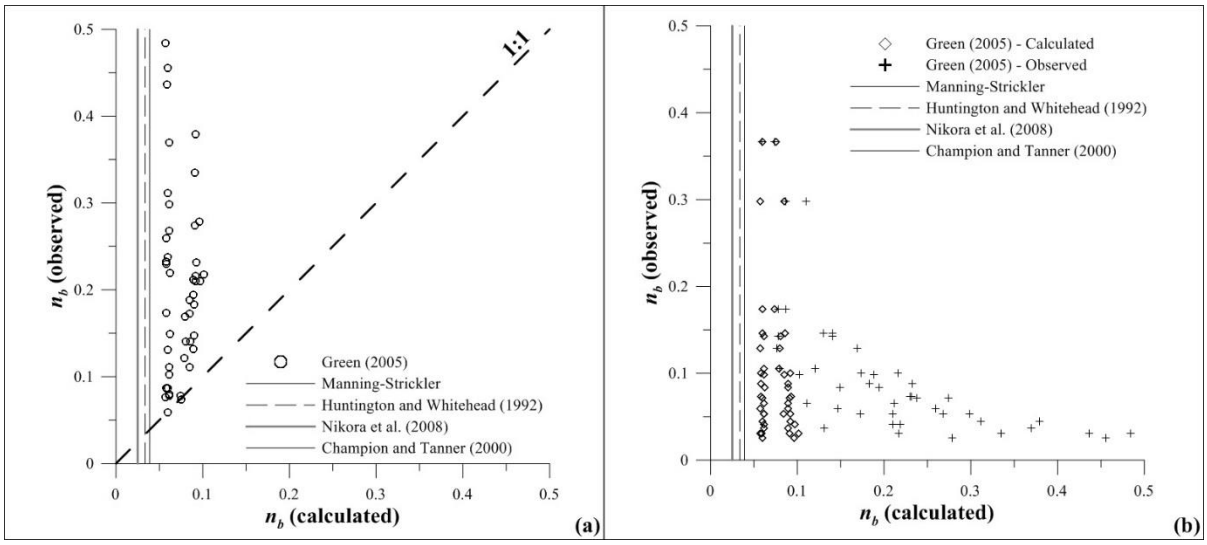

Figure 4-16: Comparison between calculated and measured base roughness using methods found in literature (a), dependence of base roughness on discharge (b) n_b values for Huntington and Whitehead (1992), Champion and Tanner (2000) and Nikora et al., (2008) were obtained setting either $B_X=0$ or $L_A=0$ in their respective equations for n.

4.5.2 Proposed correction procedure

A new procedure aimed at calculating discharge was developed based upon the findings displayed in Section 4.4.2 where K, the normalized increase in water level due to vegetation, was found proportional to $B_{X,95}$. By combining Equation (4-10) with Equation (4-14) the following expression for ΔWL is found:

$$\Delta WL = \frac{KQ^{\beta}S_w^{\beta}}{T_W^{\alpha}} = \frac{16.7e^{4.36B_{X95}}Q^{\beta}S_w^{\beta}}{T_W^{\alpha}} \quad (4\text{-}17)$$

Using $B_{X,95}$ values for each day obtained through interpolation (Figure 4-7) to correct field-measured water levels (WL), flow estimates were corrected for each seasonal hydrograph (Figure 4-17). Using this procedure, two unknowns are present (Q and ΔWL) and they were determined by solving the following system of equations:

$$\begin{cases} \Delta WL = \dfrac{16.7e^{4.36B_{X95}}Q^{\beta}S_w^{\beta}}{T_W^{\alpha}} \\ Q = f_n(WL_b) = f_n(WL - \Delta WL) \end{cases} \quad (4\text{-}18)$$

Where the second formula is equivalent to Equation (4-1).

Using the correction procedure proposed here, errors in discharge estimation caused by aquatic vegetation at Reaches 1 and 2 were significantly reduced (Figure 4-17), except for a relatively short period of time when backwater caused by accumulation of dead plants at the end of Reach 1 (as discussed in Section 4.4.1) occurred (Figure 4-17b, c). The procedure outlined in this section measures the spatial distribution of live macrophytes and as such, it is not capable of accounting for the accumulation of dead specimens. As this phenomenon, and the associated increase in backwater, only persisted for a few days, it was considered negligible when the whole flow record is considered.

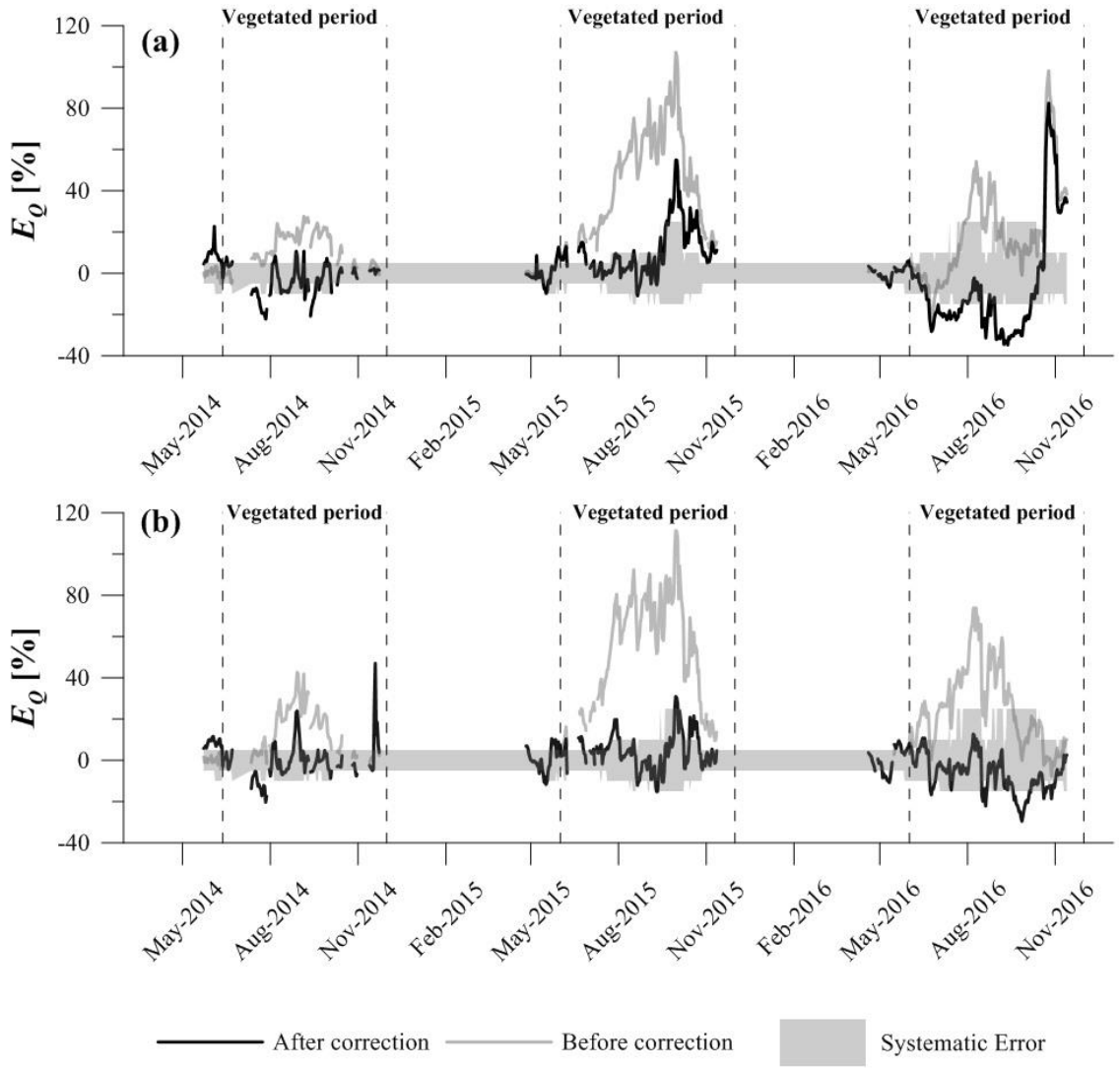

Figure 4-17: Time series of E_Q after correction procedure at (a) Reach 1 and (b) Reach 2

4.5.2.1 Implications for water management

To provide a more comprehensive understanding of the implications of these results for water management, the observed cumulative discharge volume at both reaches for each of the three years were determined. Results were then compared to calculated volumes before and after the correction procedure discussed above was applied (Figure 4-18). Clearly, the annual curves representing the observed and the non-corrected volume distribution begin to diverge when the vegetated period begins. The discharge overestimations could have significant implications on a water management perspective, as they could lead to allowing excessive water takings. In turn this could cause undesirable scarcity of water to downstream communities and damage aquatic ecosystems (Rolls et al., 2012).

Conversely, the corrected cumulative volume distribution mirrors the observed volume well, highlighting the benefits of the correction procedure in terms of discharge estimation on a yearly basis.

Benefits of this correction procedure are also evident when the average daily error is calculated. At Reach 1, the overestimation is reduced from 1,481 m^3/day to 67 m^3/day (a 95% reduction) and at Reach 2 from 1632 m^3/day to 20 m^3/day (a 99% reduction). All of these results confirm that the correction procedure outlined here is capable of correcting open-water rating curves affected by aquatic vegetation.

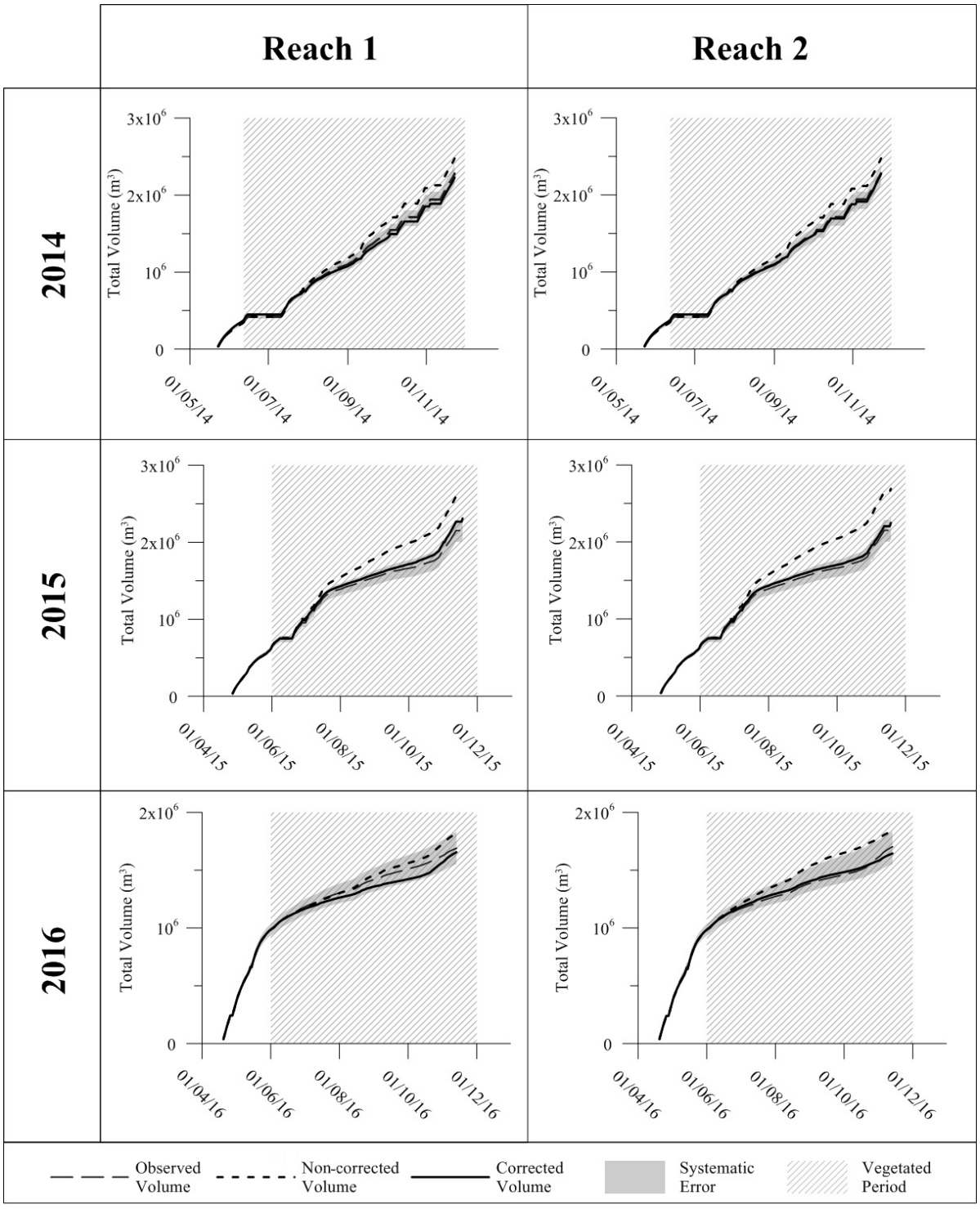

Figure 4-18: Cumulate discharge volume over the three years at both study reaches

Table 4-3: Summary of total discharged volume at Moorefield Creek (Reach 1 and 2), over the three periods investigated (520 days total). Observed volume, based on the non-vegetated site was 6.158 million m^3.

	Reach	Total Volume (10^3 m^3)	Volume Error (10^3 m^3)	Error (%)	Average Daily Volume Error (10^3 m^3)
Not corrected	**1**	6,928	769.91	12.50	1.481
	2	7,007	848.47	13.78	1.632
Corrected	**1**	6,193	34.83	0.57	0.067
	2	6,170	11.24	0.18	0.022

4.5.2.2 Effect of spatial and temporal resolution

To simulate a scenario where limited time (or budget) to collect vegetation spatial distribution is available, the proposed correction procedure was undertaken using reduced datasets, following the sensitivity analysis outlined in Section 4.3.4.2. Here, four different spatial resolutions and two different temporal resolutions were tested (Section 4.3.4.2., Table 4-4) and the impact of these changes on the total volume calculations were calculated.

Table 4-4: Summary of total discharged volume at Moorefield Creek (Reach 1 and 2), over the three periods investigated (520 days total). Observed volume, based on the non-vegetated gauge site was 6.158 million cubic metres.

	Reach	Total Volume (10^3 m^3)	Volume Error (10^3 m^3)	Error (%)	Average Daily Volume Error (10^3 m^3)
Corrected (avg. NCS ~ 1) [(a)]	**1**	6,325	166.62	2.71	0.320
	2	6,189	30.77	0.50	0.059
Corrected (avg. NCS ~ 2) [(a)]	**1**	6,398	239.45	3.89	0.460
	2	6,332	173.79	2.82	0.334
Corrected (avg. NCS ~ 3) [(a)]	**1**	6,660	502.14	8.15	0.966
	2	6,427	268.84	4.37	0.517
Corrected, low temporal resolution[(b)]	**1**	6,205	46.50	0.76	0.089
	2	6,234	75.21	1.22	0.145

(a) maximum temporal resolution used; (b) maximum spatial resolution used

The importance of achieving sufficient spatial resolution while sampling is evident as the *NCS*~3 scenario (i.e. approximately 9 times fewer cross-sections) still yielded a noticeable overestimation of discharge (Table 4-4). As expected, the error decreased as resolution increased: using one-third of the cross-sections originally surveyed, (*NCS*~1) the overestimation was reduced to 2.71% at Reach 1 (a 78% decrease) and 0.2% at Reach 2 (a 96% decrease). Conversely, temporal resolution did not impact the accuracy of the correction: one survey per month was sufficient to reduce the overestimation to 0.8% (a 94% decrease) at Reach 1 and 1.2% (a 90% decrease) at Reach 2 (Table 4-4).

Variations between results are related to differences between the polynomial curves used to determine daily $B_{X,95}$ values (Section 4.3.4.1). The curve obtained for low temporal resolution mirrors the maximum resolution data better than the one obtained with low spatial resolution (Figure 4-7). Therefore, as similar $B_{X,95}$ values are obtained using low or high temporal resolution, similar performances of the correction procedure are expected. Furthermore Figure 4-19 clearly shows that $B_{X,95}$ is affected by spatial resolution. On average, to achieve an error below 10% for $B_{x,95}$, values of *NCS* below 0.65 are required and when *NCS*>3 errors quickly rise above 20%.

From an application point of view, these results suggest that, if limited time is available, few vegetation surveys over the summer may be sufficient to capture the necessary information about plant growth and decay, as long as the spatial resolution of vegetation surveys is not minimized. However, in the presence of plants which may be able to survive over the winter, this protocol will likely have to be re-validated and modified.

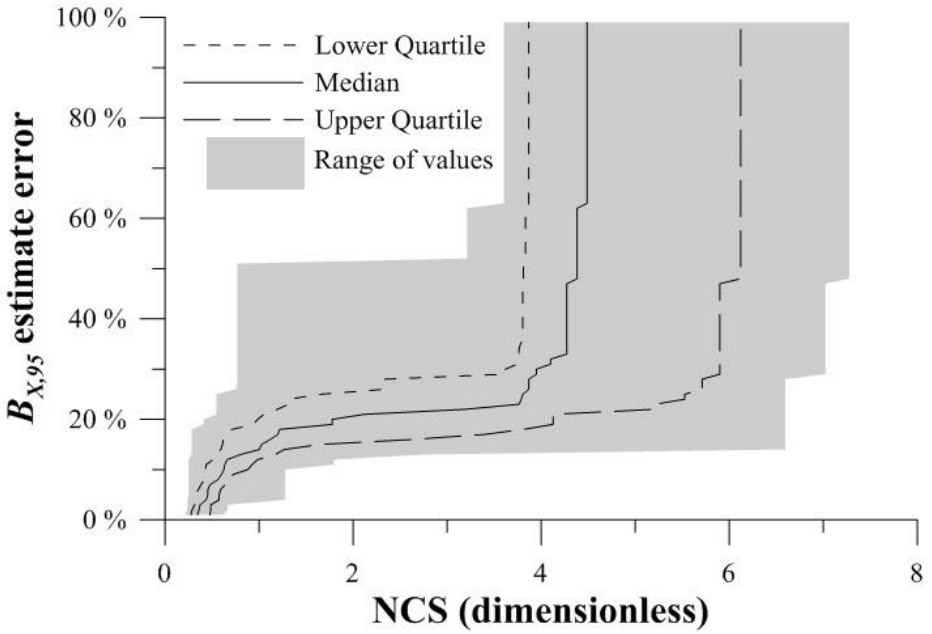

Figure 4-19: $B_{X,95}$ error as a function of normalized cross-sectional spacing (*NCS*)

4.6 Independent validation at other sites

To validate the method proposed herein, the correction procedure outlined in Section 4.5.2 was applied to three other reaches. At these sites, flows calculated with conventional open-water rating curves are often overestimated due to vegetation growth as determined by field observations and communications with agency personnel. Due to budgetary constraints, the correction procedure was applied for a single day rather than for the entire season as in the cases of Reaches 1 and 2.

Discharge overestimations were confirmed by comparing flow measurements (using the methods outlined in Section 4.3.2) to the discharge calculated with the open-water rating curve provided by the reporting government agency responsible for stream-gauging each site. Calculated error, E_Q, was found to range between 6% and 41% (Table 4-5). To reduce this error, the method proposed in Section 4.5.2 was applied.

Measures of T_W and S_W were obtained using the RTK-GPS unit described in Section 4.3. Identical methods to those used in Reaches 1 and 2 (Section 4.3.4) were adopted to inventory and analyze aquatic vegetation to obtain a VDC for each site and calculate corresponding standard errors (Figure 4-20 and Figure 4-21). *SE* values obtained at Reaches 3-5 were lower than those for Reaches 1 and 2. This was mirrored by their respective VDCs, which covered a smaller range in $B_{X,p}$ values at Reaches 3-5. Consequently, calculated values of the *SE* were lower at the validation sites. Similar to Reaches 1 and 2, it was confirmed that more dense vegetation had larger impacts on flow resistance as E_Q is directly proportional to B_{X95} (Table 4-5). Consequently, the method proposed in Section 4.5.2, undertaken by applying Equation (4-18) was capable of correcting *Q* estimates at all three sites assessed (Table 4-5).

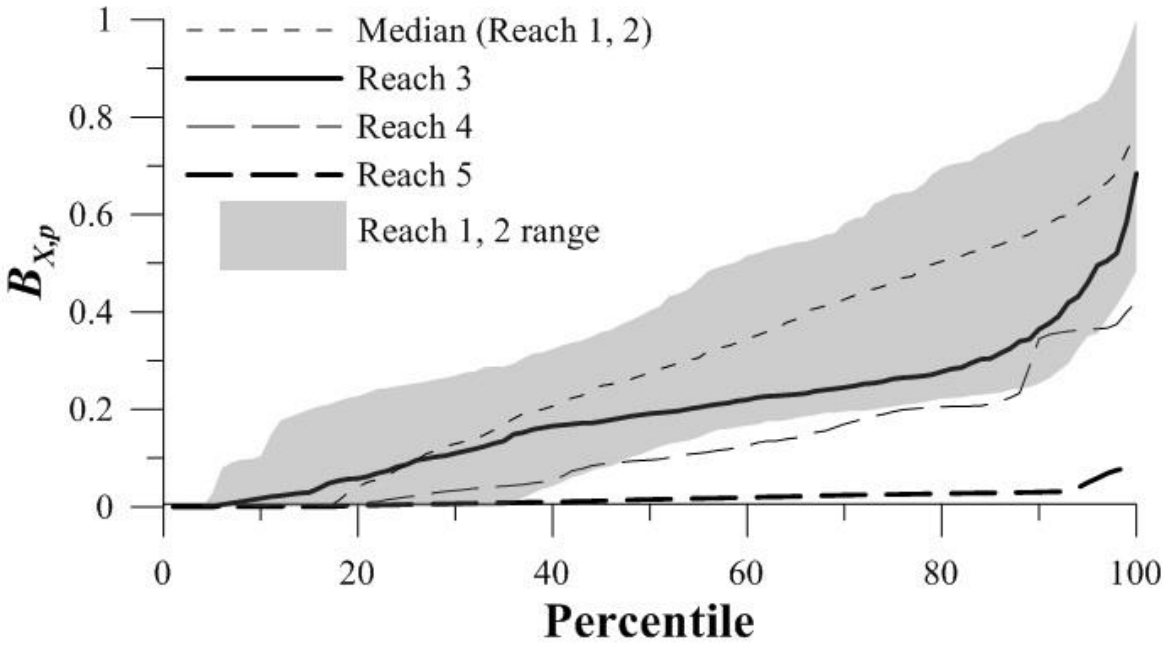

Figure 4-20 VDC's obtained at Reaches 3-5 compared to the range obtained at Reaches 1 and 2 (single VDCs are shown in the appendices).

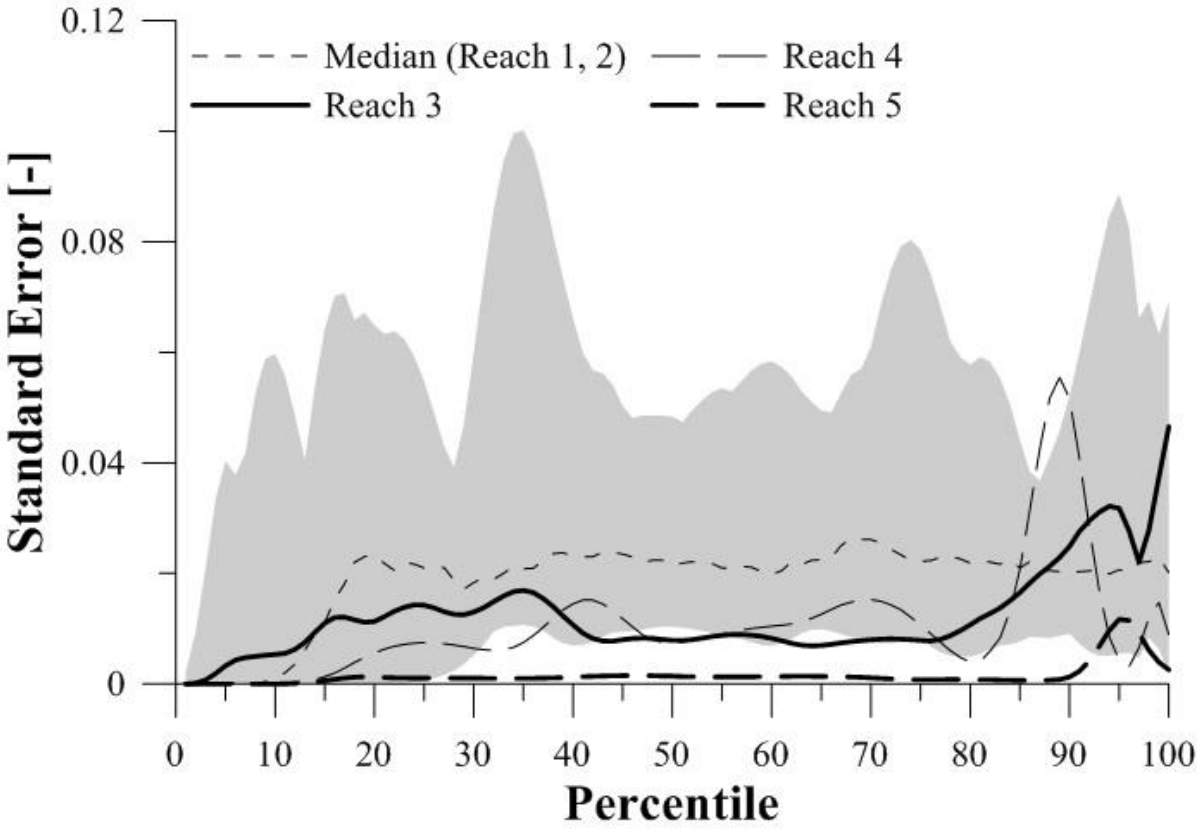

Figure 4-21: Standard Error (*SE*) for each B_X percentile at Reaches 3-5 compared to the range obtained at Reaches 1 and 2

Table 4-5: Independent validation results

	Field-measured Q (m^3/s)	**Rating curve Q (m^3/s)**	**E_Q from gauge station**	**$B_{X,95}$**	**Corrected Q (m^3/s)**	**E_Q after correction**
Reach 3	0.051	0.072	41%	0.496	0.054	5%
Reach 4	0.339	0.425	25%	0.367	0.342	1%
Reach 5	0.117	0.124	5%	0.05	0.116	-1%

At Reach 3, the error was reduced from a 41% to a 5% overestimation. This site exhibited many similarities to Reaches 1 and 2, as its vegetation distribution curve was within the range observed at Reaches 1 and 2 (Figure 4-20) while S_W and T were similar to Reach 1. However, dominant vegetation species found on this site were different than at Reaches 1 and 2, and mostly submergent (*Potamogeton* spp.). As such, successful correction of flow rates (Table 4-5) suggests that the method proposed here may be used to calculate flow resistance for different plant species.

At Reach 4, the error was reduced from a 25% to a 1% overestimation. This was the only site characterized by dense vegetation present on a riffle delimiting the downstream end of the reach. Clearly, presence of plants in a shallow area impacted upstream water levels, as it essentially acted as an increase in the riffle crest elevation, which in turn increased the backwater effect. These results confirmed comments by Green (2005b) who stated that the impact of flow resistance by plants on riffles may be higher because of the shallower depth encountered. It is worth noting that if vegetation on the riffle were neglected, correction of discharge would have reduced the error to approximately 20%.

Gauged flow rating at Reach 5 was the closest to the field measured flow rate, due to the relatively low density of plants observed at the validation reach (Figure 4-20). Nevertheless, the flow estimate was improved to a 1% error by applying Equation (4-18).

Figure 4-22 compares discrete discharge measurements at Reaches 1 and 2 with both non-corrected and corrected flow rates at Reaches 3-5 with. Both the range of errors and effect of the correction procedure observed at Reaches 3-5 is comparable to those observed at Reaches 1 and 2, further reinforcing the applicability of the technique presented herein.

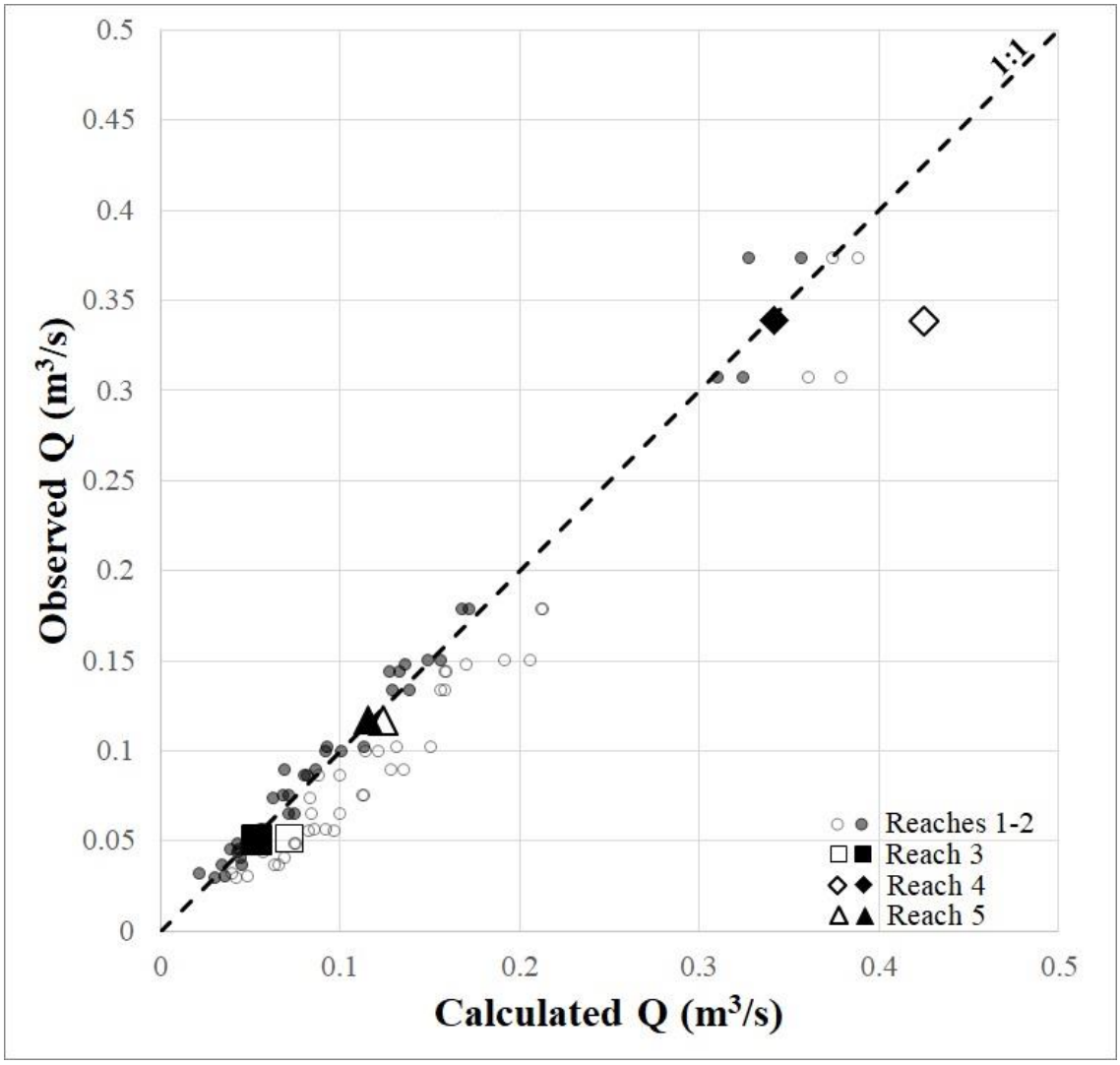

Figure 4-22: Corrected (solid symbols) and Non-corrected (hollow symbols) *Q* values at the validation reaches superimposed to discrete discharge measurements (using the flow measurement methods outlined in Section 4.3.2) at reaches 1 and 2.

4.6.1 Influence of sample size

A validation procedure of the sensitivity analysis undertaken in Section 4.3.4.2 was also conducted. The goal of this analysis was to assess whether the correction procedure was sensitive to sample size and whether results obtained at Reach 1 and 2 could be site specific. Since only a single Vegetation Distribution Curve (VDC) was obtained for each site, only spatial resolution could be assessed.

At Reach 3, the correction procedure was particularly sensitive to spatial resolution (Figure 4-23). This is related to the VDC being steeper for higher percentiles, as testified by corresponding high Standard Error values (Figure 4-21). Consequently, few cross-sections were not able to capture the spatial variability of vegetation and only high spatial resolution provided an accurate estimation of B_{X95} and

correction of Q at this reach (Table 4-6). At Reach 4, values of SE for B_X percentiles were close to the respective median values for Reaches 1 and 2 with a marked increase at the 90th percentile. This corresponds to the steeper part of the VDC (Figure 4-20) and SE was notably lower for B_{X95}. Consequently B_{X95} (Figure 4-23) and corrected discharge (Table 4-6) were not sensitive to sample size. At Reach 5, due to low plant densities, SE was well below the range observed at the other sites (Figure 4-21). As values of B_{X95} were low, errors calculated with Equation (4-12) are markedly higher. Nevertheless, their impact on discharge calculation is minimal (Table 4-6). Overall, these results confirm observations for Reaches 1 and 2, when B_{X95} is found on a steep portion of the VDC a larger sample size is needed to capture vegetation heterogeneity appropriately. If a high resolution is not achieved, B_{X95} values obtained may lead to inaccurate corrections of discharge estimates (Table 4-6).

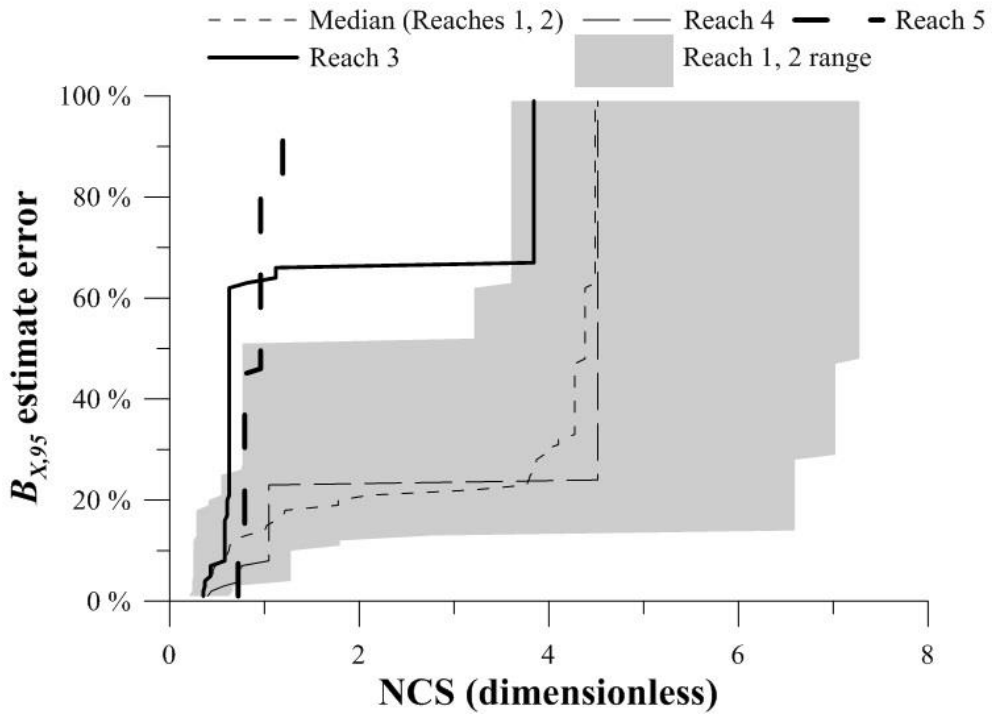

Figure 4-23: Error in $B_{X,95}$ at Reaches 3-5 as a function of normalized cross-sectional spacing (*NCS*). compared to the range obtained at Reaches 1 and 2

Table 4-6: Sensitivity analysis on validation

	$B_{X,95}$ **Standard Error**	**Error after correction**			
		Max. resolution	***NCS~1***	***NCS~2***	***NCS~3***
Reach 3	0.032	5%	13%	17%	30%
Reach 4	0.004	1%	-1%	2%	2%
Reach 5	0.012	-1%	-1%	-1%	-1%

4.7 Conclusions

This study was able to correct seasonal flow data collected over a three-year period on a natural channel affected by aquatic vegetation growth. It was first determined that if the additional resistance by aquatic plants is not accounted for, discharges calculated through an "open-water" stage-discharge relationship could exceed twice the actual flow rate recorded in the stream. Using the correction procedure proposed here, the errors in discharge estimation were reduced by 99%.

The correction procedure developed here was determined to be sensitive to the spatial frequency at which vegetation is measured. However, it is not particularly sensitive to temporal resolution, as long as the temporal boundaries of the growing season and the period of peak growth are accurately defined. Given the relatively low sampling effort required, these techniques can be readily applied to correct flow estimates for the whole period of record affected by vegetation growth. Furthermore, as testified by the successful validation of the procedure on three other streams, the methodology can be used on medium-low gradient streams affected by vegetative flow resistance, at different growth stages, and on different vegetation species.

A new method was developed by quantifying vegetative flow resistance at the reach-scale. This was achieved by comparing water levels before and during aquatic vegetation growth at coinciding flow rates and by using a Vegetation Distribution Curve (Green, 2006) to characterize plants spatial distribution. It was found that vegetation cross-sectional distribution at the densest part of the reach is highly correlated to increases in water level, flow resistance, and, as such, errors in discharge estimation. This result is partially in contradiction with findings from other studies, which found flow resistance related to the average cross-sectional blockage or aerial cover (Huntington and Whitehead, 1992; Champion and Tanner, 2000; Green, 2005a; Nikora et al., 2008; Old et al., 2014). Furthermore, Manning's n was found unsuitable to estimate vegetative flow resistance, especially at low flow. Nevertheless, given successful results by previous studies (Green, 2005a; Nikora et al., 2008; Old et al., 2014) n could be a well-suited parameter at higher flow rates. However, dependence of n on Q, should be accounted for, as evident in this and many other studies (notably, Ferguson, 2010, 2013, 2014).

In summary, the methodology developed here will be particularly useful for improving the accuracy of flow records and specifically for the estimation of low flows. Correctly assessing low flow discharges over the span of several years will improve the accuracy of flow records. These can then be used to calculate low flow indices, which are valuable to many disciplines and practices (Smakthin, 2001; Pryce, 2004, Whitfield and Hendrata, 2006). Specifically, effectively quantifying flow rates in periods

of low flow directly relates to water management decisions, such as apportionments between provinces or countries. By using the methods presented here to correct low flow records, water can be divided amongst downstream communities appropriately. Furthermore, negative impacts on ecosystems could be avoided as overestimations in flow rates, which can lead to excessive water takings, can be corrected. Finally, the use of corrected low flow indices can aid in developing regulation frameworks to assess and protect habitat sustainability for fish and benthic communities in a suitable manner.

Chapter 5: Conclusions

This thesis was able to demonstrate that vegetation growth in rivers can significantly impact the accuracy of flow records. It was determined that if the effects of aquatic vegetation on stage are neglected, errors in calculated discharge can exceed twice the actual flow present in the channel. Published equations were not able of providing a reliable correction. Therefore, new techniques and technologies to improve the estimation of low flows were developed and successfully tested, fulfilling the original research objectives of this thesis. The correction procedure introduced here is capable of largely reducing discharge estimation errors. The equipment, methodology and correction procedure presented in this thesis are easily reproduceable, improving on some of the short comings of previous research in the field. It is recommended that an application of these methods is expanded for their further refinement. This will allow to develop and implement a standardized approach to correct flow measures impaired by aquatic plants.

5.1 Key findings

Chapter 2 presented a rapid and cost-effective methodology to quantify aquatic vegetation presence using Unmanned Aerial Vehicles (UAVs) and an image processing algorithm. It was found that the proposed method performs systematically better than a manual (i.e. visual) detection and that data collection can be up to ten times quicker than conventional in-stream surveys. In-stream methods were also determined to be sensitive to spatial resolution, which, in turn, was demonstrated to affect the estimation of discharge.

Chapter 3 introduced the Settling Board Test (SBT) capable of measuring the combined effects of plants stiffness and density in situ. Artificial plants were used to develop a calibration equation which was later adopted to quantify natural vegetation stiffness. Field results show that the test is capable of detecting differences in plants densities and stiffnesses as macrophytes grow and decay. Furthermore, relative roughness measurements were found to be well correlated to plants stiffness. As the latter is known to influence flow resistance, the method can aid in the estimation of flow rates.

Chapter 4 expanded upon the findings of the previous two chapters. Here, the effects of aquatic plants growth on resistance to flow and discharge calculation were thoroughly assessed over a three-year period at two different reaches. Results indicated that flow resistance was most impacted by the cross-sectional distribution of plants at the most densely vegetated part of the reach. Using this result, a method to correct discharge estimates was developed and applied to the whole period of record affected

by plants roughness. The correction procedure reduced the average discharge calculation error by 99% over the period assessed. A thorough sensitivity analysis highlighted that accurate corrections require sampling at high spatial resolution, which was higher in this thesis than in most published studies, confirming results obtained in Chapter 2. However, as temporal resolution was not found to affect the results, the implementation of this methodology can still be time-efficient on a yearly basis.

5.2 Application for engineering practices

When aquatic vegetation presence causes seasonal discrepancies between gauge reading and flow measurements, it is common practice to use rating curve shifts. Historically, these have been based on discharge and temperature measurements as well as by confirming plant presence visually (Environment Canada, personal comm.). As such, the accuracy of the shifts is directly related to when the discharge measurements occur and their magnitude. If the lowest flows are missed, or a significant range of flow are not captured, then the shift may not be capable of estimating environmental flows correctly, leading to the introduction of systematic errors (Tomkins, 2014). Conversely, the correction procedure consists of simple and repeatable methods to inventory aquatic vegetation which was demonstrated to be directly related to increases in flow resistance and most importantly, can be used to correct stage-discharge relationship without requiring flow measurements.

Furthermore, while the method was developed at high resolution, its implementation and analysis are time-efficient. For instance, the UAV-sampling techniques presented in Chapter 2 can be deployed in less than one hour. Moreover, the sensitivity analysis undertaken in Chapter 4 demonstrated that one measurement of vegetation spatial distribution per month is sufficient to determine the start, the peak and the end of vegetation growth. This sampling frequency is comparable to that used by Water Survey of Canada, therefore the methodology introduced here could be integrated as part of the stream gauging program. Finally, should it not be possible to achieve high spatial resolution an estimate of the expected error can be gained using data from this thesis.

Practical implications from the findings of this study relate to the use of flow records and be beneficial for the calibration of hydrologic models and the evaluation of parameters such as low flow indices. For instance, Permits to Take Water in Ontario (PPTW) have different requirements based on the amount of water withdrawn and the low flow indices of the watercourse (such as the 7-day 20-year low flow, or 7Q20, and similar metrics). Low flow indices also relate to the estimation of drought severity or the evaluation of low flow passage potential for fish. Correct estimation of these depends directly on the accuracy of flow rates recorded, which during the low flow season can be greatly overestimated if aquatic vegetation is present in the channel. Using the methods presented herein, discharge can be better

estimated and the environmental impact of water withdrawals from streams can be quantified more accurately.

5.3 Future research

Results from this research have confirmed findings from other studies on vegetative flow resistance (Green, 2006; Luhar and Nepf, 2013). while contradicting others (Huntington and Whitehead, 1992; Champion and Tanner, 2000; Green, 2005a; Nikora et al, 2008; Old et al, 2014). In light of mixed results across the literature, there are opportunities for future research to further disentangle the complex interactions of plant growth and flow resistance.

For instance, being the methods produced here reproducible, they could be used to collect vegetation spatial distribution data on a wider range of channel sizes, slopes, and flow rates. In turn, as data would be collected in the same manner easier comparisons between datasets would be possible. Wider application of the method will also allow for its further validation in larger systems as a validation on larger rivers (with widths above 15 m) was not undertaken. In large streams, flow resistance is typically less sensitive to changes in discharge (Ferguson, 2010), and subject to a larger variety of roughness sources. As such, it is encouraged to use the data collection protocols presented here on larger watercourses. Moreover, results from Chapter 4 highlighted that at high vegetation densities, factors related to finer-scale flow resistance arose (such as drag at the plant/stem-scale) and cannot be accounted by the methods presented herein. As plant-scale drag is related to the biomechanical properties of plants, methods described in Chapter 3 could be adapted to capture these parameters. Further investigation and application of these methods is recommended in scenarios outside of natural streams, such as wetlands or artificial stormwater management ponds, which are often heavily vegetated. Outflow from these features is, among other things, a function of vegetation density, and could be predicted by adapting some of the methods presented here. Furthermore, in a small subset of the data collected in this study, it was found that the effects of vegetative flow resistance were significantly reduced when downstream hydraulic controls were markedly narrower than the average channel width. Given the relative small size of the dataset where this result was obtained, further research should be undertaken on this topic. A possible expansion could be to test different weir openings under different vegetation densities. In summary, future research should work towards building a larger dataset of vegetative flow resistance scenarios, under different boundary conditions, to help identify the causes of the aforementioned differences between studies results.

The methods presented in this thesis can also be improved upon by future studies. Techniques discussed in Chapter 2 could be further developed to distinguish between emergent and aquatic vegetation species

in photogrammetry data. Regarding Chapter 3, it is recommended to further refine the SBT by allowing the board to settle from the top of the vegetation canopy rather than from the water surface. Further calibration may be required, however, should the test be successful, depth would be removed as one of the parameters affecting the results and the method implementation would be simplified. Furthermore, the SBT could also be used to predict plant bending at similar growing stages, a test that could not be completed in this study due to the lack of high flow events. Successful prediction of plant bending could be used to correct higher flow rates (e.g. above the mean annual flow). While this was not assessed as part of this study, the methods presented here could be applied to investigate plant bending, which in turn can give helpful indications on the impact of aquatic plants on flood flow resistance.

Finally, results presented in Chapter 4 were achieved through detailed measurements of vegetation to identify the most densely vegetated portion of the reach. While capable of mapping vegetation in detail, this method can be time consuming and discourage its application on larger reaches. To decrease surveying time (and cost) it may be possible to visually identify the most vegetated reach portion prior to the collection of data and then measure the blockage factor on one representative cross-section located in the identified portion. While the measured cross-section may not yield the exact B_{X95}, it is reasonable to obtain one of the percentiles above 80, which were found to be suitable predictors of flow resistance. Should this assumption be successfully tested, it may result in significant cost savings.

References

Abdelsalam, M. W., Khattab, A. F., Khalifa, A. A., & Bakry, M. F. (1992). Flow Capacity Through Wide and Submerged Vegetal Channels. *Journal of Irrigation and Drainage Engineering, 118*(5).

Arcement, G. J., & Schneider, V. R. (1989). *Guide for selecting Manning's roughness coefficients for natural channels and flood plains - Water Supply Paper 2339.* USGS.

Armanini, A., Righetti, M., & Grisenti, P. (2005). Direct measurement of vegtetation resistance in prototype scale. *Journal of Hydraulic Research, 43*(5), 481-487.

Armitage, P. D., Blackburn, J. H., Winder, J. M., & Wright, J. F. (1994). Impact of vegetation management on macroinvertebrates in chalk streams. *Aquatic Conservation, 4*(2), 95-104.

Baattrup-Pedersen, A., Larsen, S. E., & Riis, T. (2002). Long-term effects of stream management on plant communities in two Danish lowland streams. *Hydrobiologia, 481*, 33-45. doi:https://doi.org/10.1023/A:1021296519187

Bal, K., Struyf, E., Vereecken, H., Viaene, P., De Doncker, L., de Deckere, E., . . . Meire, P. (2011). How do macrophyte distribution patterns affect hydraulic resistances. *Ecological Engineering, 37*, 529-533. doi:10.1016/j.ecoleng.2010.12.018

Baptist, M. J., Babovic, V., Rodríguez Uthurburu, J., Keijzer, M., Uittenbogaard, R. E., Mynett, A., & Verwey, A. (2007). On inducing equations for vegetation resistance. *Journal of Hydraulic Research, 45*(4), 435-450.

Barko, J. W., Hardin, D. G., & Matthews, M. S. (1982). Growth and morphology of sumbersed freshwater macrophytes in relation to light and temperature. *Can. J. Bot., 60*, 877-887.

Bathurst, J. C. (1982). Theoretical aspects of flow resistance. *Gravel-Bed Rivers*, 83-108.

Bathurst, J. C. (1985). Flow Resistance estimation in mountain rivers. *Jr. of the Hydr. Engg. ASCE, 111*(4), 625-643.

Beaton, A. D., & Bradford, A. (2013). Demonstration of a methodology for setting ecological flow and water level targets. *Canadian Water Resources Journal, 38*(4), 296-310. doi:10.1080/07011784.2013.830371

Beschta, R. L. (1997). Riparian shade and stream temperature: an alternative perspective. *Rangelands, 19*, 25-28.

Biggs, B. J., & Stokseth, S. (1996). Hydraulic habitat suitability for periphyton in rivers. *Regulated Rivers: Research and Management, 12*, 251-261.

Bradford, A. (2008). An Ecological Flow Assessment Framework: Building a Bridge to Implementation in Canada. *Canadian Water Resources Journal, 33*(3), 215-232.

Bradford, M. J., & Heinonen, J. S. (2008). Low Flows, Instream Flow Needs and Fish Ecology in Small Stream. *Canadian Water Resources Journal, 33*(2), 165-180.

Bradley, K., & Houser, C. (2009). Relative velocity of seagrass blades: Implications for wave attenuation in low-energy environments. *Journal of Geophysical Research, 114*. doi:10.1029/2007JF000951

Bray, D. I. (1979). Estimating average velocity in Gravel Bed Rivers. *Jr. of the Hydr. Engg. ASCE, 106*(9), 1103-1121.

Bray, D. I. (1982). Regime Equations for Gravel-Bed Rivers. In R. Hey, J. Bathurst, & C. and Thorne, *Gravel-Bed Rivers* (p. Chapter 19). John Wiley and Sons.

Carollo, F. G., Ferro, V., & Termini, D. (2005). Flow resistance law in channels with flexible submerged vegetation. *Journal of hydraulic engineering, 131*, 554-564.

Carr, G. M., Duthie, H. C., & Taylor, W. D. (1997). Models of aquatic plant productivity: a review of the factors that influence growth. *Aquatic Botany, 59*, 195-215.

Cassan, L., Belaud, G., Baume, J., Dejean, C., & Moulin, F. (2015). Velocity profiles in a real vegetated channel. *Environmental Fluid Mechanics, 15*, 1263-1279. doi:10.1007/s10652-015-9417-0

Castellarin, A., Galeati, G., Brandimarte, L., Montanari, A., & Brath, A. (2004). Regional low-duration curves: reliability for ungauged basins. *Advances in Water Resources, 27*, 953-965. doi:10.1016/j.advwatres.2004.08.005

Champion, P. D., & Tanner, C. C. (2000). Seasonality of macrophytes and interaction with flow in a New Zealand lowland stream. *Hydrobiologia, 441*, 1-12. doi:https://doi.org/10.1023/A:1017517303221

Chen, L., Acharya, K., & Stone, M. C. (2014). Using a mechanical approach to quantify flow resistance by submerged, flexible vegetation - A revisit of Kouwen's approach. *Advances in Water Resources, 73*, 198-202.

Chow, V. (1959). *Open-Channel Hydraulics.* New York, NY: McGraw-Hill.

Chubb, S. L., & Liston, C. R. (1986). Density and distribution of larval fishes in pentwater marsh a coastal wetland on Lake Michigan. *J. Great Lakes Res., 12*(4), 332-343.

Conant, B. (2004). Delineating and quantifying ground-water discharge zones using streambed temperatures. *Ground Water, 42*(2), 243-257.

Corenblit, D., Tabacchi, E., Stieger, J., & Gurnell, A. M. (2007). Reciprocal interactions and adjustments between fluvial landforms and vegetation dynamics in river corridors: A review of compementary approaches. *Earth-Science Reviews*(84), 56-86.

Cowan, W. L. (1956). Estimating hydraulic roughness coefficients. *Agricultural Engineering, 37*(7), 473-475.

Cox, M. B. (1942). *Tests on Vegetated Waterways - Technical Bulletin No. T-15.* Stillwater, OK, USA: Oklahoma agricultural and machanical college.

Dallas, H. (2008). Water temperature and riverine ecosystems: An overview of knowledge and approaches for assessing biotic responses with special reference to South Africa. *Water SA, 34*(3), 394-404.

Darby, S. E. (1999). Effect of Riparian Vegetation on Flow Resistance and Flood Potential. *Journal of Hydraulic Engineering, 125*(5).

Darby, S. E., & Thorne, C. R. (1996). Prediction Stage-Discharge Curves in Channels with Bank Vegetation. *Journal of Hydraulic Engineering, 122*, 583-586.

De Doncker, L., Troch, P., Verhoeven, R., Bal, K., Desmet, N., & Meire, P. (2009). Relation between resistance characteristics due to Aquatic Weed growth and the Hydraulic capacity of the River Aa. *River Research and Applications, 25*, 1287-1303. doi:10.1002/rra.1240

Detert, M., & Weitbrecht, V. (2015). A low-cost airborne velocimetry system: proof of concept. *Journal of Hydraulic Research, 53*(4), 532-539. doi:10.1080/00221686.2015.1054322

Dibble, E. D., Killgore, K. J., & Harrel, S. L. (1997). Assessment of Fish-Plant Interactions. *Aquatic Plant Control Research Program*. US Army Corps of Engineers.

Dunbar, M. J., Pedersen, M., Cadman, D., Extence, C., Waddingham, J., Chadd, R., & Larsen, S. E. (2010). River discharge and local-scale physical habitat influence macroinvertebrate LIFE scores. *Freshwater Biology, 55*(1), 226-242.

Dunford, R., Michel, K., Gagnage, M., Piégay, H., & Trémelo, M.-L. (2009). Potential and constraints of Unmanned Aerial Vehicle technology for the characterization of Mediterranean riparian forest. *International Journal of Remote Sensing, 30*(19), 4915-4935. doi:10.1080/01431160903023025

Eastgate, W. I. (1966). Vegetated stabilization of grasses, waterways and dam bywashes. *MEngrg. thesis*. St. Lucia, Queensland, Australia: Dept of Civ. Engrg. University of Queensland.

Fenzl, R. N., & Davis, J. R. (1964). Hydraulic resistance relationships for surface flows in vegetaed channels. *Transactions of the ASAE, 7*(1), 46-55.

Ferguson, R. (2010). Time to abandon the Manning equation? *Earth Surface Processes and Landforms*. doi:10.1002/esp.2091

Ferguson, R. (2014). Reach-Scale Flow Resistance in River Channels. In *Reference Module in Earth Systems and Environmental Sciences.* doi:10.1016/B978-0-12-409548-9.09386-6.

Ferguson, R. I. (2013). Reach-scale flow resistance. In J. F. Shroder, & E. Wohl (Eds.), *Treatise on Geomorphology* (pp. 50-68). Academic Press.

Flynn, K. F., & Chapra, S. C. (2014). Remote sensing of submerged aquatic vegetation in a shallow non-turbid river using an unmanned aerial vehicle. *Remote Sensing, 6*, 12815-12836. doi:doi:10.3390/rs61212815

Folkard, A. M. (2011). Vegetated flows in their environmental context: a review. *ICE proceedings, 164*, 3-24.

Getzin, S., Wiegand, K., & Schöning, I. (2012). Assessing biodiversity in forests using very high-resolution images and unmanned aerial vehicles. *Methods in Ecology and Evolution, 3*, 397-494. doi:10.1111/j.2041-210X.2011.00158.x

Göktoğan, A. H., Sukkarieh, S., Bryson, M., Randle, J., Lupton, T., & Hung, C. (2010). A Rotary-wing unmanned air vehicle for aquatic weed surveillance and management. *Journal of Intelligent and Robotic Systems, 57*, 467–484. doi:10.1007/s10846-009-9371-5

Green, J. (2003). The precision of sampling grain-size percentiles using the Wolman method. *Earth Surface Processes and Landforms, 28*, 979-991. doi:10.1002/esp.513

Green, J. C. (2005a). Comparison of Blockage factors in modelling the resitance of channels containing submerged macrophytes. *River Research and Applications*, 671-686.

Green, J. C. (2005b). Modelling flow resistance in vegetated streams: review and development of a new theory. *Hydrological Processes, 19*, 1245-1259.

Green, J. C. (2006). Effect of macrophyte spatial variability on channel resistance. *Advances in Water Resources, 29*, 426-438.

Guerrero, J.-L., Westerberg, I. K., Halldin, S., Xu, C.-Y., & Lundin, L.-C. (2012). Temporal variability in stage-discharge relationships. *Journal of Hydrology*, 90-102. doi:10.1016/j.jhydrol.2012.04.031

Gurnell, A. (2014). Plants as river system engineers. *Earth Surface Processes and Landforms, 39*, 4-25.

Gurnell, A. M., & Midgley, P. (1994). Aquatic weed growth and flow resistance: influence on the relationship between discharge and stage over a 25 year river gauging station record. *Hydrological Processes, 8*, 63-73. doi:10.1002/hyp.3360080105

Hamilton, A. S., & Moore, R. D. (2011). Quantifying uncertainty in streamflow records. *Canadian Water Resources Journal, 37*(1), 3-21.

Hamilton, S. (2008). Sources if uncertainty in Canadian low flow hydrometric data. *Canadian Water Resources Journal, 33*(2), 125-136.

Haslam, S. M. (1978). *River Plants.* Cambridge University Press.

Haxton, J. W., & Findlay, C. S. (2008). Meta-analysis of the impact of water management on aquatic communities. *Canadian Journal of Fisheries and Aquatic Sciences, 65*, 437-447.

Herschy, R. W. (1995). *Streamflow measurement.* London, UK: E & FN SPON.

Hey, R. D. (1979). Flow resistance in gravel-bed rivers. *Journal of hydraulic division, 105*(4), 365-379.

Hey, R. D. (1988). Bar Form Resistance in Gravel-Bed Rivers. *Journal of Hydraulic Engineering, 114*(12), 1498-1508.

Hicks, D. M., & Mason, P. D. (1991). *Roughness Characteristics of New Zealand Rivers.* Water Resources Survey.

Hill, B. H., & Webster, J. R. (1982). Aquatic macrophyte breakdown in an Appalachian river. *Hydrobiologia*, 53-59.

Holmes, N. T., Newman, J. R., Chadd, S., Rouen, K. J., Saint, L., & Dawson, F. H. (1999). *Mean Trophic Rank: A User's Manual*. Bristol, UK: Environmentl Agency R&D.

Howes, A. C. (2007). A Methodology for low-flow gauging at channel-control stations with seasonal vegetation effects. *Masters Thesis, University of Guelph*. Guelph, Ontario, Canada.

Huntington, S. W., & Whitehead, E. (1992). *The Hydraulic Roughness of Vegetated Channels - Report SR305.* Wallingford, Oxfordshire, UK: HR Wallingford Ltd.

Hussner, A., van Dam, H., Vermaat, J. E., & Hilt, S. (2014). Comparison of native and neophytic aquatic macrophyte developments in a geothermally warmed river and thermally normal channels. *Fundam. Appl. Limnol., 185*(2), 155-166. doi:10.1127/fal/2014/0629

Husson, E., Ecke, F., & Reese, H. (2016). Comparison of Manual Mapping and Automated Object-Based Image analysis of Non-submerged aquatic vegetation from Very-High-Resolution UAS images. *Remote Sensing, 8*(9), 1-18. doi:10.3390/rs8090724

Husson, E., Hagner, O., & Ecke, F. (2014). Unmanned aircraft systems help to map aquatic vegetation. *Applied vegetation science*, 567-577. doi:10.1111/avsc.12072

James, C. S., Birkhead, A. L., Jordanova, A. A., & O'Sullivan, J. J. (2004). Flow resistance of emergent vegetation. *Journal of Hydraulic Research, 42*(4), 390-398. doi:10.1080/00221686.2004.9641206

Järvelä, J. (2002). Flow resistance of flexible and stiff vegetation, a flume study with natural plants. *Journal of Hydrology, 269*, 44-54.

Järvelä, J. (2004). Flow resistance in environmental channels: Focus on vegetation. *PhD Thesis*. Espoo, Finland: Helsinki University of Technology.

Järvelä, J. (2005). Effect of submerged flexible vegetation on flow structure and resistance. *Journal of Hydrology, 307*, 233-241.

Johnson, F. A. (1971). Stream temperatures in an alpine area. *Journal of Hydrology, 14*, 322-336.

Johnson, J. A., & Newman, R. M. (2011). A comparison of two methods for sampling biomass of aquatic plants. *Journal of Aquatic Plant Management, 49*, 1-8.

Kadlec, R. (1990). Overland flow in wetlands. *Journal of Hydraulic Engineering, 116*(5), 691-706.

Kenow, K. P., Lyon, J. E., Hines, R. K., & Elfessi, A. (2007). Estimating biomass of submersed vegetation using a simple rake sampling technique. *Hydrobiologia, 575*, 447-454.

Kiang, J. E., Cohn, T. A., & Mason, Jr., R. R. (2009). Quantifying Uncertainty in Discharge Measurements: A New Approach. *World Environmental and Water Resources Congress.* ASCE.

Kouwen, N. (1970). Flow retardance in vegetated open channels. *PhD Thesis, University of Waterloo*. Waterloo, Ontario, Canada.

Kouwen, N. (1988). Field estimation of the biomechanical properties of grass. *Journal of Hydraulic Resources, 26*(5), 559-568.

Kouwen, N. (1992). Modern Approach to design of Grassed Channels. *Journal of Irrigations and Drainage Engineering, 118*(5), 733-743.

Kouwen, N., & Li, R. M. (1980). Biomechanics of vegetative channel linings. *Journal of the hydraulic division, 106*, 1085-1103.

Kouwen, N., & Unny, T. E. (1973). Flexible roughness in open channels. *Journal of the hydraulic division, 99*, 713-742.

Kouwen, N., Li, R.-M., & Simons, D. B. (1981). Flow resistance in vegetated waterways. *Transaction of the ASAE, 24*(3), 684-690, 698.

Kouwen, N., Unny, T. E., & Hill, H. M. (1969). Flow retardance in vegetated channels. *Journal of the Irrigation and Drainage Division, 95*, 329-342.

Kris, B. D., & Meire, P. (2009). The Influence of Macrophyte Cutting on the Hydraulic Resistance of Lowland Rivers. *Journal of Aquatic Plant Management, 47*, 65-68.

Kuta, R. W., Annable, W. K., & Tolson, B. A. (2010). Sensitivity of Field Data Estimates in One-Dimensional Hydraulic Modeling of Channels. *Journal of Hydraulic Engineering*, 379-384. doi:0.1061/(ASCE)HY.1943-7900.0000187

Langbein, W. B., & Leopold, L. B. (1964). Quasi-Equilibrium States in Channel Morphology. *American Journal of Science, 262*, 782-794.

Łoboda, A. (2017). The new insights on the study of biomechanics of aquatic plants. *XXXVI International School of Hydraulics.* Jachranka, Poland.

Luhar, M., & Nepf, H. M. (2011). Flow-induced reconfiguration of buoyant and flexible aquatic vegetation. *Limnology Oceanography, 56*(6), 2003-2017.

Luhar, M., & Nepf, H. M. (2013). From the blade scale to the reach scale: A characterization of aquatic vegetative drag. *Advances in Water Resources, 51*, 305-316. doi:10.1016/j.advwatres.2012.02.002

Madsen, T. V., & Brix, H. (1997). Growth, photosynthesis and acclimation by two submerged macrophytes in relation to temperature. *Oecologia, 110*, 320-327.

Magnuszewski, A., & Moran, S. (2014). Vistula River bed erosion processes and their influence on Warsaw's flood safety. *Sediment Dynamics from the Summit to the Sea. 367*, pp. 147-153. New Orleans, LA, USA: IAHS. doi:doi:10.5194/piahs-367-147-2015

Marcus, W. A., & Fonstad, M. A. (2010). Remote sensing of rivers: the emergence of a subdiscipline in the river sciences. *Earth Surface Processes and Landforms, 35*, 1867-1872. doi:10.1002/esp.2094

Marion, A., Nikora, V., Puijalon, S., Bouma, T., Koll, K., Ballio, F., . . . Statzner, B. (2014). Aquatic interfaces: a hydrodynamic and ecological perspective. *Journal of Hydraulic Research, 52*(6), 744-758. doi:10.1080/00221686.2014.968887

Marjoribanks, T. I., Hardy, R. J., Lane, S. N., & Parsons, D. R. (2014). High-resolution numerical modelling of flow-vegetation interactions. *Journal of Hydraulic Research, 52*(6), 775-793. doi:0.1080/00221686.2014.948502

Marjoribanks, T. I., Hardy, R. J., Lane, S. N., & Tancock, M. J. (2017). Patch-scale representation of vegetation within hydraulic models. *Earth surface processes and landforms, 42*, 699-710. doi:10.1002/esp.4015

Marr, D., & Hildreth, E. (1980). Theory of edge detection. *Proceedings of the Royal Society B, 207*(1167), 187-217.

Mathworks, T. (2018). *Detecting a cell using image segmentation*. Retrieved from https://www.mathworks.com/help/images/examples/detecting-a-cell-using-image-segmentation.html

Miler, O., Albayrak, I., Nikora, V., & O'Hare, M. (2012). Biomechanical properties of aquatic plants and their effects on plant-flow interactions in streams and rivers. *Aquatic Sciences, 74*, 31-41.

Miler, O., Albayrak, I., Nikora, V., & O'Hare, M. (2014). Biomechanical properties and morphological characteristics of lake and river plants: implications for adaptations to flow conditions. *Aquatic Science, 76*, 465-481.

Millar, R. G. (1999). Grain and form resistance in gravel-bed rivers. *Journal of Hydraulic Research, 37*(3), 303-312.

Millar, R. G. (2000). Influence of bank vegetation on alluvial channel patterns. *Water resources research, 36*, 1109-1118.

Naden, P., Rameshwaran, P., Mountford, O., & Robertson, C. (2006). The influence of macrophyte growth, typical of eutrophic conditions, on river flow velocities and turbulence production. *Hyrdological Processes, 20*, 3915-3938. doi:10.1002/hyp.6165

Neary, V. S. (2003). Numerical Solution of Fully Developed Flow with Vegetative Resistance. *Journal of Engineering Mechanics, 129*, 558-563. doi:10.1061/(ASCE)0733-9399(2003)129:5(558)

Nebel, S., Porter, J. L., & Kingsford, R. T. (2008). Long-term trends of shorebird populations in eastern Australia and impacts of freshwater extraction. *Biological Conservation, 141*, 971-980.

Nepf, H. M. (2012). Hydrodynamics of vegetated channels. *Journal of Hydraulic Research, 50*(3), 262-279. doi:10.1080/00221686.2012.696559

Nikora, V. (2010). Hydrodynamics of aquatic ecosystems: an interface between ecology, biomechanics and environmental fluid mechanics. *River Research and Application, 26*, 367-384. doi:10.1002/rra.1291

Nikora, V., Larned, S., Nikora, N., Debnath, K., Cooper, G., & Reid, M. (2008). Hydraulic resistance due to aquatic vegetation in small streams: field study. *Journal of Hydraulic Engineering, 134*(9), 1326-1332. doi:10.1061/(ASCE)0733-9429(2008)134:9(1326)

Nikora, V., Learned, S., Debnath, K., Cooper, G., Reid, M., & Nikora, N. (2006). Effects of aquatic and bank-side vegetation on hydraulic performance of small streams. *River Flow 2006* (pp. 639-646). Taylor and Francis, London.

O'Hare, M. T., Hutchinson, K. A., & Clarke, R. T. (2007). The drag and reconfiguration experienced by five macrophytes from a lowland river. *Aquatic botany, 86*, 253-259. doi:10.1016/j.aquabot.2006.11.004

O'Hare, M. T., McGahey, C., Bissett, N., Cailes, C., Henville, P., & Scarlett, P. (2010). Variability in roughness measurements for vegetated rivers near base flow in England and Scotland. *Hournal of Hydrology, 385*, 361-370. doi:10.1016/j.jhydrol.2010.02.036

Old, G. H., Naden, P. S., Rameshwaran, P., Acreman, M. C., Baker, S., Edwards, F. K., . . . Neal, M. (2014). Instream and riparian implications of weed cutting in a chalk river. *Ecological Engineering, 71*, 290-300.

Paine, D. P., & Kiser, J. D. (2003). *Aerial photography and image interpretation.* Hoboken, New Jersey, USA: John Wiley & Sons, Inc.

Palmer, S. C., Kutser, T., & Hunter, P. D. (2015). Remote sensing of inland waters: Challenges, progress and future directions. *Remote Sensing of Environment, 157*, 1-8. doi:10.1016/j.rse.2014.09.021

Palmer, V. J. (1945). A Method for designing vegetated waterways. *Agricultural Engineering, 26*(12), 516-520.

Palmer, V. J. (1946). Retardance coefficients for low flow in channels lined with vegetation. *Transactions, American Geophysical Union, 27*(2), 187-197.

Pelletier, P. M. (1988). Uncertainty in the single determination of river discharge: a literature review. *Canadian Journal of Civil Engineering, 15*, 834-850.

Pelletier, P. M. (1989). Uncertainty in streamflow measurement under winter ice conditions a case study: the Red River at Emerson, Manitoba, Canada. *Water Resource Research, 25*(8), 1857-1867.

Petryk, S., & Bosmajian, G. (1975). Analysis of flow through vegetation. *Journal of the hydraulic division, 101*, 871-884.

Piñeiro, G., Perelman, S., Guerschman, J., & Paruelo, J. (2008). How to Evaluate Models: Observed vs. Predicted or Predicted vs. Observed? *Ecological Modelling, 216*, 316-322. doi:10.1016/j.ecolmodel.2008.05.006

Pryce, R. (2004). Hydrological Low Flow Indices and their Uses. *WSC Report No. 04-2004*. Watershed Science Centre.

Quick, M. C. (1991). Reliability of flood discharge estimates. *Canadian Journal of Civil Engineering, 18*, 624-630.

Quilbé, R., Rousseau, A. M., Moquet, J.-S., Trinh, N. B., Yonas, D., Gachon, P., & Chaumont, D. (2008). Assessing the Effect of Climate Change on River Flow Using General Circulation Models and Hydrological Modelling – Application to the Chaudière River, Québec, Canada. *Canadian Water Resources Journal, 33*(1), 73-94.

Ree, W. O. (1939). Some experiments on shallow flows over a grassed slope. *Transactions of the American Geophysical Union, 20*, 653-656.

Ree, W. O. (1941). Hydraulic Tests of Kudzu as a Conservation Channel Lining. *Agricultural Engineering*(1).

Ree, W. O. (1941). Hydraulic Tests of Kudzu as a Conservation Channel Lining. *Agricultural Engineering, 22*(1).

Ree, W. O. (1949, April). Hydraulic characteristics of vegetation for vegetated waterways. *Agricultural Engineering*, 184-189.

Ree, W. O. (1958). Retardation Coefficients for Row Crops in Diversion Terraces. *Transactions of the ASAE, 1*(1), 78-80.

Ree, W. O., & Palmer, V. J. (1949). *Flow of water in channels protected by vegetative linings.* Washington DC: U.S. Soil Conservation Service Technical Bulletin vol. 967.

Reitan, T., & Petersen-Øverleir, A. (2011). Dynamic rating curve assessment in unstable rivers using Ornstein-Uhlenback processes. *Water Resources Research, 47*. doi:10.1029/2010WR009504

Rice, S., & Church, M. (1996). Sampling surficial fluvial gravels: the precision of size distribution percentile estimates. *Journal of Sedimentary Research, 66*(3), 654-665. doi:1079-130X/96/D66-654/$03.00

Rodusky, A. J., Sharfstein, B., East, T. L., & Maki, R. P. (2005). A comparison of three methods to collect submerged aquatic vegetation in a shallow lake. *Environmental Monitoring and Assessment, 110*, 87-97.

Rolls, R. J., Leigh, C., & Sheldon, F. (2012). Mechanistic effects of low-flow hydrology on riverine ecosystems: ecological principles and consequences of alteration. *Freshwater Science, 31*(4), 1163-1186. doi:10.1899/12-002.1

Samani, J., & Kouwen, N. (2002). Stability and Erosion in grassed channels. *Journal of hydraulic engineering, 128*(1), 40-45.

Samuels, P. G. (1990). Cross-section location in 1-d models. *International conference on river flood hydraulics* (pp. 339-350). Wallingford, UK: HR Wallingford.

Sand-Jensen, K. (2003). Drag and reconfiguration of freshwater macrophytes. *Freshwater biology, 48*, 271-283.

Sand-Jensen, K., & Pedersen, M. (2008). Streamlining of plant patches in streams. *Freshwater Biology, 53,* 714-726. doi:10.1111/j.1365-2427.2007.01928.x

Scheffer, M., & Carpenter, S. R. (2003). Catastrophic regime shifts in ecosystems: linking theory to observation. *Trends in Ecology and Evolution, 18*, 648-656.

Schmidt, A. R. (2004). Uncertainties in Discharges from Stations where Rating Shifts are Utilized. *Critical Transitions in Water and Environmental Resources Management.* ASCE.

Sellin, R. H., & van Beesten, D. P. (2004). Conveyance of a managed vegetated two-stage river channel. *Proceedings of the Institution of Civil Engineers, Water Management 157*(WM1), 21-33.

Serra, J. (1983). *Image Analysis and Mathematical Morphology.* Orlando, Florida, USA: Academic Press Inc.

Serway, R. A. (1986). *Physics for Scientists and Engineers.* Saunders College Publishing.

Shahbazi, M., Théau, J., & Ménard, P. (2014). Recent applications of unmanned aerial imagery in natural resource management. *GIScience & Remote Sensing, 51*(4), 339-365. doi:10.1080/15481603.2014.926650

Sheldon, R. B., & Boylen, C. W. (1978). An underwater survey method for estimating submerged macrophyte population density and biomass. *Aquatic Botany, 4*, 5-72.

Smakthin, V. U. (2001). Low Flow Hydrology: a review. *Journal of Hydrology, 240*, 147-186.

Sobel, I., & Feldman, G. (1968). A 3x3 Isotropic Gradient Operator for Image Processing. Stanford Artificial Intelligence Project.

Standardization, I. O. (1997). ISO 748 Measurement of liquid flow in open channels -- Velocity-area methods.

Statzner, B., Lamouroux, N., Nikora, V., & Sagner, P. (2006). The debate about drag and reconfiguration of freshwater macrophytes: comparing results obtained by three recently discussed approaches. *Freshwater Biology, 51*, 2173-2183.

Stone, M. C., Chen, L., McKay, S. K., Goreham, J., Acharya, K., Fischenich, C., & Stone, A. B. (2013). Bending of submerged woody riparian vegetation as a function of hydraulic flow conditions. *River Research and Applications, 29*, 195-205.

Suren, A. M., & Jowett, I. G. (2006). Effects of floods versus low flows on invertebrates in a New Zealand gravel-bed river. *Freshwater Biology*, *51*(12), 2207-2227. doi:10.1111/j.1365-2427.2006.01646.x

Tamminga, A. D., Eaton, B. C., & Hugenholtz, C. H. (2015). UAS-based remote sensing of fluvial change following an extreme flood event. *Earth Surface Processes and Landforms, 40*, 1464-1476. doi:10.1002/esp.3728

Tanino, Y., & Nepf, H. M. (2008). Lateral dispersion in random cylinder arrays at high Reynolds number. *Journal of Fluid Mechanics, 600*, 339-371.

Task Force on Friction in Open Channels. (1963). Friction factors in open channels. *Journal of the Hydraulics Division, 89*, 97-143.

Temple, D. M. (1980). Tractive force design of vegetated channels. *Transactions of the ASAE, 23*(4), 884-890.

Tomkins, K. M. (2014). Uncertainty in streamflow rating curves: methods, controls and consequences. *Hydrological processes*, 464-481. doi:10.1002/hyp.9567

Trepel, M., Holsten, B., Kieckbusch, J., Otten, I., & Pieper, F. (2003). Influence of macrophytes on water level and flood dynamics in a riverine wetland in Northern Germany. *International conference 'Towards natural flood reduction strategies'*. Warsaw.

USDA. (2007). Chapter 7: Grassed Waterways. In *Part 650: Engineering Field Handbook*.

van der Heide, T., Roijackers, R. M., van Nes, E. H., & Peeters, E. T. (2006). A simple equation for describing the temperature dependent frowth of free-floating macrophytes. *Aquatic Botany, 84*, 171-175.

Verschoren, V., Meire, D., Schoelynk, J., Buis, K., Bal, K. D., Troch, P., . . . Temmerman, S. (2016). Resistance and reconfiguration of natural flexible submerged vegetation in hydrodynamic river modeling. *Environmental Fluid Mechanics, 16*, 245-265. doi:10.1007/s10652-015-9432-1

Verschoren, V., Schoelynck, J., Buis, K., Visser, F., Meire, P., & Temmerman, S. (2017). Mapping the spatio-temporal distribution of key vegetation cover properties in lowland river reaches, using digital photography. *Environmental Monitoring Assessments, 189: 294*. doi:https://doi.org/10.1007/s10661-017-6004-5

Visser, F., Buis, K., Verschoren, V., & Schoelynck, J. (2016). Mapping of submerged aquatic vegetation in rivers from very high-resolutions image data, using object-based image analysis combined with expert knowledge. *Hydrobiologia*, 1-19. doi:10.1007/s10750-016-2928-y

Whitfield, P. H., & Hendrata, M. (2006). Assessing detectability of changes in low flow in future climates from stage discharge measuremetns. *Canadian Water Resource Journal, 31*, 1-12.

Wilson, C. A. (2007). Flow resistance models for flexible submerged vegetation. *Journal of Hydrology*, 213-222. doi:10.1016/j.jhydrol.2007.04.022

Wilson, C. A., & Horritt, M. S. (2002). Measuring the flow resistance of submerged grass. *Hydrological processes, 16*, 2589-2598. doi:10.1002/hyp.1049

Wolman, G. M. (1954). A method of sampling coarse river-bed material. *TransactionsAmerican Geophisical Union, 35*(6), 951-956.

Yin, Y., & Kreiling, R. M. (2011). The evaluation of a rake method to quantify submersed vegetation in the Upper Mississippi River. *Hydrobiologia, 675*, 187-195.

Appendix A : Additional analyses and calculations

A.1 Extrapolation of water levels

Flow rates during the vegetative period may be lower than those recorded in the non-vegetated period. In these cases, a direct comparison between non-vegetated water levels (WL_b) and vegetated water levels (WL_v) is not possible. Thus, WL_b were extrapolated based on the water level at the non-vegetated section, WL_C recorded at the same time. The procedure is as follows: first, a best-fit function between WL_C and WL_b in Reach 1 and 2 is determined for the non-vegetated period (Section 4.3.3.2):

$$WL_b(t) = a + bWL_C(t) \quad for\ t < t_{veg} \tag{A-1}$$

Where t denotes the time at which WL_C and WL_b were recorded and t_{veg} the end of the non-vegetated period (Section 4.3.3.2).

Then, using the water level at the non-vegetated section WL_C (Section 4.3.2), WL_b at Reaches 1 and 2 are calculated for the vegetated period using the formula:

$$WL_b(t) = a + bWL_C(t) \quad for\ t > t_{veg} \tag{A-2}$$

This procedure allows to compare vegetated and non-vegetated water levels at the same value of discharge.

Accuracy of the extrapolation procedure was determined by calculating errors by comparing known WL_b values (i.e. recorded during the non-vegetated period) with calculated ones.

$$\epsilon = |WL_{b\ meas}(t) - WL_{b\ calc}(t)| \tag{A-3}$$

Where $WL_{b,\ meas}$ and $WL_{b,\ calc}$ are the measured and calculated (using Equation (A-2)) non-vegetated water levels. Average value of ϵ was 0.003 m, which is the accuracy of the water level loggers used in this study. As such, the extrapolation procedure was deemed accurate.

A.2 Outliers

At reaches 1 and 2, out of 46 surveys undertaken, 5 (11%) were excluded. Of these, three (7%) were removed because of detected measurement errors, and two (4%) because of singularities that could not be accounted by the methodology used.

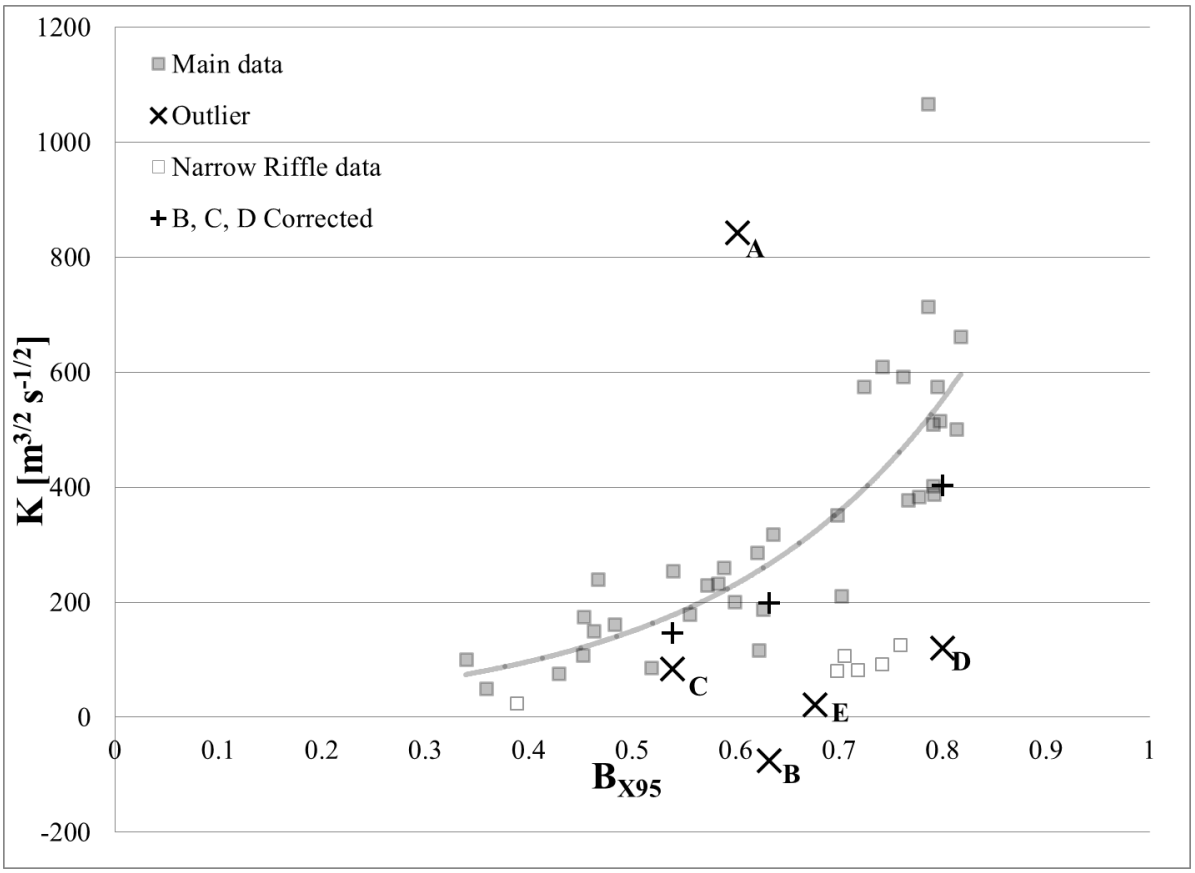

Figure A-1: Outliers recorded at Reaches 1 and 2

Point A (Figure A-1) in Reach 1 plots to the left of the interpolating curve, having a *K* value much higher than predicted based on its B_{X95}. The point was collected in early October 2015 when a large part of aquatic plants died, as testified by the value of B_X being 37% lower than the September average. Nevertheless, it was observed that most of these plants remained in the reach, spanning the whole width and (Figure A-2), adding to the backwater effect. As the methodology measures distribution of live vegetation, it cannot account for backwater caused by dead plants. Consequently, Point A was excluded from the analysis. A similar result was observed the following year in the form of a "spike" in E_Q in early October 2016, which did not occur in 2014(Figure 4-8). In the latter case, high flows were recorded in the fall, removing the dead plants from the reach and preventing them from accumulating and causing backwater. Conversely, no high flows were observed in 2015 and 2016 in early October and dead plants added to the resistance to flow by accumulating. As such, field observations should be undertaken to assess whether the site used is prone to these issues. It should be noted that this phenomenon was not recorded at Reach 2, where field observations of plants showed a lower accumulation of dead specimens (Figure A-2).

Figure A-2: accumulation of dead specimens spanning the whole cross-sectional width (Reach 1, left) and scattered around the reach, thus not affecting backwater (Reach 2, right).

Points B and C correspond to vegetation surveys undertaken at Reaches 1 and 2 on June 29th. These data points were removed after an issue with the water level recorded at the non-vegetated location (Section 4.3.2) between June 22nd and July 1st was detected. This data is used to estimate ΔWL and consequently K. As such, this issue caused an underestimation of K, of approximately 275 $m^{3/2}s^{-1/2}$ at Reach 1 and 62 $m^{3/2}s^{-1/2}$ at Reach 2. If the points are corrected (by compensating for the aforementioned drop), they fall close to the curve defined by Equation (4-14). However, it should be noted that these corrected points were not used in developing Equations (4-14), (4-15), and (4-16).

Point D was removed after an analysis showed an anomalous drop in ΔWL for Reach 1 immediately following a field visit to download data from the loggers. The causes of this drop are unknown, but are likely related to measurement error due to the abrupt nature of the drop in ΔWL, which is similar to what was observed for points B and C. This drop was not observed in Reach 2. Similar to Points B and C, if the anomalous drop is compensated, the "corrected" point falls close to the curve defined by Equation (4-14), however this point was not used to develop Equations (4-14), (4-15), and (4-16).

Point E was removed as it had an uncharacteristically low K value (~20 $m^{3/2}s^{-1/2}$) as, for similar values of B_{X95} (~0.68) K was usually one order of magnitude higher, at both reaches. A possible explanation is that larger than usual groundwater loss occurred between Reach 1 and the non-vegetated control, thus affecting ΔWL. Naturally, methods used here are not able to detect this phenomenon thus point E was removed.

A.3 Daily water level fluctuations

Previous research (Haslam, 1978; Howes, 2007) indicated how daily fluctuations in water levels during summer low flows may be due to changes in vegetative flow resistance due to changes in plants respiration between night and day. These changes are believed to affect plants buoyancy and stiffness, and thus vegetative flow resistance.

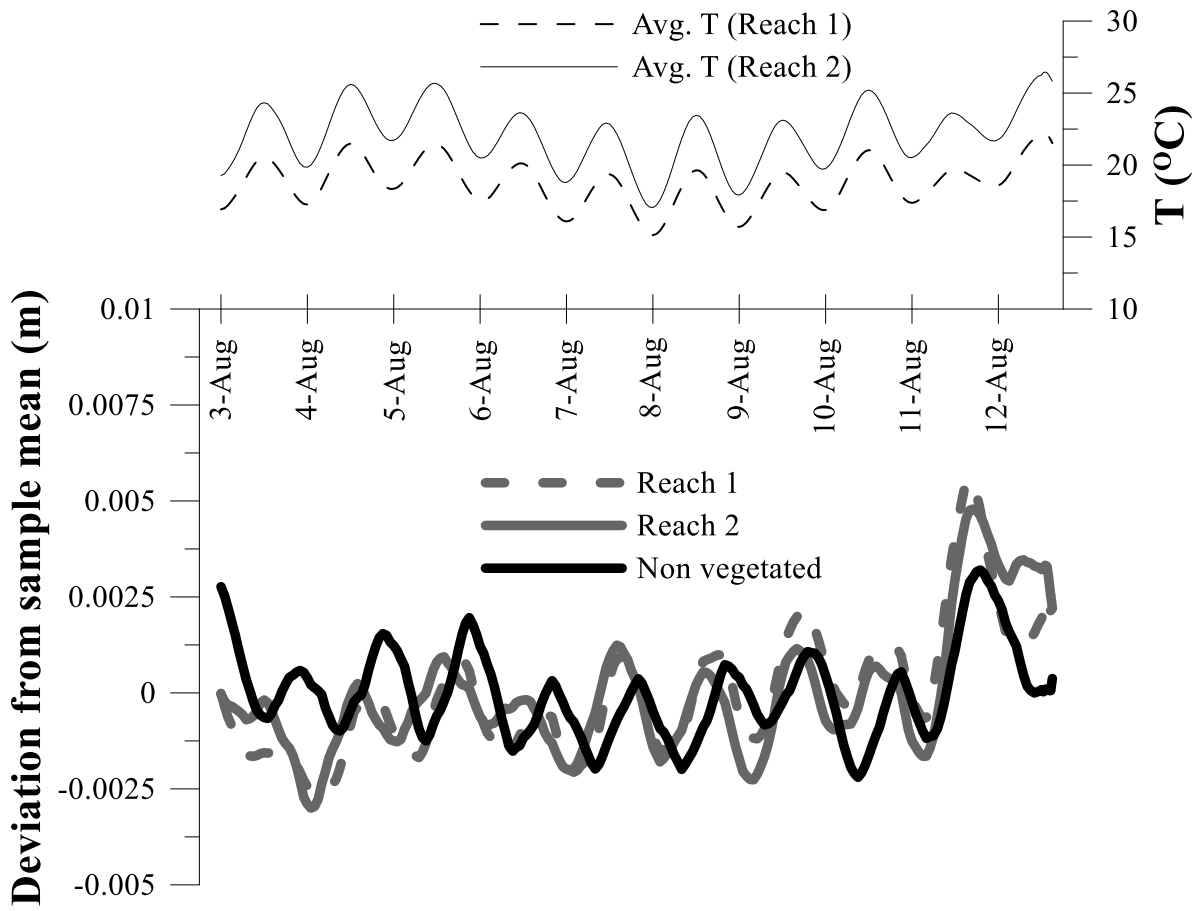

Figure A-3: Daily fluctuations in water temperature and water level between non-vegetated location and Reaches 1 and 2 (12 hour moving average)

Daily fluctuations were recorded at Reaches 1 and 2 during the summer, ranging 4 and 6 mm respectively, nevertheless, almost identical fluctuations were also recorded at a non-vegetated location which is not affected by vegetative growth (Section 4.3.2). Therefore, while daily changes in plant respiration effects on flow resistance cannot be ruled out, other diurnal effects were also recorded. These may be due to groundwater/surface water exchanges or changes in water viscosity reflecting water temperature fluctuations (Figure 3-8). All of these phenomena were outside the scope of this study and, for this reason, were not assessed.

Appendix B : Additional data

B.1 Monitoring data

Table B-1: Discharge measurements valid for Reaches 1 and 2

Stage [m]	Discharge [m^3/s]	Number of panels	Inaccuracy [ISO 1997]
0.211	0.270	25	2.90%
0.204	0.254	29	2.60%
0.180	0.123	29	2.60%
0.188	0.150	29	2.60%
0.229	0.329	29	5.10%
0.234	0.361	29	2.70%
0.175	0.131	29	2.70%
0.180	0.134	28	2.80%
0.168	0.100	28	2.70%
0.155	0.078	27	2.80%
0.172	0.110	29	2.70%
0.182	0.142	30	2.70%
0.178	0.120	30	2.80%
0.240	0.410	31	2.60%
0.196	0.198	29	2.70%
0.200	0.223	30	2.60%
0.220	0.319	32	2.60%
0.185	0.167	30	2.70%
0.168	0.106	30	2.80%
0.150	0.052	29	2.90%
0.149	0.053	35	2.60%
0.156	0.061	35	2.60%
0.160	0.066	30	2.80%
0.144	0.045	31	2.80%
0.137	0.036	30	2.70%
0.141	0.037	30	2.80%
0.218	0.248	33	2.40%
0.159	0.081	33	2.50%
0.163	0.097	40	2.20%
0.151	0.052	33	2.50%
0.151	0.055	37	2.30%
0.156	0.056	38	2.30%
0.134	0.024	31	2.70%
0.136	0.028	35	5.00%

Table B-2: Discharge measurements at Reaches 3, 4, and 5

Reach	**Discharge (m^3/s)**	**# panels**	**Inaccuracy (ISO 1997)**
Reach 3	0.051	35	2.30%
Reach 4	0.339	35	2.40%
Reach 5	0.117	38	2.20%

Table B-3:Summary of data obtained at Reach 1

Date	**Q [m^3/s] [a]**	**T [m]**	**S_W [-]**	**ΔWL (mm)**	**K ($m^{3/2}s^{-1/2}$)**
17-Jul-2014	0.367	10.17	1.56E-04	9	116
07-Aug-2014	0.129	10.54	2.99E-05	11	610
14-Aug-2014	0.143	10.13	5.27E-05	10	388
22-Aug-2014	0.098	10.36	4.98E-05	8	403
28-Aug-2014	0.065	10.17	2.47E-05	6	510
10-Sep-2014	0.106	10.01	2.80E-05	12	714
17-Sep-2014	0.173	10.52	8.58E-05	13	384
03-Jul-2015	0.298	10.48	1.71E-04	15	233
13-Jul-2015	0.147	10.13	1.57E-04	16	352
22-Jul-2015	0.101	9.65	1.35E-04	15	378
29-Jul-2015	0.054	9.91	1.41E-04	17	592
07-Aug-2015	0.054	10.00	1.74E-04	18	575
21-Aug-2015	0.088	10.34	1.79E-04	19	516
10-Sep-2015	0.071	9.46	1.82E-04	20	501
16-Sep-2015	0.045	9.81	1.39E-04	17	662
23-Sep-2015	0.031	9.91	1.21E-04	21	1066
[b]*07-Oct-2015*	[b]*0.037*	[b]*9.98*	[b]*1.20E-04*	[b]*18*	[b]*842*
10-Jun-2016	0.084	9.91	9.70E-05	2	76
[b]*29-Jun-2016*	[b]*0.059*	[b]*9.52*	[b]*1.28E-04*	[b]*-2*	[b]*-76*
[b]*15-Jul-2016*	[b]*0.073*	[b]*9.52*	[b]*1.56E-04*	[b]*1*	[b]*21*
11-Aug-2016	0.025	9.45	1.14E-04	11	575
[b]*14-Sep-2016*	[b]*0.031*	[b]*9.46*	[b]*1.31E-04*	[b]*3*	[b]*120*
19-Oct-2016	0.041	9.83	5.42E-05	5	318

[a]From rating curve [b]Outlier data

Table B-4: Summary of data obtained at Reach 2

Date	Q [m^3/s] [a]	T [m]	S_W [-]	ΔWL (mm)	K ($m^{3/2}s^{-1/2}$)
17-Jul-2014	0.367	7.08	4.78E-04	6	24
07-Aug-2014	0.129	7.78	5.14E-04	12	91
14-Aug-2014	0.143	7.40	5.19E-04	13	80
22-Aug-2014	0.098	7.60	5.64E-04	14	107
28-Aug-2014	0.065	6.71	5.32E-04	16	126
17-Sep-2014	0.173	6.69	4.96E-04	17	82
03-Jul-2015	0.298	7.14	4.45E-04	23	101
13-Jul-2015	0.147	7.01	4.61E-04	25	150
22-Jul-2015	0.101	6.89	4.57E-04	25	175
[b]*29-Jul-2015*	[b]*0.054*	[b]*6.88*	[b]*4.62E-04*	[b]*27*	[b]*260*
07-Aug-2015	0.054	6.99	4.94E-04	24	230
21-Aug-2015	0.088	7.54	5.04E-04	25	211
10-Sep-2015	0.071	6.97	5.29E-04	23	179
16-Sep-2015	0.045	6.92	5.30E-04	20	200
23-Sep-2015	0.031	6.92	4.99E-04	23	287
07-Oct-2015	0.037	7.00	5.18E-04	23	255
10-Jun-2016	0.084	7.10	3.04E-04	11	108
29-Jun-2016	0.059	7.12	3.47E-04	7	83
15-Jul-2016	0.073	7.23	2.93E-04	8	87
19-Jul-2016	0.041	6.86	3.12E-04	12	161
15-Aug-2016	0.028	6.54	3.03E-04	16	240
14-Sep-2016	0.031	6.31	2.89E-04	9	116
19-Oct-2016	0.041	6.40	3.13E-04	4	50

[a]From rating curve [b]Outlier data

Table B-5: Width of the downstream control at the study reaches

	Channel top width (m)		Reduction in top width
	Average	Control	
Reach 1	9.5	5	47%
Reach 2 (2014)	**7**	**1.8***	**76%**
Reach 2 (2015)	7	2.8*	60%
Reach 2 (2016)	7	4	29%
Reach 3	9	8	11%
Reach 4	12	11	8%
Reach 5	8	5.6	30%

*2.2 m width of bedform in 2014 (measured with RTK-GPS), 1.2 m in 2015 (measured from aerial photographs), absent in 2016; riffle width = 4m

B.2 Vegetation distribution curves

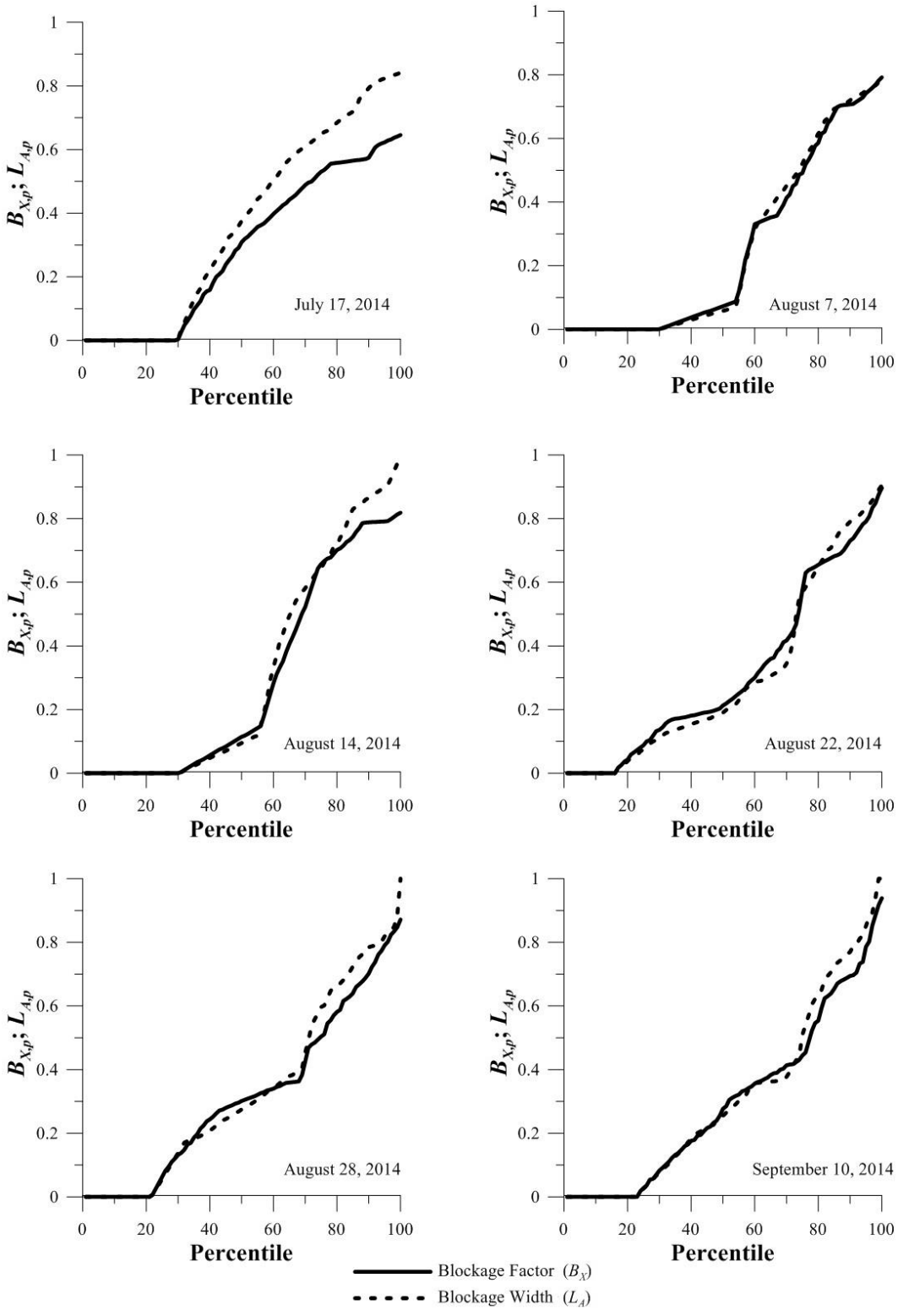

Figure B-1: VDCs for Reach 1 (1)

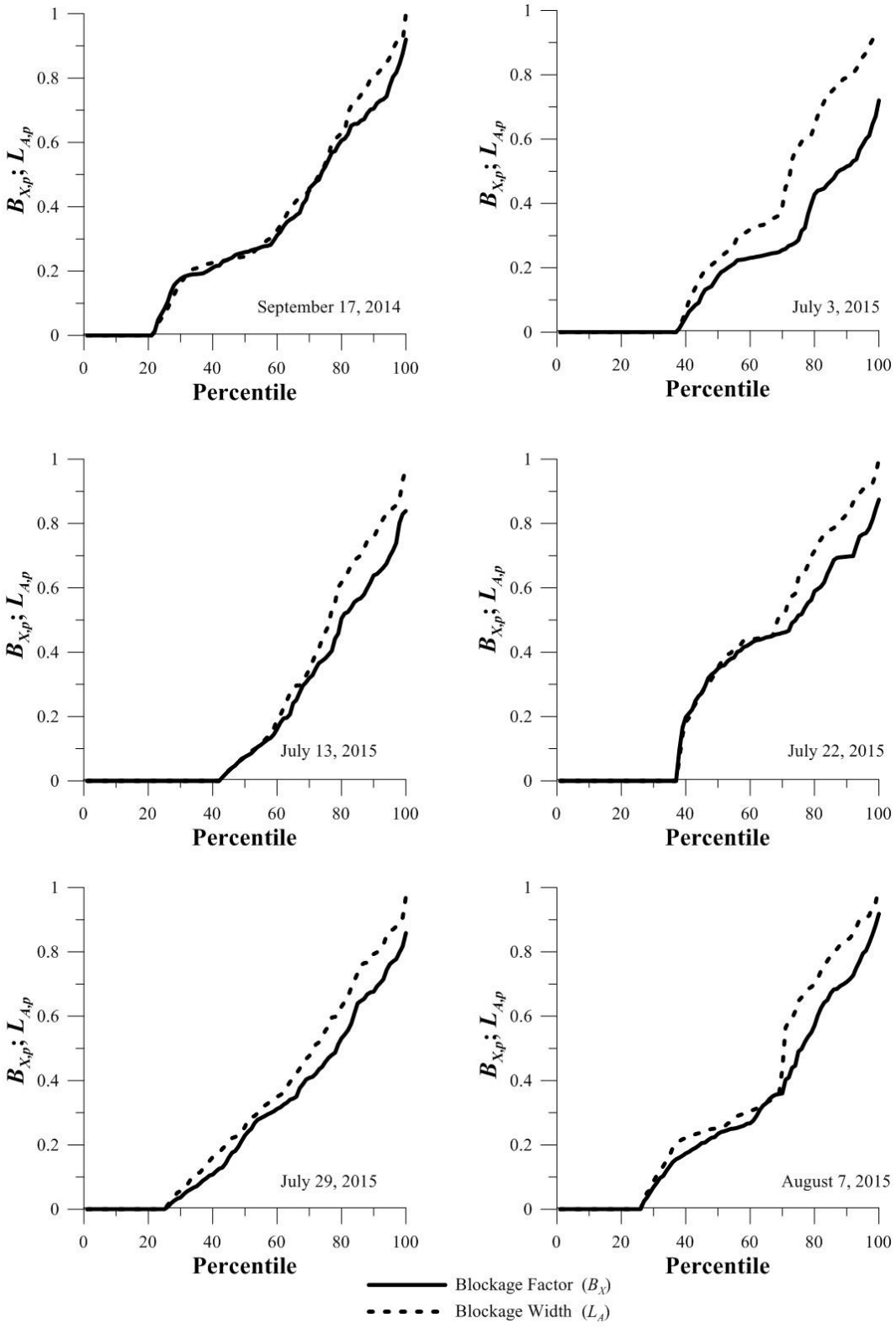

Figure B-2: VDCs for Reach 1; (2)

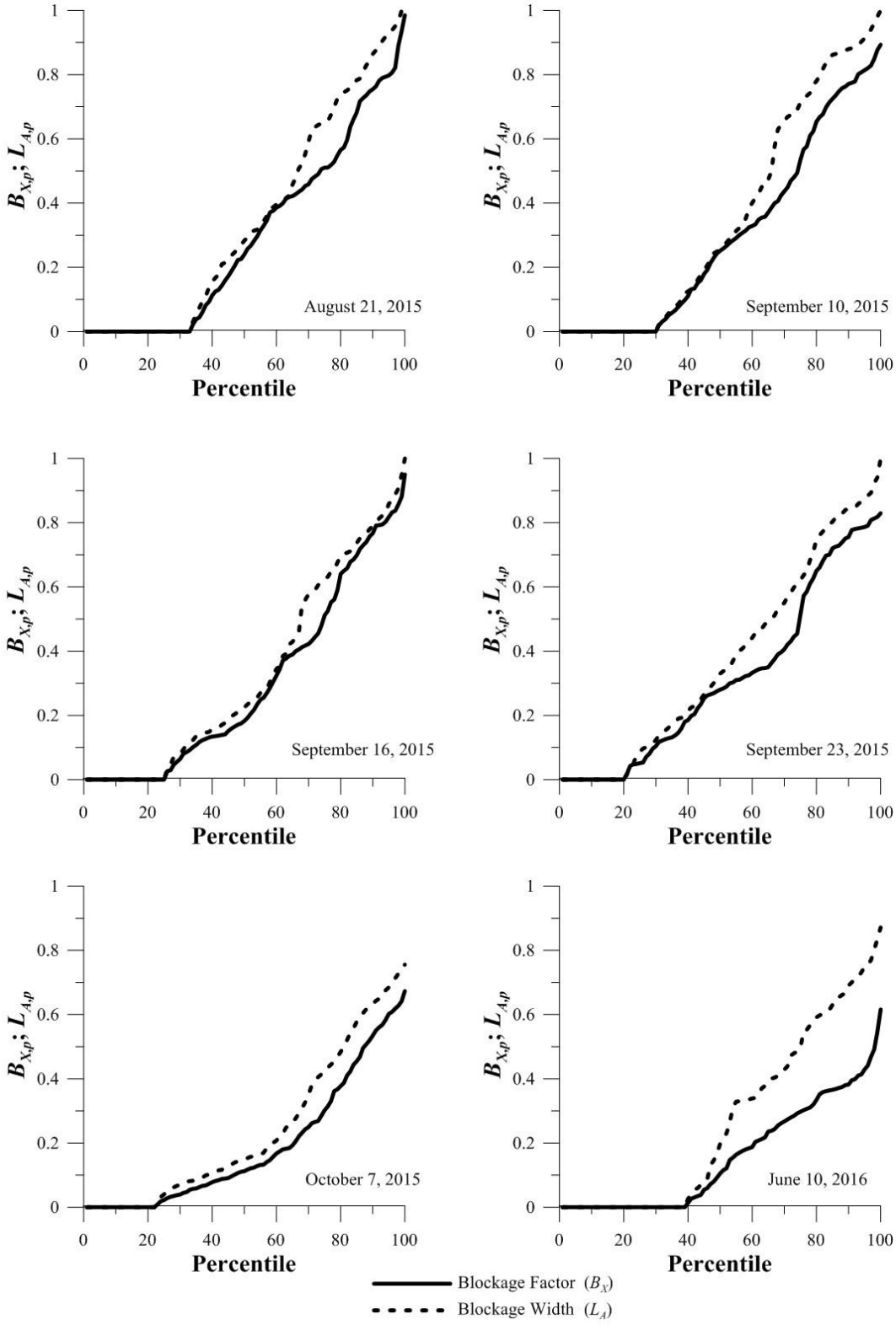

Figure B-3: VDCs for Reach 1; (3)

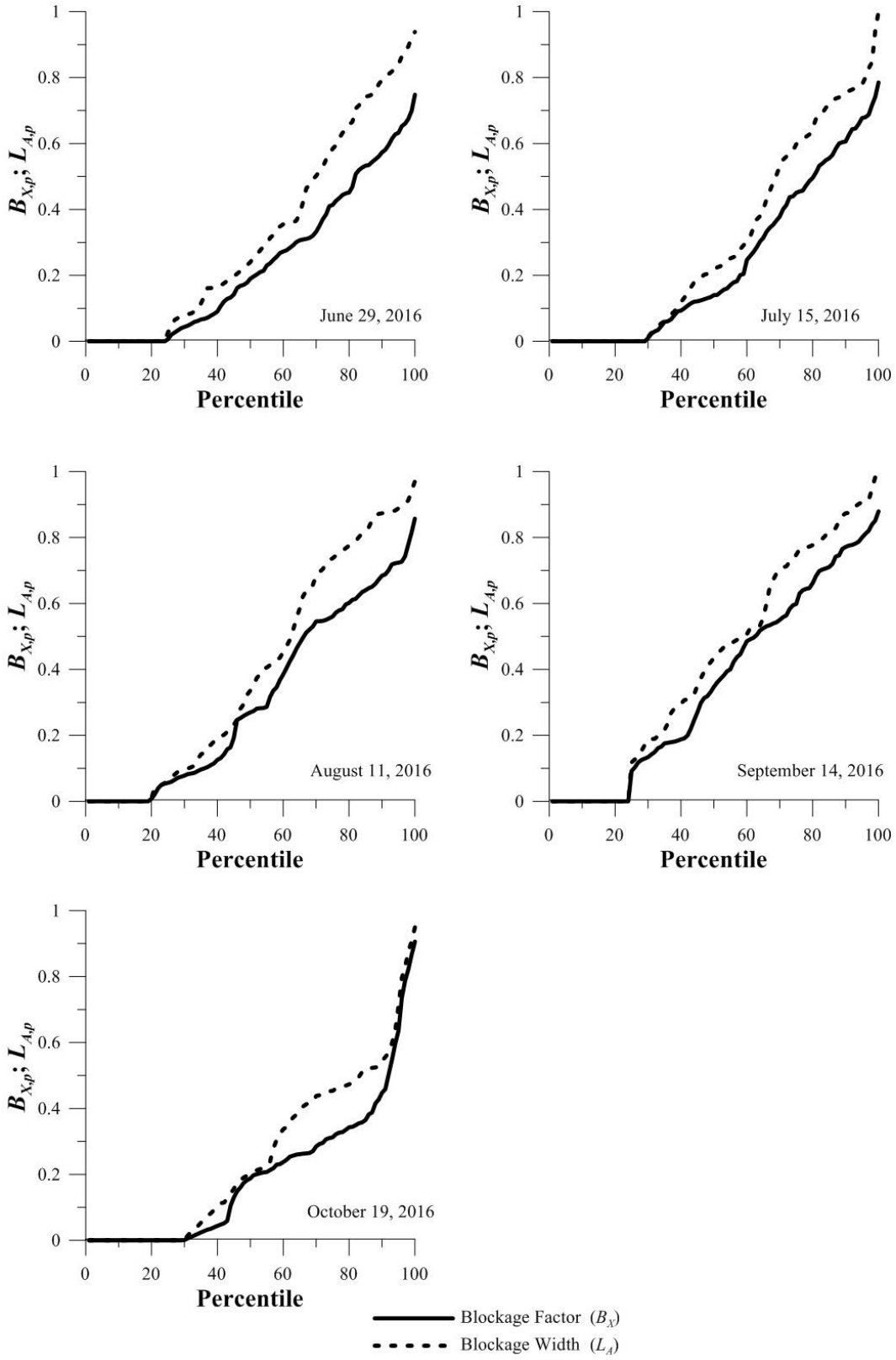

Figure B-4VDCs for Reach 1; (4)

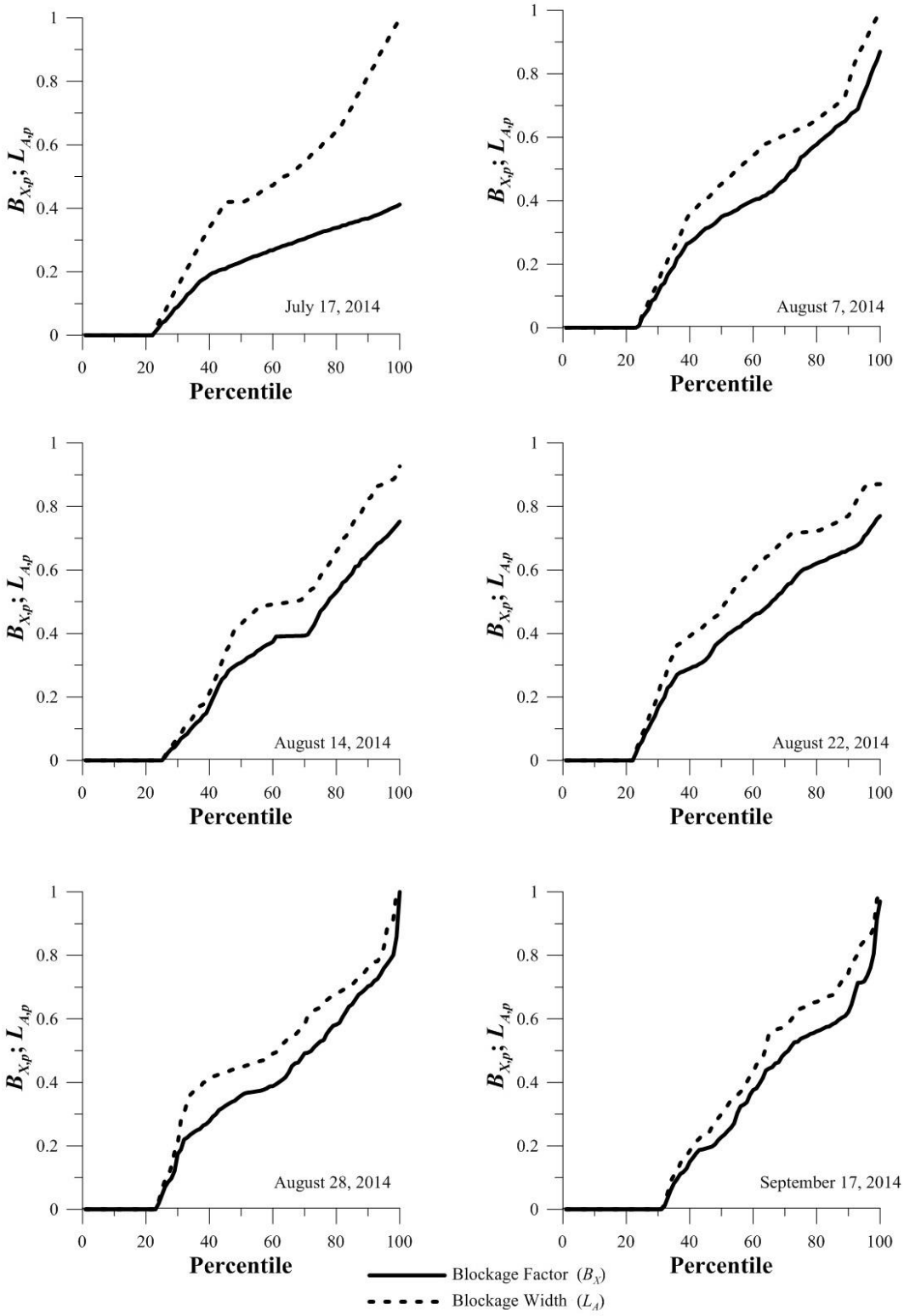

Figure B-5: VDCs for Reach 2; (1)

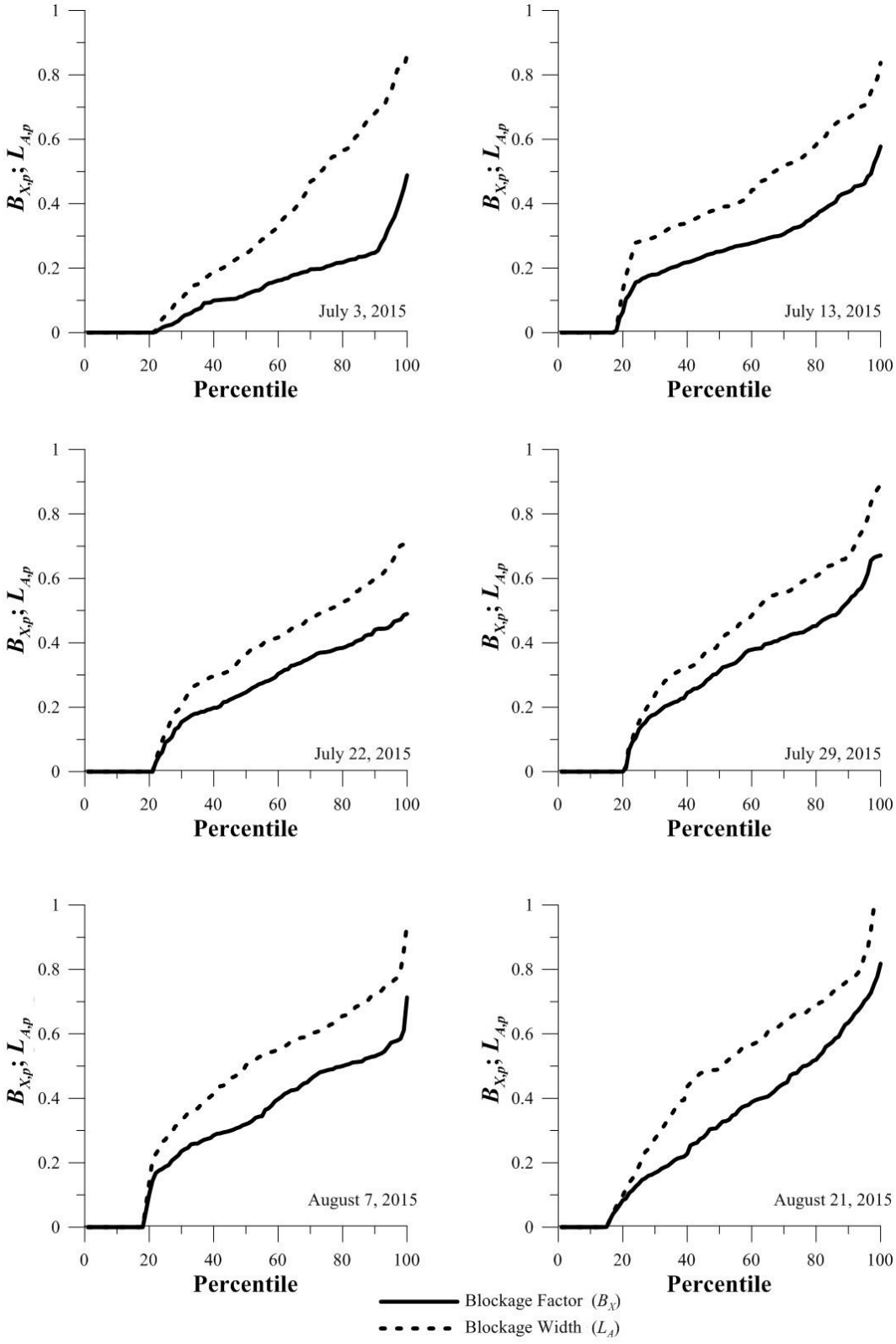

Figure B-6: VDCs for Reach 2; (2)

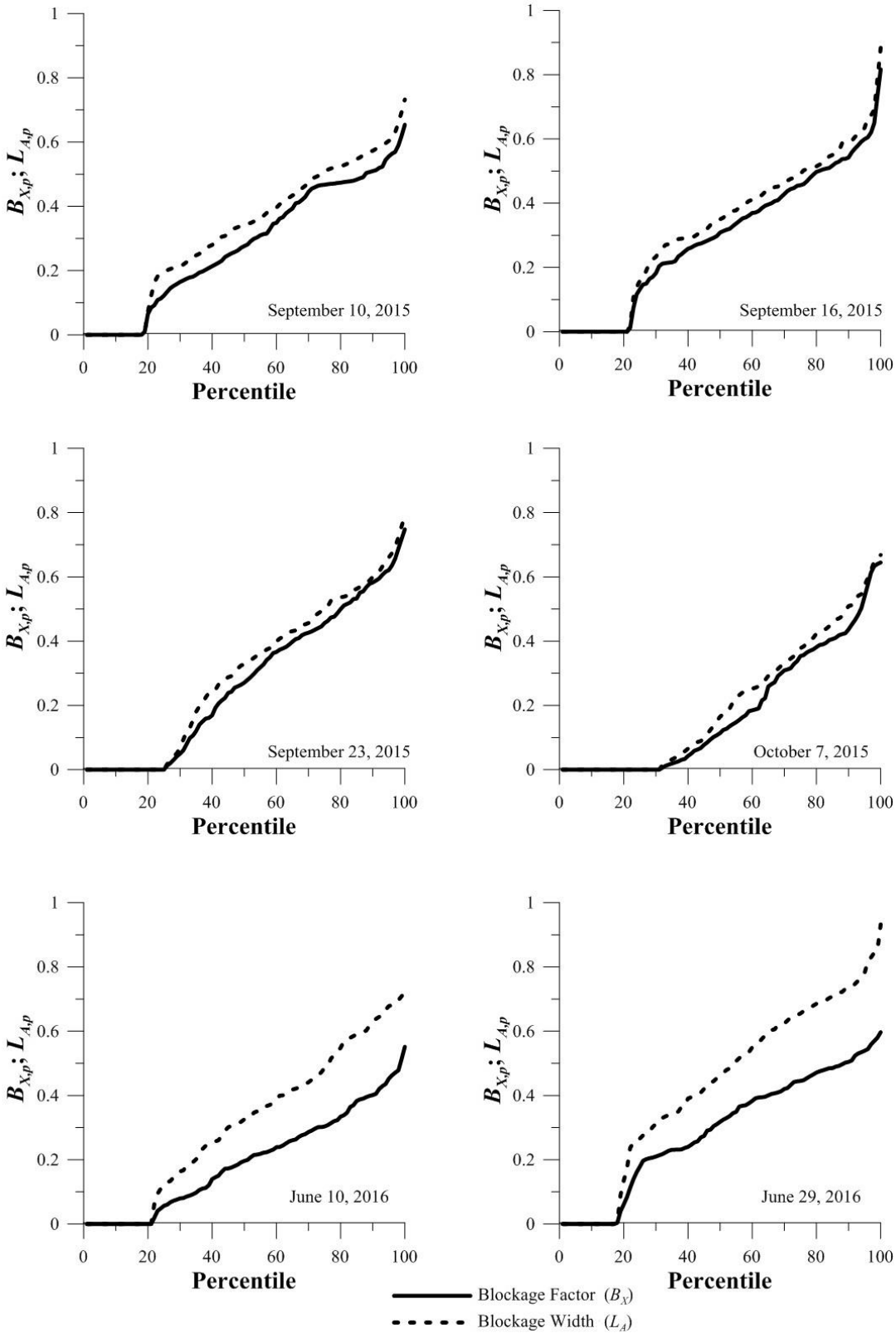

Figure B-7: VDCs for Reach 2; (3)

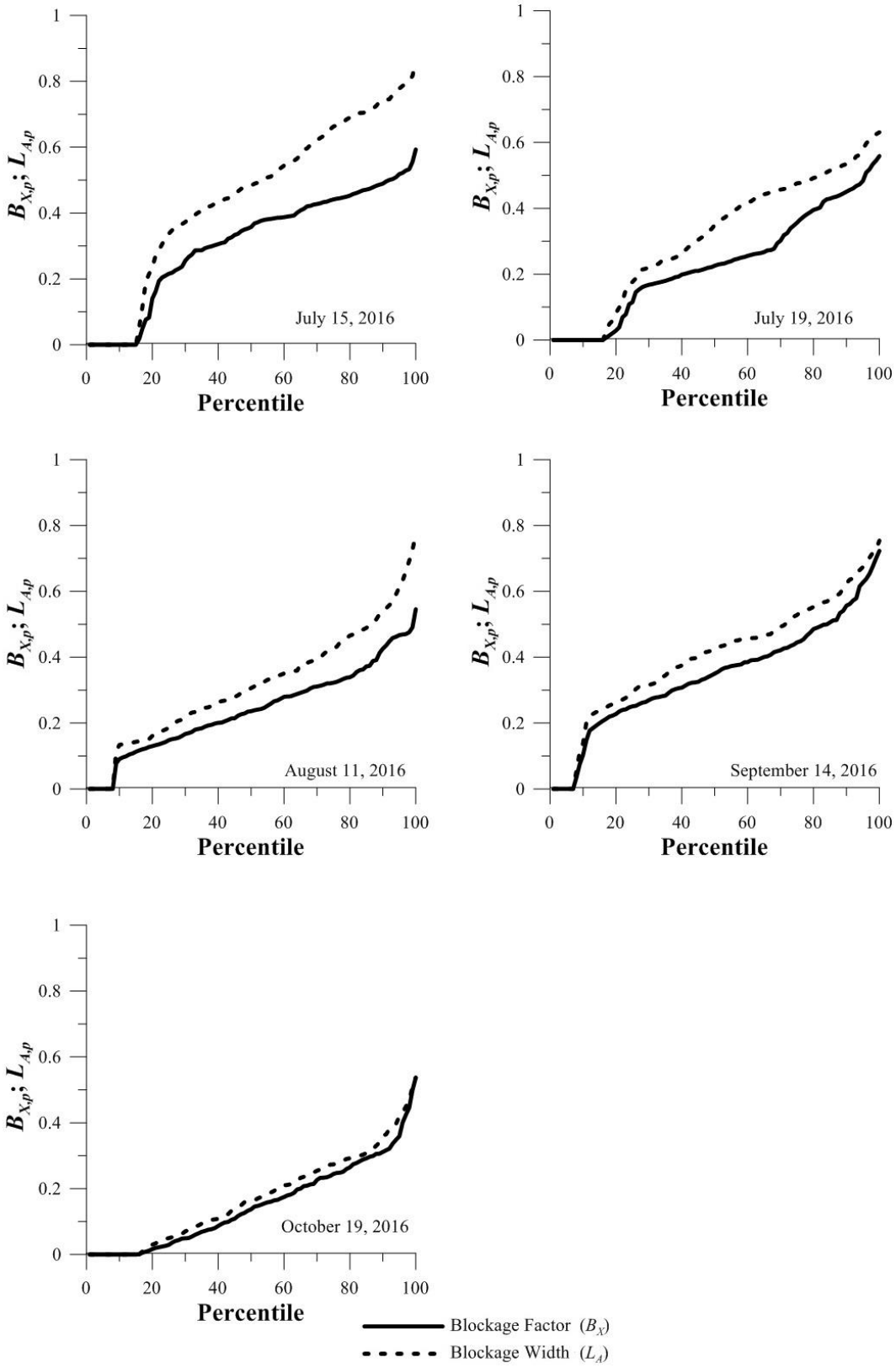

Figure B-8: VDCs for Reach 2; (4)

B.3 Polynomial functions by interpolation

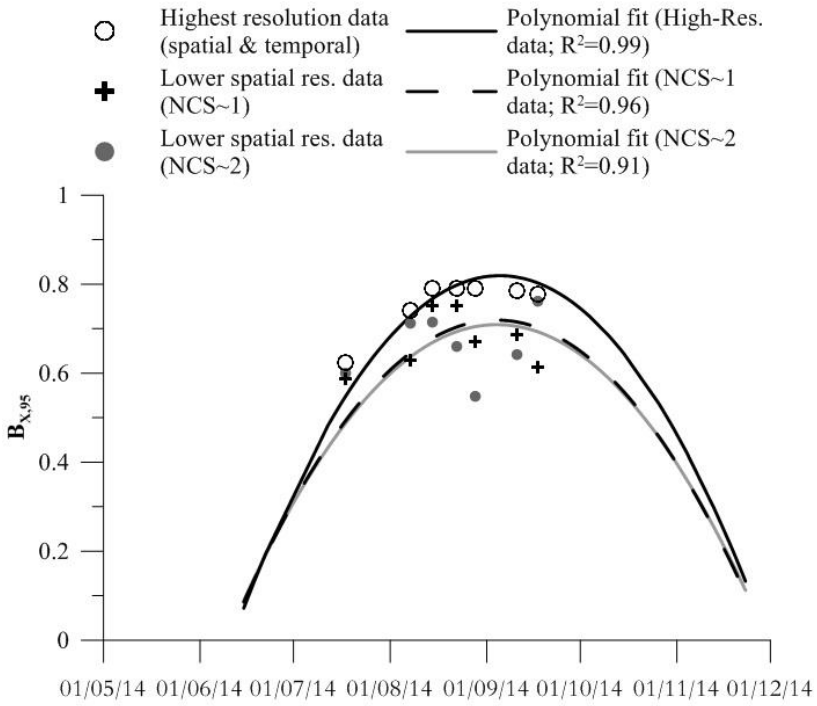

Figure B-9: Interpolation through polynomial curves (2nd order) of $B_{X,95}$ values obtained in 2014 (Year 1) at Reach 1 using data with different spatial resolutions

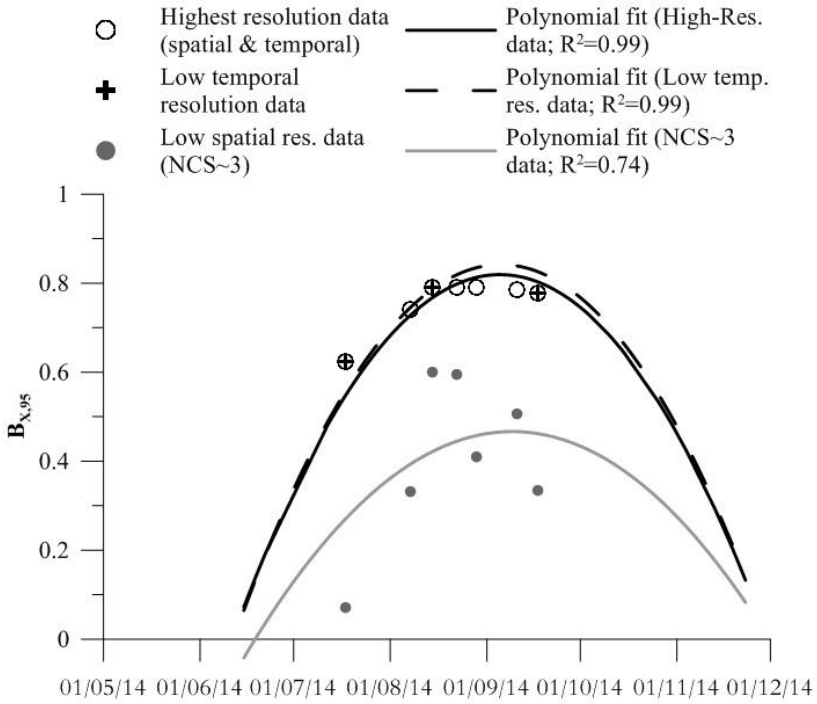

Figure B-10: Interpolation through polynomial curves (2nd order) of $B_{X,95}$ values obtained in 2014 (Year 1) at Reach 1 using data with different spatial and temporal resolutions

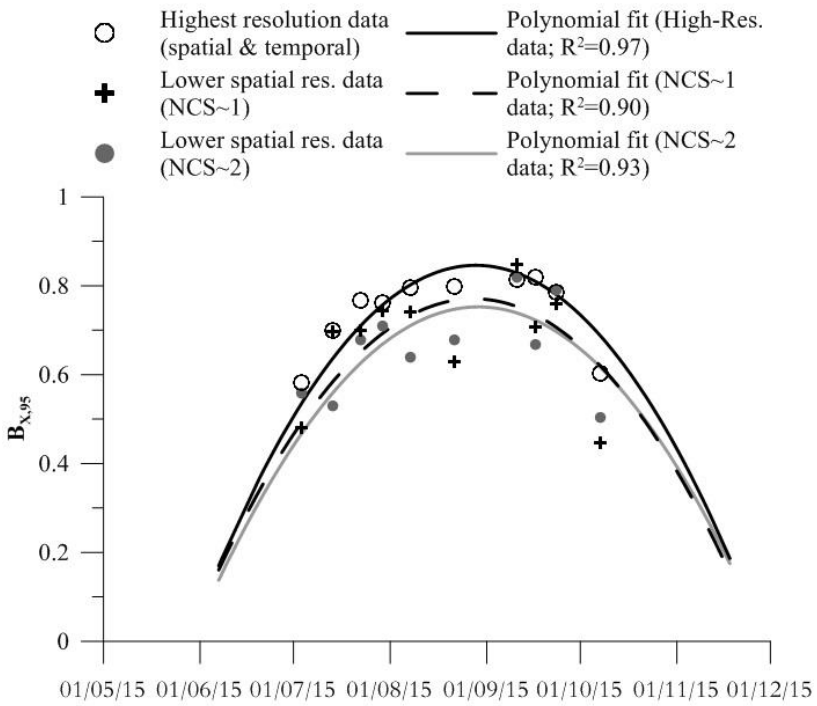

Figure B-11: Interpolation through polynomial curves (2nd order) of $B_{X,95}$ values obtained in 2015 (Year 2) at Reach 1 using data with different spatial resolutions

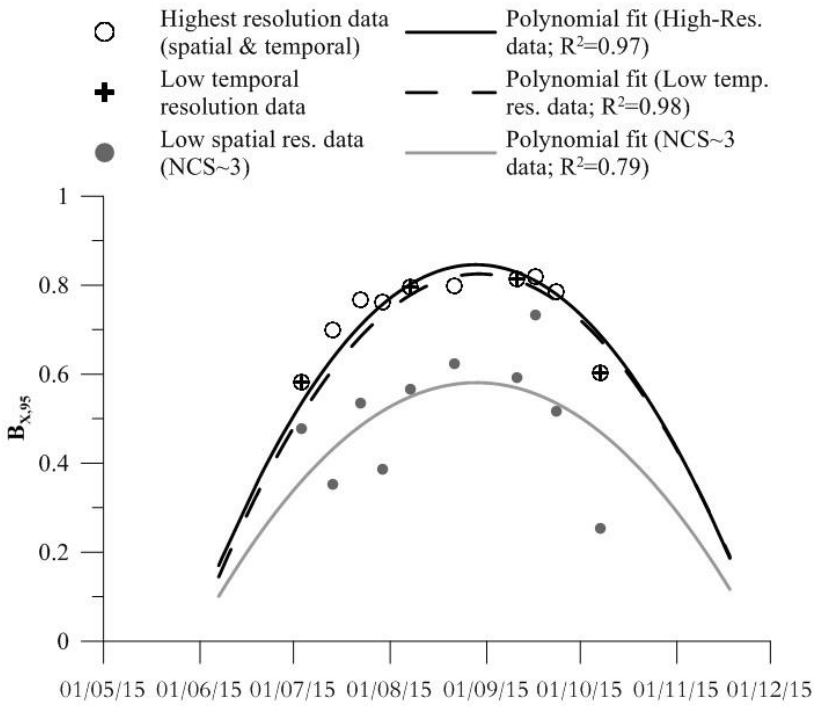

Figure B-12: Interpolation through polynomial curves (2nd order) of $B_{X,95}$ values obtained in 2015 (Year 2) at Reach 1 using data with different spatial and temporal resolutions

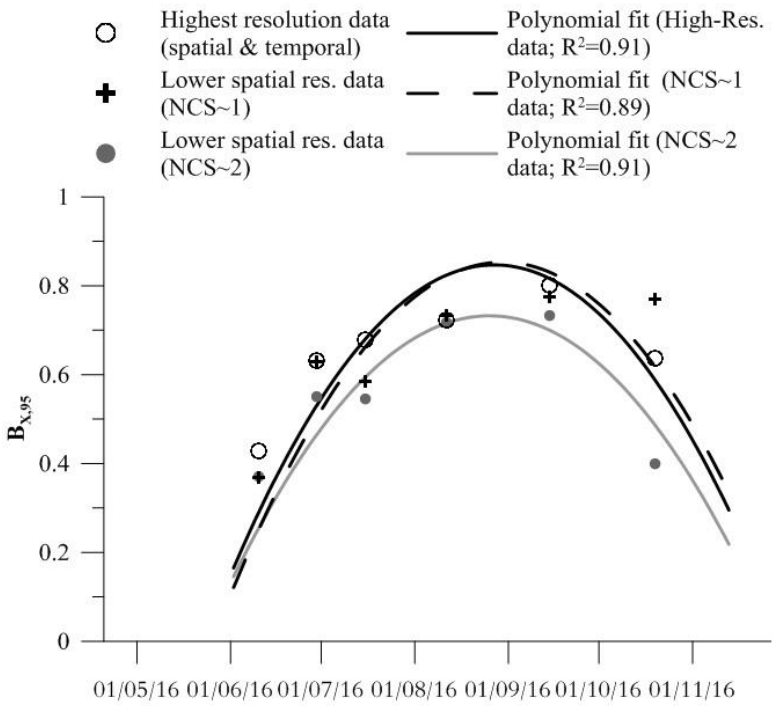

Figure B-13: Interpolation through polynomial curves (2nd order) of $B_{X,95}$ values obtained in 2016 (Year 3) at Reach 1 using data with different spatial resolutions

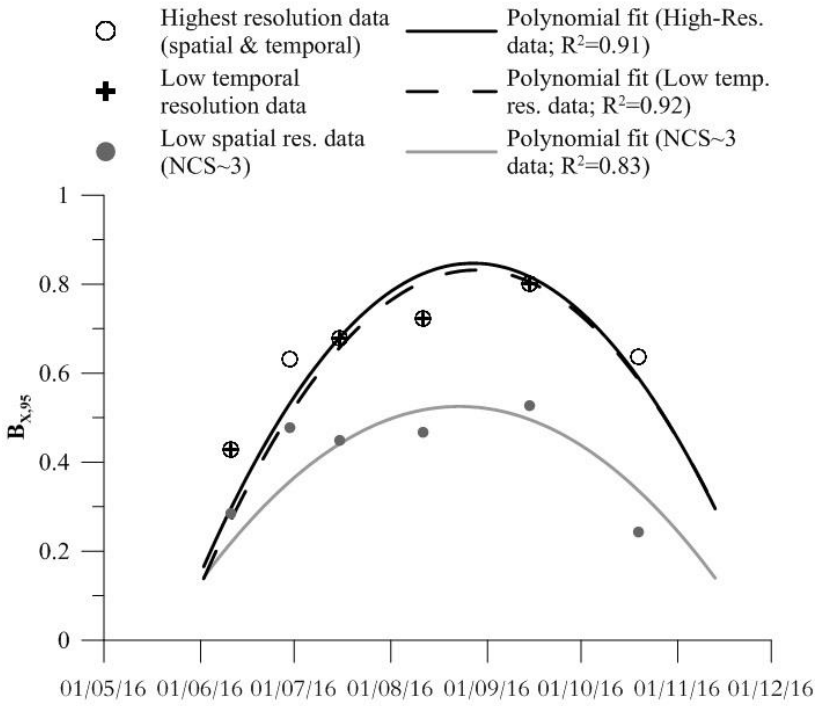

Figure B-14: Interpolation through polynomial curves (2nd order) of $B_{X,95}$ values obtained in 2016 (Year 3) at Reach 1 using data with different spatial and temporal resolutions

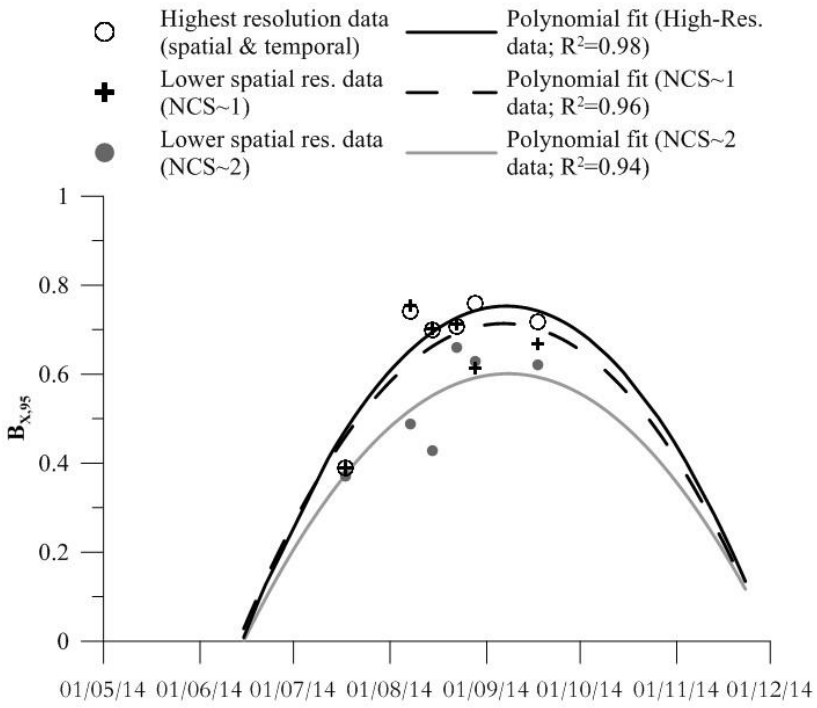

Figure B-15: Interpolation through polynomial curves (2nd order) of $B_{X,95}$ values obtained in 2014 (Year 1) at Reach 2 using data with different spatial resolutions

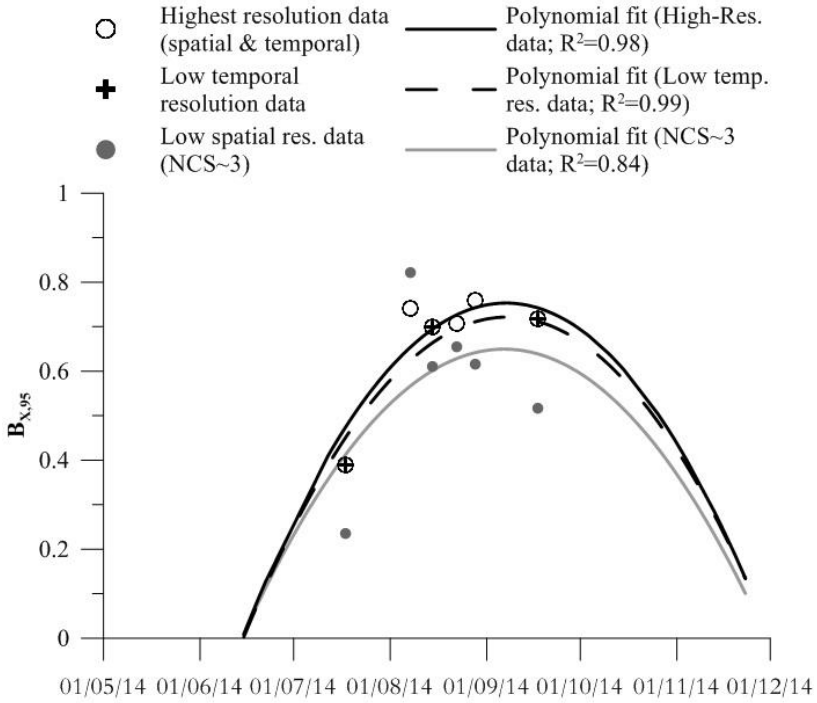

Figure B-16: Interpolation through polynomial curves (2nd order) of $B_{X,95}$ values obtained in 2014 (Year 1) at Reach 2 using data with different spatial and temporal resolutions

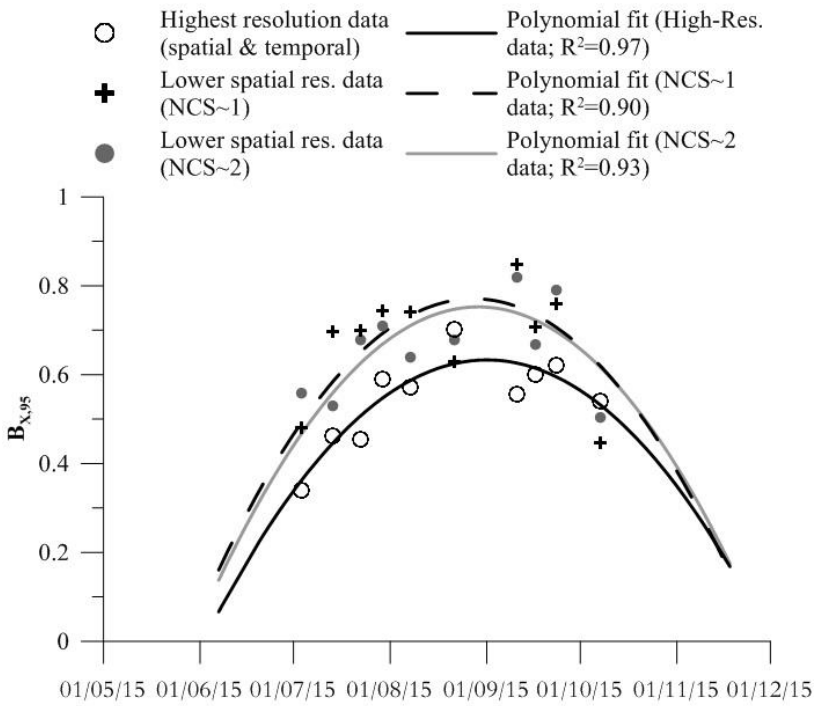

Figure B-17: Interpolation through polynomial curves (2nd order) of $B_{X,95}$ values obtained in 2015 (Year 2) at Reach 2 using data with different spatial resolutions

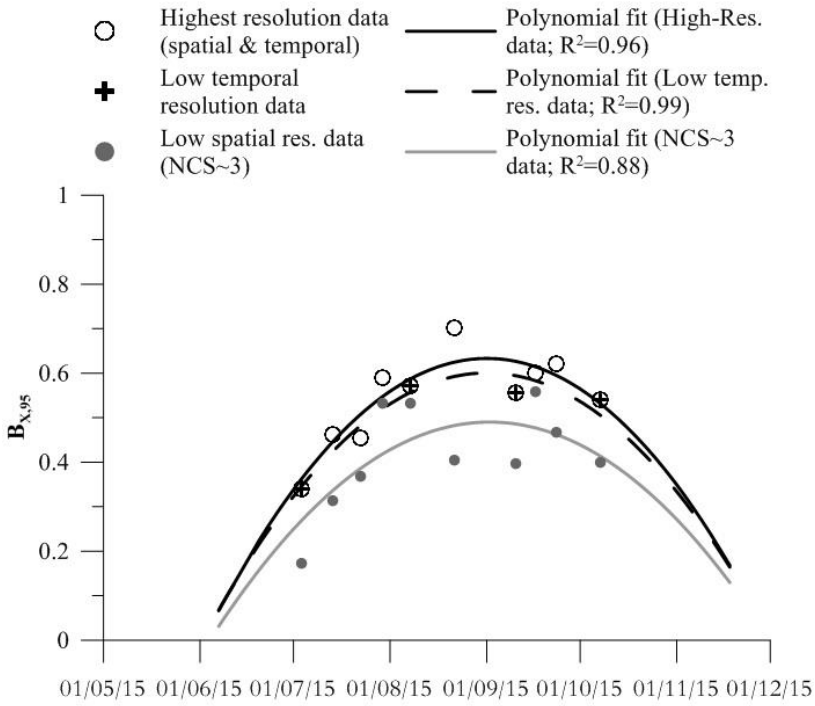

Figure B-18: Interpolation through polynomial curves (2nd order) of $B_{X,95}$ values obtained in 2015 (Year 2) at Reach 2 using data with different spatial and temporal resolutions

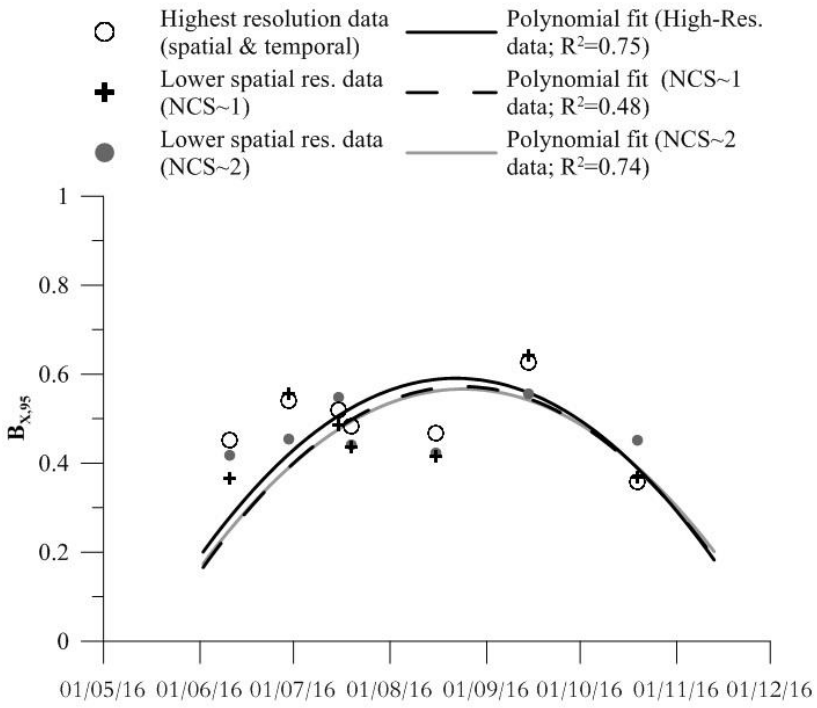

Figure B-19: Interpolation through polynomial curves (2nd order) of $B_{X,95}$ values obtained in 2016 (Year 3) at Reach 2 using data with different spatial resolutions

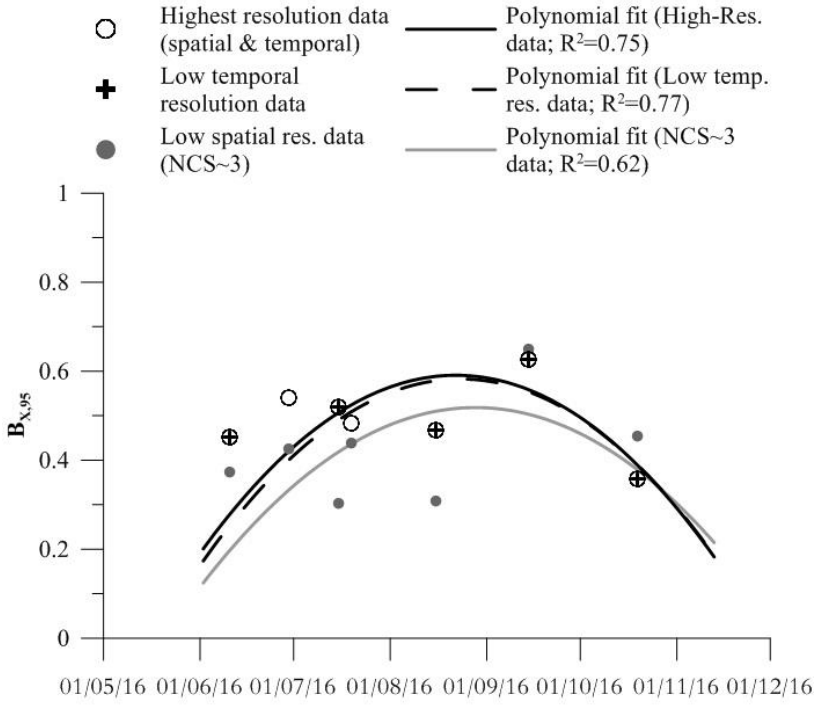

Figure B-20: Interpolation through polynomial curves (2nd order) of $B_{X,95}$ values obtained in 2016 (Year 3) at Reach 2 using data with different spatial and temporal resolutions

B.4 Vegetation stiffness testing data

Table B-6: *MEIh* values (in Nm) obtained at Reach 1 in 2015; Note average value shown was calculated using for tests 1 – 5 as test GDT 6 was not completed on 3 occasions. The acronym *S.a.* denotes *Sparganium americanum*

	GDT 1	GDT 2	GDT 3	GDT 4	GDT 5	GDT 6	Average
Test date	*S. a.*	*S. a.*	*S. a.*	*S. a.*	*S. a.*	*S. a.*	
29-Jul-15	7.32E-04	5.30E-03	5.07E-03	6.30E-03	1.15E-03	n/a	3.71E-03
07-Aug-15	6.85E-04	5.92E-04	1.15E-02	4.67E-03	3.23E-04	n/a	3.56E-03
04-Sep-15	6.39E-04	5.92E-04	1.13E-02	4.24E-03	3.00E-04	n/a	3.42E-03
10-Sep-15	6.39E-04	5.92E-04	7.17E-03	7.78E-04	8.71E-04	1.49E-02	2.01E-03
16-Sep-15	2.77E-04	4.85E-03	1.32E-02	6.85E-04	8.71E-04	1.85E-02	3.98E-03
23-Sep-15	7.32E-04	7.32E-04	1.10E-02	4.03E-03	4.20E-03	1.54E-02	4.15E-03
07-Oct-15	2.69E-03	2.54E-04	7.49E-03	2.54E-04	3.47E-04	1.04E-02	2.21E-03

Table B-7: *MEIh* values (in Nm) obtained at Reach 2 in 2015; Note average value shown was calculated using for tests 1 – 5 as test GDT 6 was not completed on 2 occasions. The acronym *S.a.* denotes *Sparganium americanum*;

	GDT 1	GDT 2	GDT 3	GDT 4	GDT 5	GDT 6	Average*
Test date	*S. a.*	*S. a.*	*S. a.*	*S. a.*	*S. a.*	*S. a.*	
29-Jul-15	1.01E-03	4.47E-03	4.71E-03	1.01E-03	7.68E-03	n/a	3.78E-03
07-Aug-15	9.17E-04	9.13E-03	8.71E-04	1.15E-03	1.24E-03	n/a	2.66E-03
04-Sep-15	1.05E-02	1.35E-02	4.62E-04	1.18E-02	5.08E-04	2.30E-02	7.36E-03
10-Sep-15	9.28E-03	1.49E-02	9.17E-04	1.06E-02	7.32E-03	3.81E-02	8.59E-03
16-Sep-15	1.16E-02	1.44E-02	1.01E-03	9.93E-03	5.43E-04	2.93E-02	7.49E-03
23-Sep-15	1.27E-02	1.29E-02	1.06E-03	9.52E-03	9.74E-03	2.59E-02	9.19E-03
07-Oct-15	1.10E-03	9.03E-03	4.62E-04	5.08E-04	5.43E-04	5.43E-04	2.33E-03

Table B-8: *MEIh* values (in Nm) obtained at Reach 1 in 2016. The acronym *S.a.* denotes *Sparganium americanum*; while *E.c.* denotes *Elodea canadensis*

	GDT 1	GDT 2	GDT 3	GDT 4	GDT 5	GDT 6	GDT 7	GDT 8	GDT 9	GDT 10	Average
Test date	*S. a.*	*S. a.*	*S. a.*	*S. a.*	*S. a.*	*S. a.*	*S. a.*	*S. a.*	*S. a.*	*E. c.*	
19-Jul-16	4.39E-04	2.44E-03	2.31E-04	NA	1.06E-03	6.66E-03	6.90E-03	9.41E-04	8.66E-03	7.45E-03	3.87E-03
11-Aug-16	8.70E-03	3.47E-04	7.32E-04	NA	3.47E-04	1.10E-02	8.03E-03	1.06E-03	7.32E-04	1.00E-02	4.56E-03
30-Aug-16	1.01E-02	3.47E-04	1.40E-02	NA	1.07E-02	1.35E-02	7.78E-04	6.66E-03	9.84E-03	1.19E-02	8.65E-03
14-Sep-16	4.62E-04	3.93E-04	1.26E-02	NA	1.52E-02	9.17E-04	8.80E-03	3.81E-04	1.13E-02	1.15E-02	6.85E-03
19-Oct-16	4.85E-04	4.16E-04	2.43E-04	NA	4.85E-04	3.93E-04	3.81E-04	4.04E-04	3.12E-04	9.40E-03	1.39E-03

Table B-9: *MEIh* values (in Nm) obtained at Reach 2 in 2016 The acronym *S.a.* denotes *Sparganium americanum*; *P.n.* denotes *Potamogeton natans* and *N.* denotes *Nasturtium*

	GDT 1	GDT 2	GDT 3	GDT 4	GDT 5	GDT 6	GDT 7	GDT 8	Average
Test date	*S. a.*	*S. a.*	*S. a.*	*P. n.*	*S. a.*	*S. a.*	*S. a.*	*N.*	
19-Jul-16	5.55E-04	5.78E-04	5.78E-04	1.16E-04	4.85E-04	5.08E-04	5.78E-04	6.24E-04	4.13E-04
11-Aug-16	1.29E-03	5.78E-04	5.78E-04	3.44E-03	2.92E-02	3.48E-02	1.34E-03	6.24E-04	5.20E-03
30-Aug-16	1.13E-03	5.78E-04	5.78E-04	5.04E-03	3.42E-02	Above WS	2.28E-02	NA	9.19E-03
14-Sep-16	1.77E-02	5.78E-04	5.78E-04	4.10E-03	3.20E-02	Above WS	3.48E-02	2.57E-02	1.28E-02
19-Oct-16	0	0	0	0	0	0	0	0	0

B.5 Effect of sample size

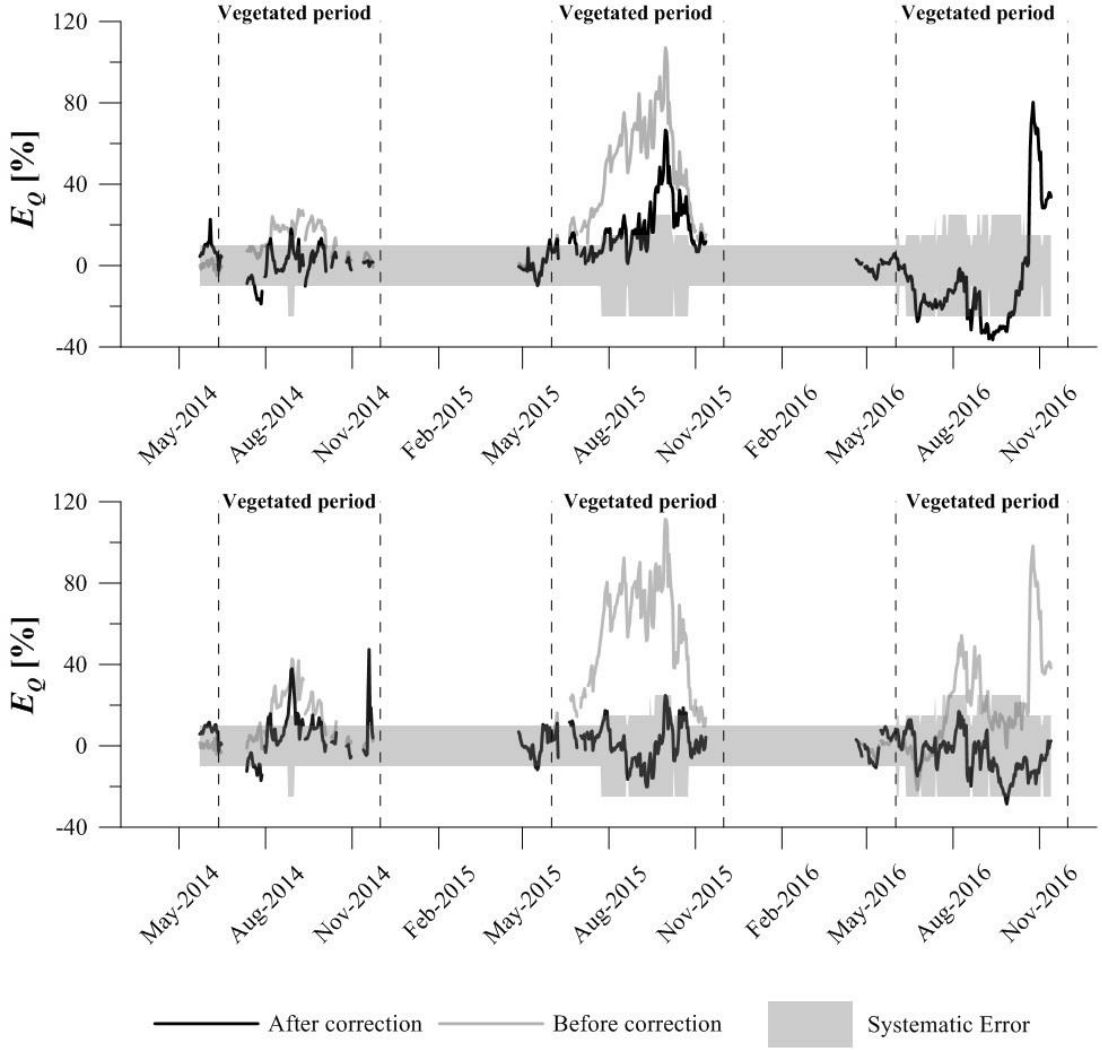

Figure B-21: Time series of E_Q after correction procedure at Reach 1 (top) and Reach 2 (bottom) with a normalized cross-sectional spacing (*NCS*) equal to 1

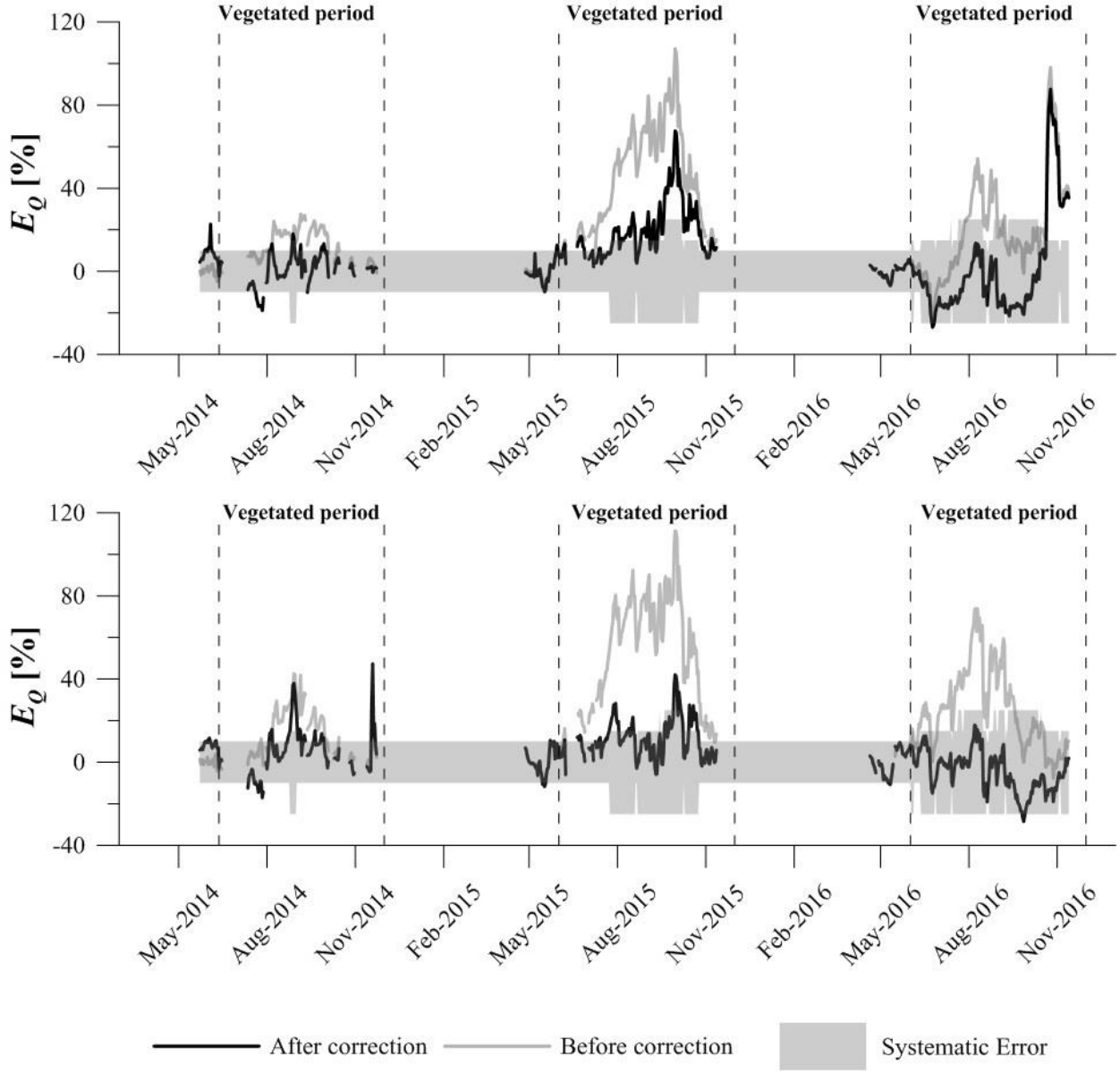

Figure B-22: Time series of E_Q after correction procedure at Reach 1 (top) and Reach 2 (bottom) with a normalized cross-sectional spacing (*NCS*) equal to 2

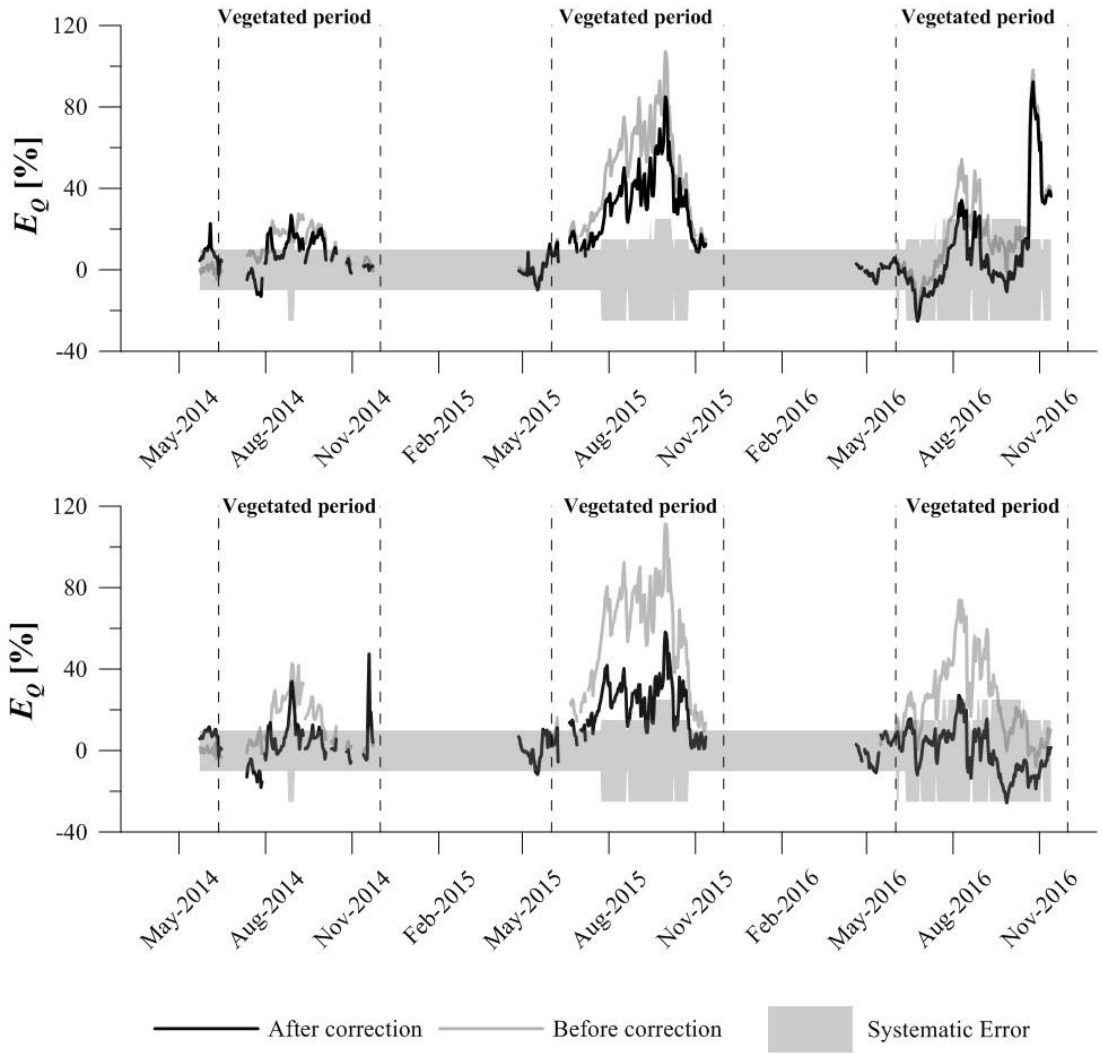

Figure B-23: Time series of E_Q after correction procedure at Reach 1 (top) and Reach 2 (bottom) with a normalized cross-sectional spacing (*NCS*) equal to 3

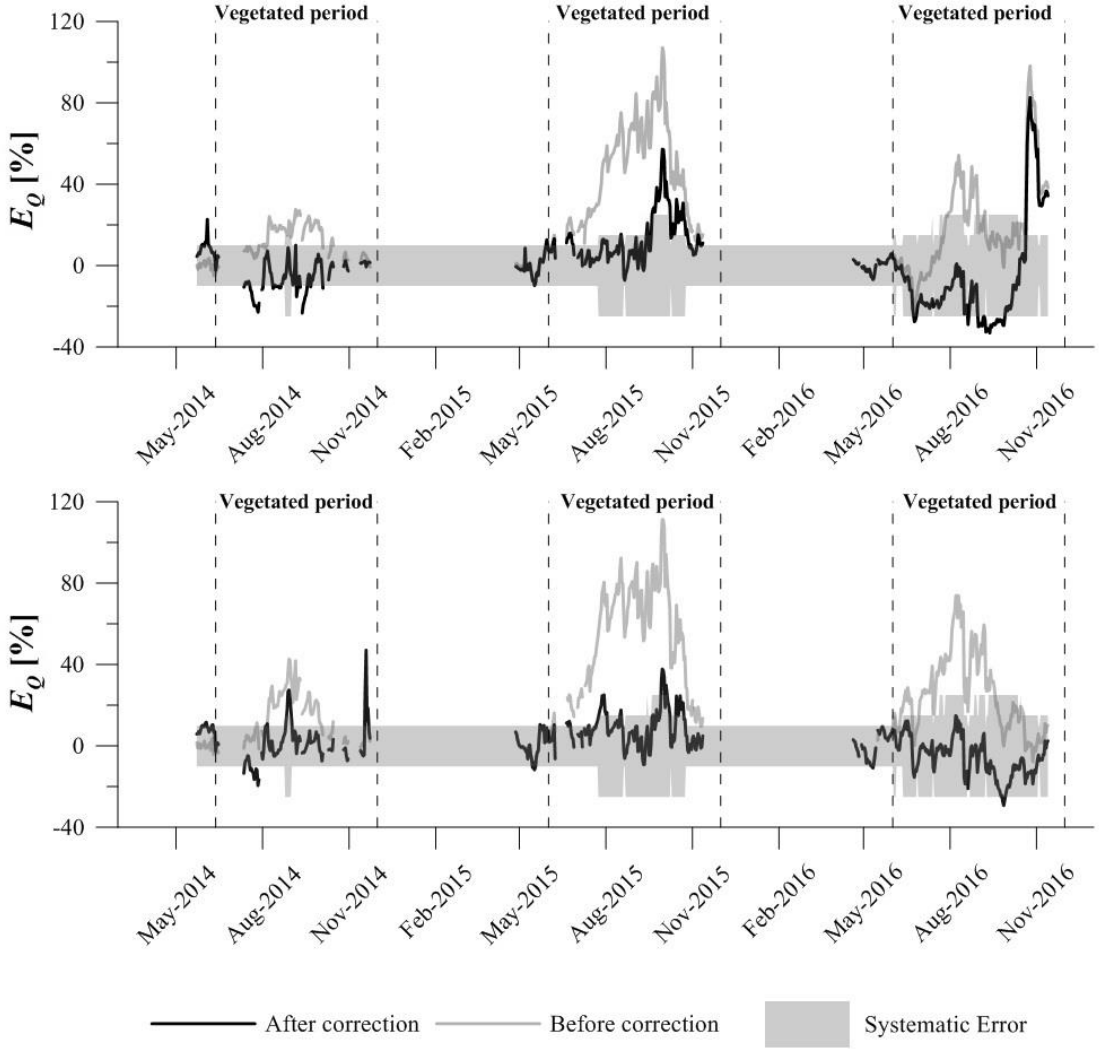

Figure B-24: Time series of E_Q after correction procedure at Reach 1 (top) and Reach 2 (bottom) with a low temporal resolution (approximately one vegetation survey per month) and using the maximum spatial resolution.

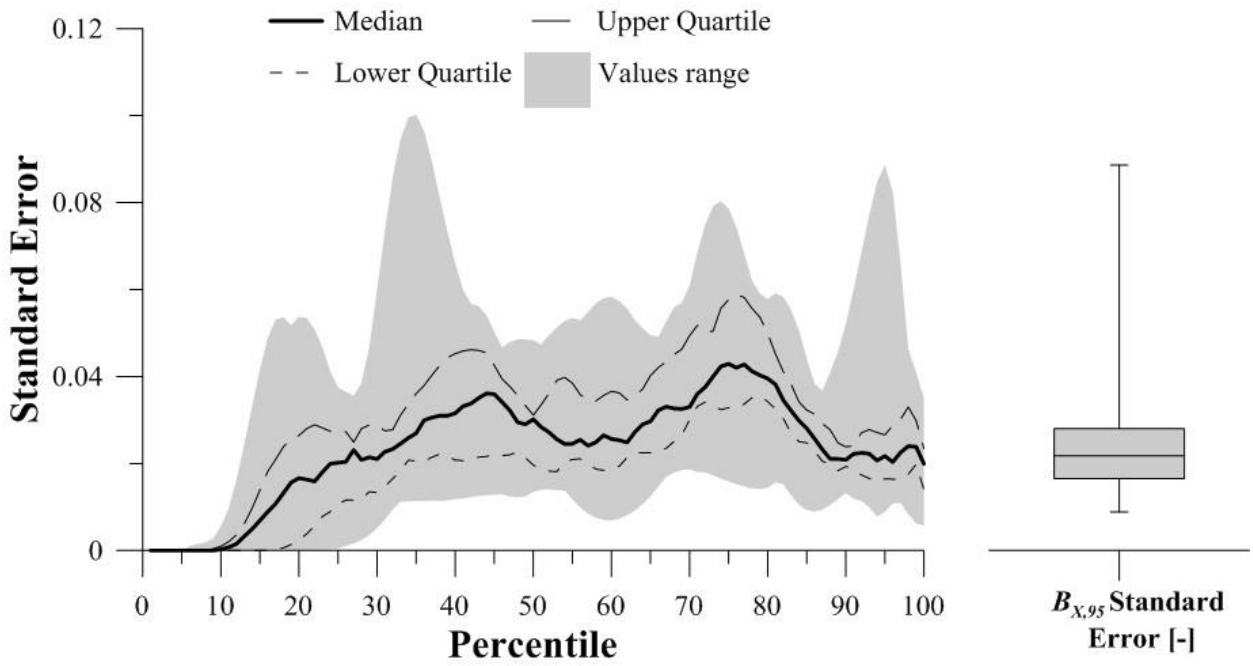

Figure B-25: Distribution of Standard errors for VDC percentiles at Reach 1

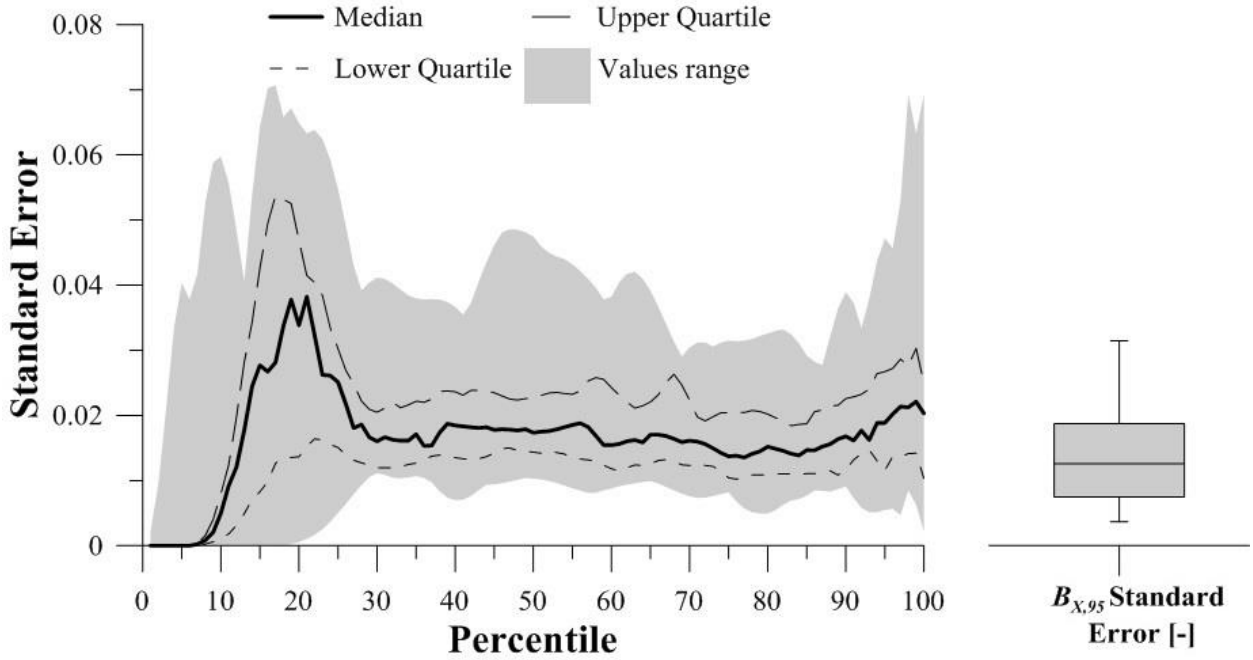

Figure B-26: Distribution of Standard errors for VDC percentiles at Reach 2

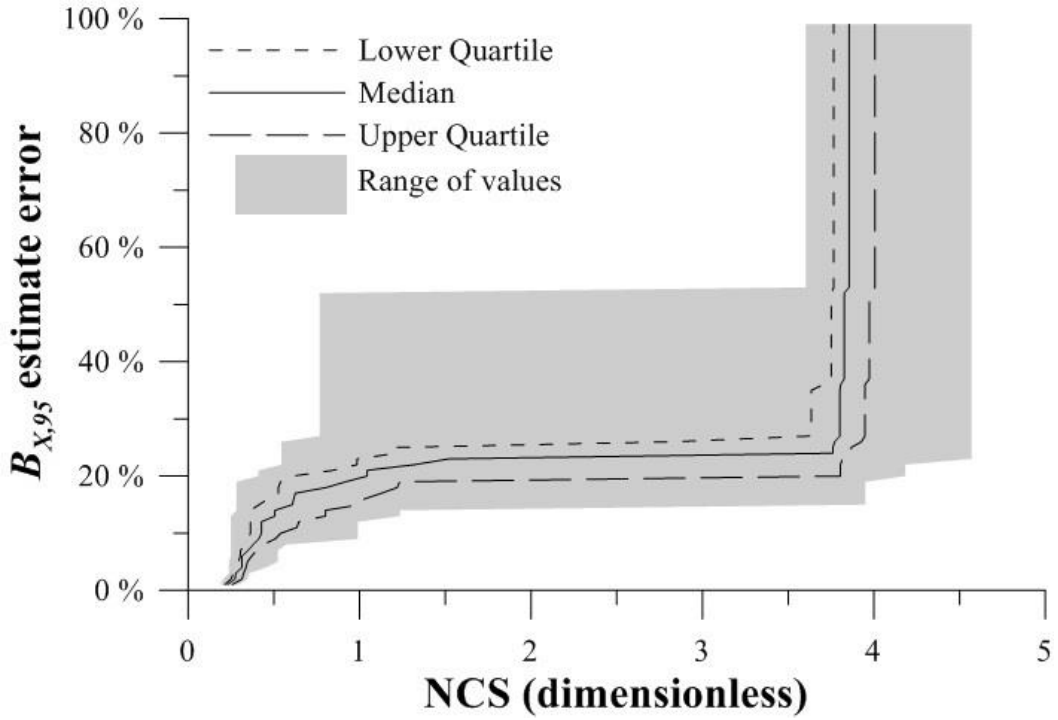

Figure B-27: Errors in $B_{X,95}$ as a function of *NCS* at Reach 1

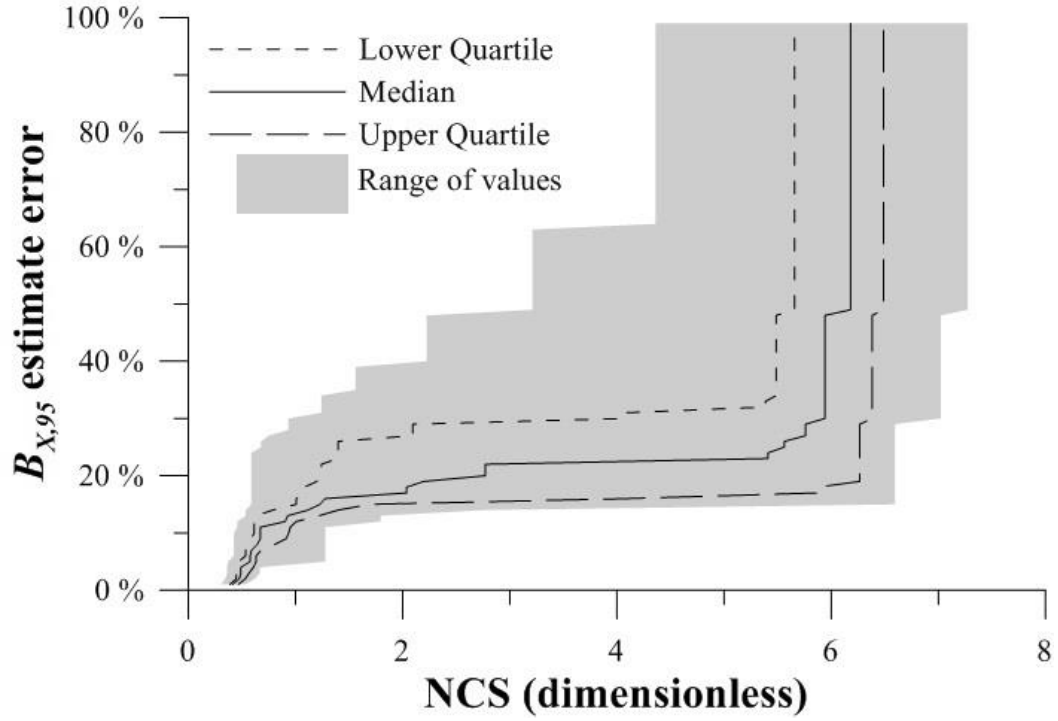

Figure B-28: Errors in $B_{X,95}$ as a function of NCS at Reach 2